GRID AND CLOUD COMPUTING FOR E-SCIENCE APPLICATIONS

Politecnico di Torino
I Facoltá di Ingegneria
Dottorato in Matematica per le Scienze dell'Ingegneria

Doctor of Philosophy Dissertation

Mathematical Models and Methods related to Cell–Extracellular Matrix Interactions

by

Guido Vitale (matricola 160790)

Supervisors:
Prof. Davide Ambrosi (Politecnico di Milano)
Prof. Luigi Preziosi (Politecnico di Torino)

MAT - 07

Contents

Quieto s'asside ciascheduno al suo posto: il sol Tersite di gracchiar non si resta, e fa tumulto parlator petulante. Avea costui di scurrili indigeste dicere pieno il cerebro, e fuor di tempo, e senza o ritegno o pudor le vomitava contro i re tutti; e quanto a destar riso infra gli Achivi gli venia sul labbro, tanto il protervo beffator dicea.

from *Iliad*, Homerus (Italian translation by *Vincenzo Monti*)

Acknowledgements

Apart from my supervisors, other people had given (directly or indirectly) a contribution to this Dissertation Thesis.
Among them I would like to thank *prof. Paolo Tilli* (*Politecnico di Torino*) for assisting me with patience during the work of analytical well posedness shown in the first part of this work.
The numerical and analytical issues of the first part has also improved thanks to the help of *prof. Marco Verani* and *dr. Simone Pezzuto* (*Politecnico di Milano*) who gave me me an envaluable help.
Major issues from what concerning the second part of this work where discussed with *prof. Franco Pellerey* (*Politecnico di Torino*) and *dr. Andrea Tosin* (*IAC–CNR, Roma*): they give important ideas and answer to crucial questions.

Preludio

This Doctor of Philosophy Dissertation in *Matematica per le Scienze dell'Ingegneria* is composed by two distinct parts having in common the study of the interactions between cells and extracellular-matrix. This is the result of a three year working project supervised by professors *Davide Ambrosi* (*Politecnico di Milano*) and *Luigi Preziosi* (*Politecnico di Torino*). In the spirit of the aims and scopes of the Doctoral degree, both modelling and applications of analytical/numerical methods constitute the backbone of such a work; in fact, the first part emphasizes the latter aspect whilst the second part is more focused on the former. Specifically:

1. *Part I* deals with the mathematical aspects of Force Traction Microscopy. This is an inversion method that allows to reconstruct the stress field acting on a substratum knowing the displacement of the substrate itself, measured at some points. The formulation of this problem in the Inverse/Optimal Control framework together with its analytical and numerical study constitutes the real aim of this part of dissertation. Remarkably, some contents of this part had been submitted [70].

2. *Part II* deals with the mathematical modeling of cell-tissue adhesion. Such an adhesive property of living tissue seems to be of importance in the developing of biological process. Moreover, quite a huge amount of experimental data can be found in the specialistic literature. A Continuum Mechanics point of view is adopted to describe adhesion and the outcome of our model is qualitatively compared with experiments. Remarkably, some contents of this part had been published [59].

Last, the relevant symbols used in this work are collected at the end for reader convenience.

Part I

Mathematical Methods in Force Traction Microscopy

Chapter 1

Motivations

Many living cells have the ability to migrate, in both physiological and pathological conditions; examples include wound healing, embryonic morphogenesis and the formation of new vessels in tumours. The motility of a cell is driven by the reorganization of its inner structure, the cytoskeleton, according to a complex machinery. The net effect of this process is that a cell is able to apply a stress on the environment, pulling the surrounding material mainly in the direction of the movement. The biophysical details of the internal engine of a cell are far from being fully understood or rephrased in terms of a mathematical model; nevertheless its inverse counterpart, that is the determination of forces on the basis of measured displacement, is quite a popular problem in the biophysical community.

The early idea to study the force applied by cells in their migration as an inverse problem dates back to the work of Harris and coworkers in the eighties [30]. They consider the action of fibroblasts (cells with a high degree of contractility) laying on a flat poliethylene sheet. They argue that the wrinkles produced by the cells on the substrate are a good indicator of the stress exerted by the cells on the surface itself: direction, height and length of the buckles correlate with the direction and intensity of the force, respectively.

After several efforts, the correct methodology to translate such a qualitative argument above into a quantitative procedure was formulated by Dembo and Wang in a seminal paper about twenty years later [24, 23]. Their technique was new, both in a technological and in a methodological sense. The use of a soft poliacrilamide substrate avoids the emergence of wrinkles, that are typically produced in a nonlinear elasticity range. Thus restricting to a linear elastic regime, the displacement of fluorescent beads dispersed in the elastic material can be evaluated from different images. Finally, they solve the direct problem in terms of Green elasticity functions and then minimize the error under regularization by a discrete Tichonov method. This method has become a standard in biophysics.

An alternative approach addressing the same issue can be stated in a continuous variational framework [2]. Again, the starting point is a Tichonov functional defined as the error norm plus a penalization of the magnitude of the force. If a variation of the cost functional is operated at a continuous level, the definition of an adjoint problem for the unknown force naturally arises. This way, two elliptic partial differential equations

coupled by the (linear) source terms are obtained and their approximate solution can be addressed, for instance, by a finite element discretization. The adjoint method has been applied to evaluate the surface traction generated by different cell lines, solving a two–dimensional depth–averaged elasticity set of equations.

Although the optimal control approach is less popular than the standard inverse method based on Green functions, it has some attractive features that make it worth to investigate further.
The first reason is of numerical type: a variational formulation, based on forward and adjoint problem to be solved jointly, can be addressed by a finite element code where local approximating polinomials might be computationally more efficient than convolution of global Green functions plus a decoupled minimizing algorithm.
The second, more relevant, issue is that Green functions of the elasticity problem are known explicitly only in few simple geometrical configurations, including the infinite half–space. As a matter of fact, the typical biological domain where cells apply stress in their three dimensional migration is geometrically complex and Green functions are not known a priori. Legant et al. [39] actually calculate those Green functions in approximated form by finite elements and then minimize the Tichonov penalty functional to find the optimal traction.
Last but not least, the optimum control theory offers a framework for a natural generalization of the forward model to a number of important physical characterizations of the substrate, in particular nonlinear elastic materials, possibly including non–homogeneities and anisotropy due to fibres embedded in the material itself.

One goal of this work is of strictly mathematical nature. The rigorous theory of inversion of force traction microscopy is, at our knowledge, still lacking and this work aims to fill this gap. The availability of pointwise observations makes it impossible to state the well posedness of the problem using Hilbert spaces only, and we resort to the theory developed by Casas [18], [19], [20]. Existence and uniqueness of the solution is proved in a general context encompassing distributed and boundary control in two and three dimensions.
The second goal of this part of the dissertation is to extend the issue of the numerical reconstruction of boundary cell traction in a three dimensional environment. To the best of our knowledge, these calculations has up to now been tackled only in [39] using the Green function approach. Conversely to [39], the strategy we implement leads to the numerical approximation of a three dimensional elasticity problem with boundary control and mixed boundary conditions. This problem leads to a set of two coupled elliptic differential equations, namely the forward and the adjoint problem. The latter system can be implemented quite straightforwardly using a finite element code. An important applicative issue is to ascertain the degree of confidence that one can have in the results of a numerical inversion of the 3D data generated by a cell encapsulated in a soft gel. We have implemented a Finite Element discretization of the forward and adjoint equations. The numerical code has been therefore applied to a test case that reproduces *in silico* most of the relevant dynamical aspects of a living cell migrating in a three dimensional environment: the cavity in the gel, representing the space occupied by the embedded cell, has a size of 10-20 microns and the surrounding material has the typical elastic moduli of poliacriamide gel. We first apply a zero–average traction at the surface of such a hole, which is here the "true" force per unit surface to be captured at best by the inversion

algorithm. The displacement in the gel produced by the applied traction evaluated in some nodes of the finite element grid then becomes our data, the starting point to chase algorithmically the value of the stress exerted by the virtual cell.
Producing a large number of numerical simulations, we are able to evaluate the error, defined as the absolute value of the difference between the "true" traction and the reconstructed one for different values of the physical and numerical parameters. Possible different configurations include the number and location of the observation points (the "fluorescent beads" in an experimental setting), the regularization parameters and the number of nodes of the finite element mesh. This way we are able to check at what extent the inversion procedure is sensitive to variations of the parameters and, working in a test case very near to the real biophysical conditions, fix the optimal parameters configuration to be adopted for experimental data.

Chapter 2

Background

In this Chapter we resume some basic results in Elasticity, Functional Analysis and Inverse Problem.

In Section 1, an outline of *Continuum Mechanics* is exposed in order to introduce the Linear Theory of Elasticity. The latter constitutes the mathematical model of the behavior of the gel used in the experimental setup of Force Traction Microscopy. The treatment is based on a *configurational* approach, which allows to find the fundamental balance law and invariance requirement via a *virtual power* argument [29].

Section 2 contains some definitions and theorems of Mathematical Analysis that will be instrumental to study the equations we are interested in, i.e those arising from the problem of traction reconstruction.

Section 3 contains an informal introduction to *Inverse*, *Ill–Posed* and *Optimal Control* problems and tries to emphasize the links among them. Those notions are crucial when facing the estimate of quantities from information provided by experimental measures.

2.1 Basic Continuum Mechanics of Elastic Media

In this Section we introduce the few notions of Continuum Mechanics necessary to introduce the *Theory of Linearized Elasticity*. This Section will also be helpful when reading the second Part of this dissertation, that faces the Continuum Mixture theory.

2.1.1 Kinematics and Balance Equations

Consider the ambient space as a $n-$dimensional affine space ($n \leq 3$), say $\mathcal{A}$ and a time line $[0, T) \subseteq \mathbb{R}$. The space $\mathcal{A}$ is endowed with a translation space, the vector space $\mathcal{V}$. Consider a body in a compatible reference configuration as a smooth $n-$dimensional manifold $\mathcal{B} \subset \mathcal{A}$ *.

The *motion* χ is a smooth one parameter group which maps the reference configuration into the actual one $\mathcal{B}_t$ (i.e. the configuration of the body at the time t):

$$\chi(\cdot, t) : \mathcal{B} \subseteq \mathcal{A} \to \mathcal{B}_t \subseteq \mathcal{A} \tag{2.1}$$

*The notion of a reference configuration can be avoided in the development of the mechanics as well as the request of compatibility [50]. However we follow this approach because is generally simpler and does not affects the fundamental aim of the work

The material gradient of the motion map (performed on $\mathcal{B}$) is the celebrated *Deformation Gradient*:

$$\mathbf{F}(X,t) := \nabla\chi(\cdot,t)(X) \in \mathsf{Lin}(\mathbb{T}_X\mathcal{B},\mathcal{V}) \tag{2.2}$$

In this Section we follow a virtual work approach to deduce balance equations of a continuum medium [29]. We define the *external power* expended on a sub-body $\mathcal{P} \subseteq \mathcal{B}_t$ provided by a surface and a bulk force fields, $\mathbf{c} : \mathcal{B}_t \mapsto \mathcal{V}$ and $\mathbf{b} : \mathcal{B}_t \mapsto \mathcal{V}$ respectively:

$$w^{ext}(\mathcal{P},\mathbf{v}) := \int_{\mathcal{P}} \mathbf{b}\cdot\mathbf{v} + \int_{\partial\mathcal{P}} \mathbf{c}\cdot\mathbf{v}, \tag{2.3}$$

where $\mathbf{v} : \mathcal{B}_t \to \mathcal{V}$ has the role of *arbitrary test velocity field*. To define an *inner power* expenditure, we have to introduce the Cauchy Stress Tensor field $\mathbf{T} : \mathcal{B}_t \mapsto \mathsf{Lin}\mathcal{V}$ and the stress vector field $\mathbf{s} : \mathcal{B}_t \mapsto \mathcal{V}$:

$$w^{int}(\mathcal{P},\mathbf{v}) := \int_{\mathcal{P}} \mathbf{s}\cdot\mathbf{v} + \mathbf{T}\cdot\nabla\mathbf{v} \tag{2.4}$$

Following [29], we require:

Axiom 2.1. *The Internal Power expenditure is Frame Indifferent* [†] *, i.e.:*

$$w^{int}(\mathcal{P},\mathbf{v}) = w^{int\,*}(\mathcal{P},\mathbf{v}^*)$$

for any $\mathbf{v} : \mathcal{B}_t \to \mathcal{V}$ *and sub-body* $\mathcal{P} \subseteq \mathcal{B}_t$*.*

The previous axiom in action give us the frame invariance of (2.4), which leads to the following well known results:

- the inconsistency of a non trivial valued $\mathbf{s}$:

$$\mathbf{s} = 0 \tag{2.5}$$

- the objectivity of $\mathbf{T}$:

$$\mathbf{T}^* = \mathbf{Q}\mathbf{T}\mathbf{Q}^T \qquad \forall\mathbf{Q} \in \mathsf{Ort}(\mathcal{V}) \tag{2.6}$$

- the symmetry of $\mathbf{T}$:

$$\mathbf{T} = \mathbf{T}^T \tag{2.7}$$

The other fundamental axiom involving the virtual power is:

Axiom 2.2. *The Internal Power expenditure equals the power exerted by outer actions, i.e.:*

$$w^{int}(\mathcal{P},\mathbf{v}) = w^{ext}(\mathcal{P},\mathbf{v})$$

for all test fields $\mathbf{v} : \mathcal{B}_t \to \mathcal{V}$ *and material sub-body* $\mathcal{P} \subseteq \mathcal{B}_t$*.*

[†]We intend as a *change of frame* a list $([\mathbf{Q},o,\mathbf{c}],\tau) : [[0,T) \to \mathsf{Ort}(\mathcal{V}) \times \mathcal{A} \times \mathcal{V}] \times \mathbb{R}$ such that the motion and the time measured in the new frame (labeled with a superposed star '*') can be written as [42]:

$$\begin{cases} \chi^* = o + \mathbf{c} + \mathbf{Q}(\chi - o) \\ t^* = t + \tau \end{cases}$$

From the previous Axiom 2.2 one finds the equivalence between (2.3) and (2.4):

$$\int_{\mathcal{P}} \mathbf{T} \cdot \nabla \mathbf{v} = \int_{\mathcal{P}} \mathbf{b} \cdot \mathbf{v} + \int_{\partial \mathcal{P}} \mathbf{c} \cdot \mathbf{v} \tag{2.8}$$

that can be localized using the standard procedure:

$$\begin{cases} -\operatorname{div} \mathbf{T} & = \mathbf{b}, \text{ in } \mathcal{B}_t \\ \mathbf{T}\mathbf{n} & = \mathbf{c}, \text{ on } \partial \mathcal{B}_t \end{cases} \tag{2.9}$$

where div denotes the divergence operator on the actual configuration $\mathcal{B}_t$.

2.1.2 Constitutive Theory for an Elastic Material

Equations (2.9) and (2.7) are not sufficient to determine the actual motion χ of the body (the only unknown in this purely mechanical theory) unless the stress tensor $\mathbf{T}$ is related with kinematical quantities by the so called *constitutive map*. The latter is the mathematical statement that rigorously introduces the intuitive notion of material response and writes as:

$$\mathbf{T}(X,t) = \hat{\mathbf{T}}(\chi; \mathcal{B}_t) \tag{2.10}$$

To reduce the possible forms of the constitutive functional in the above equation, some additional hypothesis have to be introduced. First, the *principle of objectivity* for constitutive mappings which states the correct transformation of (2.10) under a change of frame (see the footnote at page 14). Second, since we are interested in elastic behavior, we rule out the dependence on the history of the motion and long range effects from the map $\hat{\mathbf{T}}$. Under these conditions, the following representation theorem holds (see [42] for the rationale behind such a *vulgata*):

$$\mathbf{T}(X,t) = \mathbf{F}\hat{\mathbf{S}}(\mathbf{C}(X,t); X)\mathbf{F}^T \tag{2.11}$$

where $\mathbf{C} := \mathbf{F}^T\mathbf{F}$ is the *right Cauchy Green Tensor* and $\hat{\mathbf{S}} : \mathsf{Lin}\mathcal{V} \times \mathcal{B} \to \mathsf{Lin}\mathcal{V}$ is a smooth constitutive map. Another restriction on constitutive maps is imposed by *Thermodynamics*. If we follow the rules of exploitation of the Second Principle of Thermodynamics stated by Coleman and Noll [29], a free energy depending on the motion (say $\psi = \hat{\psi}(\mathbf{F}; X)$) should be postulated. Then one has the following relationship when considering the material homogeneous (i.e. leaving aside the explicit dependence on X) for sake of simplicity:

$$\mathbf{T} = \hat{\psi}'(\mathbf{F}) \tag{2.12}$$

where the prime ($'$) means differentiation.

2.1.3 Linearized Elasticity

Suppose we are dealing with small deformations, i.e $|\mathbf{F}| \ll 1$ everywhere at any time ($|\cdot|$ is a norm on $\mathsf{Lin}\mathcal{V}$). Then, by easy calculations: $\mathbf{C} = \mathsf{sym}\mathbf{F} + o(|\mathbf{F} - \mathbf{1}|)$. In the latter equation $\mathbf{1}$ is the identity on $\mathsf{Lin}\mathcal{V}$, sym is the projection on the space of symmetric tensor Sym and the 'o' is the usual Landau symbol (that is any function such that $\lim_{|z|\to 0} \frac{o(z)}{|z|} = 0$).

Introducing the displacement vector $\mathbf{u}(X,t) = \chi(X,t) - X$ then the deformation gradient writes as $\mathbf{F} = \nabla\mathbf{u} + \mathbf{1}$ and the Cauchy Green tensor becomes

$$\mathbf{C} = \mathsf{sym}\big(\nabla\mathbf{u} + \mathbf{1}\big) + o(|\nabla\mathbf{u}|).$$

If the constitutive map in (2.11) is sufficiently regular, dealing with small deformation and dropping the explicit dependence on X, one can write:

$$\begin{aligned}\hat{\mathbf{S}}(\mathbf{C}) &= \hat{\mathbf{S}}\left(\mathbf{1} + \mathsf{sym}\nabla\mathbf{u} + o(|\nabla\mathbf{u}|)\right)\\ &= \hat{\mathbf{S}}(\mathbf{1}) + \hat{\mathbf{S}}'(\mathbf{1})\left[\mathsf{sym}\nabla\mathbf{u}\right] + o(|\nabla\mathbf{u}|)\end{aligned}$$

If the reference configuration is relaxed (i.e $\hat{\mathbf{S}}(\mathbf{1}) = 0$) then, at the first order of approximation:

$$\mathbf{T} = \mathbb{C}\left[\mathsf{sym}\nabla\mathbf{u}\right] \tag{2.13}$$

where $\mathbb{C} := \hat{\mathbf{S}}'(\mathbf{1}) \in \mathsf{Lin}(\mathsf{Lin}(\mathcal{V}))$ is a linear isomorphism on $\mathsf{Lin}(\mathcal{V})$ and it is called the *Hooke Linear Elasticity Tensor*.
Remarkably, when dealing with small deformation, $\mathcal{B} \approx \mathcal{B}_t$. It is thus meaningless in this regime to distinguish spatial and material description.
Note also that, in the linearized case, $\psi = \mathbf{H} \in \mathsf{Lin}(\mathcal{V}) \mapsto \frac{1}{2}\mathbf{H}\cdot\mathbb{C}\mathbf{H} \in \mathbb{R}$ thanks to the (2.12). The latter implies $\psi''(\mathbf{1}) = \mathbb{C}$. Following [21, 47], we claim that $\mathbb{C}$ satisfies the following conditions:

$$\mathbb{C}[\mathbf{S}] = \mathbb{C}[\mathbf{S}^T], \quad \forall\mathbf{S} \in \mathsf{Lin}(\mathcal{V}), \tag{2.14}$$

$$\mathbf{S}\cdot\mathbb{C}[\mathbf{S}] \geq \alpha\mathbf{S}\cdot\mathbf{S}, \quad \alpha > 0, \forall\mathbf{S} \in \mathsf{Sym}(\mathcal{V}), \tag{2.15}$$

$$\mathbf{S}\cdot\mathbb{C}[\mathbf{H}] = \mathbf{H}\cdot\mathbb{C}[\mathbf{S}], \quad \forall\mathbf{H},\mathbf{S} \in \mathsf{Sym}(\mathcal{V}). \tag{2.16}$$

The condition (2.14) accounts for objectivity in the linearized case. The symmetry property (2.16) reflects torque balance: it descents from the Eqns. (2.7) and (2.13). The inequality (2.15) is, instead, postulated: it is a requirement of stability since it forces the convexity of the energy functional ψ. The latter inequality will be fundamental when study the analytical well–posedness of the equations characterizing the linear elastic regime.

2.2 A Brief Review of Selected Analysis Tools

We now give some technical results useful for the following.

2.2.1 Functional spaces

The theory of linear elliptic equations is classically based on the definition and properties of some suitable functional spaces. We sketch here below the main notions to be used in this work; more details can be found, for instance, in [1] and [49] [‡].

Definition 2.3. *Given Ω an open set in $\mathbb{R}^n$, we set the following Sobolev spaces:*

- $L^p(\Omega) := \{\mathbf{u} : \Omega \to \mathbb{R}^m \mid \int_\Omega |\mathbf{u}|^p < \infty\}$;
- $W^{k,p}(\Omega) := \{\mathbf{u} \in L^p(\Omega) \mid \nabla^i \mathbf{u} \in L^p(\Omega),\ \forall i \in \{1, \dots, k\}\}$.

where ∇^i is the i-th gradient and $\nabla^0 := \mathbf{1}$ is the identity tensor.

Non integer indexed Sobolev spaces (i.e. when $k \in \mathbb{R}$) can be also defined, see [1], and they will turn useful in the following. Relevant examples of Sobolev spaces are the following Hilbert spaces:

- $L^2(\Omega)$ with the scalar product $(\mathbf{u}|\mathbf{v})_{L^2(\Omega)} := \int_\Omega \mathbf{u} \cdot \mathbf{v}$;
- $H^k(\Omega) := W^{k,2}(\Omega)$ with the scalar product $(\mathbf{u}|\mathbf{v})_{H^k(\Omega)} := \sum_{i=0}^k \int_\Omega \nabla^i \mathbf{u} \cdot \nabla^i \mathbf{v}$.

The following inequality is a milestone for the L^p spaces [49].

Theorem 2.4. *(Hölder inequality) Let $\mathbf{u} \in L^s(\Omega)$, $\mathbf{v} \in L^{s'}(\Omega)$ with s' conjugate to s (i.e. $\frac{1}{s} + \frac{1}{s'} = 1$). It holds:*

$$\int_\Omega \mathbf{u} \cdot \mathbf{v} \leq \sqrt[s]{\int_\Omega |\mathbf{u}|^s} \sqrt[s']{\int_\Omega |\mathbf{v}|^{s'}}.$$

The trace operator $\mathcal{T}_{\partial\Omega}$ is defined as the restriction of a function defined on $\Omega \subset \mathbb{R}^n$ over its boundary $\partial\Omega$, having dimension $n-1$. Traces are characterized by [1]:

Theorem 2.5. *(Trace Theorem) Let $\Omega \in \mathbb{R}^n$ be an open bounded set with boundary $\partial\Omega$. The trace $\mathcal{T}_{\partial\Omega}$ is a linear and continuous functional such that:*

- *it injects $W^{1,p}(\Omega)$ in $L^p(\partial\Omega)$ if $p < n$;*
- *if $\mathbf{u} \in H^k(\Omega)$ then $\mathcal{T}(\nabla^i \mathbf{u}) \in H^{k-1/2}(\partial\Omega)$.*

Using traces, we can define subspaces of Sobolev spaces that allow us to treat boundary conditions. Let us define the space of fields in $H^1(\Omega)$ satisfying homogeneous Dirichlet boundary condition on Γ_D:

$$H^1_{0,\Gamma_D}(\Omega) := H^1(\Omega) \cap \mathsf{ker}(\mathcal{T}_{\Gamma_D}).$$

[‡]In this work I tacitly assume that we are dealing with domains enjoying some special properties. The interested reader may find in [1, 49] the hypothesis needed to develop the theory. In the following, sections, we will stick us with a bounded C^2-regular boundary, which is enough to prove the results shown here.

A similar construction allows us to define, more generally, the space $W^{1,s}_{0,\Gamma_D}$ ($s > 0$), see [1, 49]. It is worth noting that (thanks to Poincare Lemma [62]) $H^1_{0,\Gamma_D}(\Omega)$ can be equipped with the scalar product $(\mathbf{u}|\mathbf{v})_{H^1_{0,\Gamma_D}(\Omega)} := \int_\Omega \nabla\mathbf{u}\cdot\nabla\mathbf{v}$ equivalent to the one given above.
The following special case of Sobolev Embedding theorem [1] holds:

Theorem 2.6. *Let $\Omega \subset \mathbb{R}^n$ an open bounded domain $n = 2, 3$. Then:*

- $W^{1,p}(\Omega) \hookrightarrow C^0(\mathsf{cl}\Omega)$, $p > n$;
- $H^2(\Omega) \hookrightarrow W^{1,p}(\Omega)$, $p \in [1, \frac{2n}{n-2}]$;
- $W^{1,p}(\Omega) \hookrightarrow L^2(\Omega)$, $p \geq \frac{2n}{n+2}$;

where $\hookrightarrow$ means that the inclusion is continuous and the symbol cl *denote the closure of a set.*

2.2.2 Convex Functionals

A functional $\mathcal{J}$ is a (not necessarily linear) map from a possibly infinite dimensional linear space to the set of real numbers. In symbols $\mathcal{J} : \mathsf{F} \to \mathbb{R}$. For simplicity the theory outlined below is restricted to the situation in which F is an Hilbert space. Our interest will be focused on the properties that guarantee both existence and uniqueness of the minimum point for the aforementioned functionals, since their range is a totally ordered set. In order to pursue such an issue, the study of *convex* functionals is fundamental:

Definition 2.7. *A functional $\mathcal{J} : \mathsf{F} \to \mathbb{R}$ is called* convex *in F if, for every $t \in [0, 1]$ and $\mathbf{f}, \mathbf{g} \in \mathsf{F}$, $\mathcal{J}(t\mathbf{f} + (1-t)\mathbf{g}) \leq t\mathcal{J}(\mathbf{f}) + (1-t)\mathcal{J}(\mathbf{g})$. The latter is said* strictly convex *if the last equation holds with the strict inequality sign.*

Another important notion arises when looking for extremum points:

Definition 2.8. *A functional $\mathcal{J} : \mathsf{F} \to \mathbb{R}$ is called* coercive *if, given a sequence $(\mathbf{f}_n)_{n\in\mathbb{N}}$ such that $\lim_{n\to\infty} \|\mathbf{f}_n\|_\mathsf{F} = +\infty$, then $\lim_{n\to\infty} \mathcal{J}(\mathbf{f}_n) \to +\infty$.*

We are ready to recall a classical theorem [40]:

Theorem 2.9. *Let $\mathcal{J} : \mathsf{F} \to \mathbb{R}$ be a continuous, coercive and strictly convex functional. Let F_0 be a closed subspace of F. Then a unique minimum point of $\mathcal{J}$ in F_0 exists.*

An important operation that can be extended quite easily from finite to infinite dimensional spaces is the *differentiation*:

Definition 2.10. *Let $\mathcal{J} : \mathsf{F} \to \mathbb{R}$ a functional. Its (Frechet–)differential in $\mathbf{f} \in \mathsf{F}$ is defined (if meaningful) as the unique linear map $\mathcal{J}'(\mathbf{f}) \in \mathsf{F}^*$ such that:*

$$\mathcal{J}(\mathbf{f} + \mathbf{h}) - \mathcal{J}(\mathbf{f}) = \mathcal{J}'(\mathbf{f})\mathbf{h} + o\big(\|\mathbf{h}\|_\mathsf{F}\big). \qquad \forall \mathbf{h} \in \mathsf{F} \tag{2.17}$$

Under suitable hypothesis, the minimum of such a functional (say $\mathbf{f} \in \mathsf{F}$) can be characterized by the Euler equation $\mathcal{J}'(\mathbf{f}) = 0$. It can be shown that:

Theorem 2.11. *Let $\mathcal{J} : \mathsf{F} \to \mathbb{R}$ be a differentiable, coercive and strictly convex functional. If F_0 is a closed subspace of F, then the unique minimum point of $\mathcal{J}$ in F_0 is also the unique solution of $\mathcal{P}\mathcal{J}'(\mathbf{f}) = 0$ and viceversa, being $\mathcal{P} : \mathsf{F} \to \mathsf{F}_0 \subset \mathsf{F}$ the orthogonal projection onto F_0.*

2.2.3 Linear Elliptic Differential Equation

Consider a $n-$dimensional affine space, $\mathcal{A}$, having as a translation space the vector space $\mathcal{V}$ and being endowed with a metric structure (thanks to the scalar product '$\cdot$' on $\mathcal{V}$). It was noted in Section 2.1 that such a mathematical structure is a good model for the classical physical space which is, of course, essential to build up a mechanical theory.

We now define the notion of differential operator acting on fields attached on affine spaces:

Definition 2.12. *A* Linear Second Order Differential Operator *on $\mathcal{A}$ that acts on the field $u : \mathcal{A} \to \mathcal{U}$ (where $\mathcal{U}$ is any finite dimensional linear space) can be written as:*

$$\Big[u : \mathcal{A} \to \mathcal{U}\Big] \mapsto \Big[\mathrm{div}\mathbb{A}\left[\nabla u\right] + \mathbb{D}\left[\nabla u\right] + \mathbb{F}u : (\mathcal{A} \to \mathcal{U})\Big]$$

where $\mathbb{A} : \mathcal{A} \to \mathsf{Lin}(\mathsf{Lin}(\mathcal{V},\mathcal{U}))$, $\mathbb{D} : \mathcal{A} \to \mathsf{Lin}(\mathsf{Lin}(\mathcal{V},\mathcal{U}),\mathcal{U})$ and $\mathbb{F} : \mathcal{A} \to \mathsf{Lin}(\mathcal{U})$.

We recall that div is the divergence operator (see [51] for the details) which associates to a field with range in $\mathsf{Lin}(\mathcal{V},\mathcal{U})$ another field that takes value in $\mathcal{U}$.
In the following we consider the latter coefficient smooth enough to apply the theorems of interest, for example we assume $\mathbb{A}, \mathbb{D}, \mathbb{F} \in C^\infty(\mathcal{A})$ or even constant on $\mathcal{A}$. The following definition characterizes an important class of differential operators:

Definition 2.13. *The Linear Differential Operator above is called* strongly elliptic *if an $\alpha > 0$ exists such that, for almost all $x \in \mathcal{A}$:*

$$\mathbf{S} \cdot \mathbb{A}(x)\mathbf{S} \geq \alpha \mathbf{S} \cdot \mathbf{S} \tag{2.18}$$

for all $\mathbf{S} \in \mathsf{Lin}(\mathcal{V},\mathcal{U})$. Here the centered dot '$\cdot$' is the scalar product in $\mathsf{Lin}(\mathcal{V},\mathcal{U})$.

Actually, a weakened definition of ellipticity holds for the tensor $\mathbb{A}$, the so called Baker–Ericksen type inequality (or Rank One ellipticity):

$$(\mathbf{s} \otimes \mathbf{r}) \cdot \mathbb{A}[\mathbf{s} \otimes \mathbf{r}] \geq \alpha(\mathbf{s} \cdot \mathbf{s})(\mathbf{r} \cdot \mathbf{r})$$

for all $\mathbf{r} \in \mathcal{U}, \mathbf{s} \in \mathcal{V}$. In this case, roughly speaking, $\mathbb{A}$ is 'elliptic only on the dyads'. This mollified definition is actually sufficient to prove the theorems of our interest (see [21, 47] for a deeper discussion).

A *Linear Elliptic Differential Equation* is thus an equality involving the Linear Elliptic Differential operator introduced above, formally:

$$\begin{cases} \mathrm{div}\mathbb{A}\left[\nabla u\right] + \mathbb{D}\left[\nabla u\right] + \mathbb{F}u & = y \qquad \text{in } \Omega, \\ \mathcal{B}u & = z \qquad \text{in } \partial\Omega \end{cases}$$

where $x : \Omega \subset \mathcal{A} \to \mathcal{U}$ is the unknown field and $y : \Omega \subset \mathcal{A} \to \mathcal{U}$ and $z : \partial\Omega \subset \mathcal{A}$ are given data and $\mathcal{W}$ is a suitable linear space. When the above equality is defined over a proper open subset $\Omega \subsetneq \mathcal{A}$, additional conditions must be given in order to solve the equation properly. These additional informations are given at the boundary $\partial\Omega$, namely *boundary conditions*, and are expressed by the operator $\mathcal{B} : (\Omega \subset \mathcal{A} \to \mathcal{U}) \to (\partial\Omega \subset \mathcal{A} \to \mathcal{W})$.

The Differential Equation literature deals almost exclusively with fields defined on $\mathbb{R}^n$. The results obtained could be in principle extended to our affine $\mathcal{A}$ and vector

spaces $\mathcal{U}, \mathcal{V}, \mathcal{W}$ using a suitable homeomorphism.
The Differential Equation theory has gained some striking development in the last century when formalized in the *Sobolev Space* setting. Here, we deal exclusively with such a theory, which also fits well with the Virtual Power framework introduced in the previous section at page 14.

Linear Elliptic Differential Equations usually come up from real world applications; the one of our interest is an outcome of the Linear Theory of Elasticity sketched in the previous Section. From the first of (2.9), the (2.13) and the hypothesis (2.15) we can easily find that the Linear Elasticity equations can be expressed by means of an elliptic differential operator. Moreover the second of the (2.9) introduce a condition must be fulfilled at the boundary of Ω.
In what follows, consistently with the Differential Equation literature, we consider the continuous body introduced in the Section as a suitable open set $\Omega \subset \mathbb{R}^3$. In addition we treat the force and displacement fields as maps $\mathbb{R}^3 \to \mathbb{R}^3$.
Under such hypothesis, the Linear Elasticity equations can be obtained incorporating the Eqn. (2.13) in the Eqn. (2.9):

$$\begin{cases} -\operatorname{div} \mathbb{C}[\nabla \mathbf{u}] & = \mathbf{b}, \qquad \text{in } \Omega, \\ \mathbb{C}[\nabla \mathbf{u}]\mathbf{n} & = \mathbf{f}, \qquad \text{on } \Gamma_N, \\ \mathbf{u} & = 0, \qquad \text{on } \Gamma_D. \end{cases} \tag{2.19}$$

where the boundaries $\Gamma_D, \Gamma_N \subset \partial\Omega$ are such that $\mathsf{in}(\Gamma_N) \cap \mathsf{in}(\Gamma_D) = \emptyset$, $\mathsf{cl}(\Gamma_N \cap \Gamma_D) = \partial\Omega$. A known traction is prescribed on Γ_N and a null displacement on Γ_D. These are the so called mixed Dirichlet–Neumann boundary conditions, usually general enough to treat a lot of cases of practical interest.
The variational form of (2.19), under the hypothesis of a linear elastic behavior, can be directly obtained from (2.8) and the (2.13):

$$\int_\Omega \mathbb{C}[\nabla \mathbf{u}] \cdot \nabla \mathbf{v} = \int_\Omega \mathbf{b} \cdot \mathbf{v} + \int_{\Gamma_N} \mathbf{c} \cdot \mathbf{v}, \tag{2.20}$$

for all suitable test fields $\mathbf{v} : \mathbb{R}^3 \to \mathbb{R}^3$. The problem (2.19) (or, equivalently (2.20)) has been studied in great detail, [21, 47]. Several results for well posedness and regularity are known and we resume here only the strictly needed ones for our purposes. The notion of solution we adopt here is the classical Hadamard one [62]; another mollified notion of solution will be introduced in the following. First of all, it holds:

Theorem 2.14. *(Lax–Milgram Lemma) Given the problem in* (2.20) *with* $\mathbf{b} \in L^2(\Omega)$, $\mathbf{c} \in L^2(\Gamma_N)$, Ω *a bounded open set with Lipschitz boundary and* $\Gamma_D \neq \emptyset$. *Let the coefficient* $\mathbb{C}$ *satisfy the conditions in* (2.15),(2.16). *Then, Eqn.* (2.20) *admits a unique solution in* $H^1_{0,\Gamma_D}(\Omega)$ *which depends continuously on the data.*

From here to the end of this work, we assume to work with a bounded, open domain Ω with smooth enough boundary $\partial\Omega$ (C^2-regularity is enough). The weak solution of an elliptic problem possesses remarkable regularity properties [21], [48]:

Theorem 2.15. *Let the problem (2.20) be given with* $\mathbf{b} \in L^2(\Omega)$, $\mathbf{c} \in H^{\frac{1}{2}}(\Gamma_N)$ *and let* Ω *be a bounded open set such that its boundary* $\partial\Omega$ *is* C^2-*regular. If* $\Gamma_D \neq \emptyset$ *and* $\Gamma_N = \emptyset$

or $\mathsf{cl}(\Gamma_N) \cap \mathsf{cl}(\Gamma_D) = \emptyset$ *then the solution* $\mathbf{u}$ *of* (2.20) *belongs to* $H^1_{0,\Gamma_D}(\Omega) \cap H^2(\Omega)$ *and depends continuously on the data.*

According to Theorems 2.6 and 2.15, the solution of an elliptic problem is continuous when the above hypothesis of regularity holds.
For reasons that will be clear in the following, we need to extend the above theory to the case of forcing terms of the linear elasticity operator that are Borel measures (i.e. elements of the dual space of C^0, see [61]). Following Casas [20], [18] the following theorem holds for the pure Dirichlet and pure Neumann cases, although a generalization to the mixed case is quite straightforward when Ω is sufficiently regular:

Theorem 2.16. *Let* Ω *a bounded open set such that its boundary* $\partial\Omega$ *is* C^2-*regular. Set* $s \in [1, \frac{n}{n-1})$ *and* s' *such that* $\frac{1}{s} + \frac{1}{s'} = 1$. *Then, the variational problem: find* $\mathbf{u} \in W^{1,s}(\Omega)$ *such that* $\forall \mathbf{v} \in W^{1,s'}(\Omega)$ *equation* (2.20) *holds, given* $\mathbf{b}$ *and* $\mathbf{c}$ *regular Borel measure, admits a unique solution which depends continuously on the data.*

2.3 Introduction to Inverse and Optimal Control Problems

In this Section we introduce the notion of *Inverse Problem*. Since inverse problems are often *ill posed* in the classical Hadamard sense, there is the need to introduce a weaker notion of solution for those problems. We then discuss briefly the *regularization* of an inverse problem, a mathematical technique that allows to obtain a sequence of solvable problems; the solutions of the latter is actually a sequence that may converge to the aforementioned mollified solution of the inverse problem at hand. A problem taken from such a regularization sequence happens to be solvable in practice borrowing techniques from the *Optimal Control Theory*.

2.3.1 Inverse Problems

To introduce the definition of an inverse problem, let me quote verbatim from the Introduction of [26]:

"When using the term *Inverse Problem*, one immediately is tempted to ask 'inverse to what?' Following J.B. Keller (*reference omitted*) one calls *two* problems *inverse to each other* if the formulation of one problem involves the other one. For mostly historic reasons one might call one of these problem (usually the simpler one or the one which was studied earlier) the *direct problem*, the other one the *inverse problem*. However, if there is a real world problem behind the mathematical problem studied, there is, in most cases, a quite natural distinction between the direct and the inverse problem. "

In the case of our interest, the physical feature which permit us to distinguish the direct (or forward) problem from the inverse one is the dicotomy *internal/external*, introduced in the first Section of this Chapter when writing the definitions (2.4) and (2.3) and the Axiom 2.2 at page 14. We thus call the problem in (2.19) *direct* (or *forward*) if *external* actions (the body force $\mathbf{b}$, the boundary conditions, possible constraints) are assumed to be known and the unknown field is the motion (equivalently, the displacement $\mathbf{u}$). Viceversa if some external fields are to be inferred (in our case will be the body force and/or the boundary traction) from some information on the motion map, we call such a problem the *inverse* one.

Now, we come back to more general issues. Let $\mathcal{M} : \mathsf{F} \to \mathsf{H}$ a linear operator between the Hilbert spaces F and H and consider, formally, the problem:

$$\text{find } \mathbf{f} \in \mathsf{F} \text{ such that } \mathcal{M}\mathbf{f} = \mathbf{h} \tag{2.21}$$

If the latter happens to be an inverse problem, it may fail in principle one or more Hadamard Well Posedness Conditions [62] [§] , as noted many time in practical applications [71]. For example, due to the noise always present in real world measurements, the data $\mathbf{h}$ can in principle not belong to the range of the operator $\mathcal{M}$ thus leading to the lack of existence of the solution. In addition, the data can perhaps be very few, so the operator $\mathcal{M}$ would fail to be injective. Eventually, the lack of stability usually happens not by faulty data, but for intrinsic irreversibility of physical processes (as a paradigmatic example, think at the Backward Heat Equation [26]).

[§] we may also say for brevity: it may be ill-posed.

2.3.2 Ill–Posed Problems

Ill–posed problems, which occur frequently in practice, call for a weakened notion of solution.

Definition 2.17. *We call* $\mathbf{f}_{BAS} \in \mathsf{F}$ *the* Best Approximation Solution *of* (2.21) *if:*

$$\mathbf{f}_{BAS} = \arg\min_{\mathsf{F}}\{\|\mathbf{g}\|_{\mathsf{F}} \text{ such that } \mathbf{g} = \arg\min_{\mathsf{F}} \left(\mathbf{n} \mapsto \|\mathcal{M}\mathbf{n} - \mathbf{h}\|^2_{\mathsf{H}}\right)\} \tag{2.22}$$

This definition naturally induces a weakened concept of the inverse map of $\mathcal{M}$, namely the *Moore Penrose Generalized Inverse*, usually indicated with $\mathcal{M}^\dagger$. Apart of its technical definition, we can recall its most interesting properties. From [26], we have:

Theorem 2.18. *The Moore–Penrose generalized inverse* $\mathcal{M}^\dagger$ *satisfies:*

$$\mathsf{dom}(\mathcal{M}^\dagger) := \mathsf{ran}\mathcal{M} + (\mathsf{ran}\mathcal{M})^\perp$$

moreover, it is continuous if and only if $\mathsf{ran}\mathcal{M}$ *is closed.*
Let $\mathbf{h} \in \mathsf{dom}(\mathcal{M}^\dagger)$*, then* $\mathcal{M}\mathbf{f} = \mathbf{h}$ *has the unique Best Approximation Solution* $\mathcal{M}^\dagger\mathbf{h}$*.*

For some problems, including the one discussed in this Part of the work, the Definition (2.22) is usually not suitable for a straightforward numerical implementation. Mainly to overcome this difficulty, a regularization technique has to be introduced. In this work we only consider the Tichonov regularization [26, 71]. The application of the aforementioned tool consists in approximating the Eq. (2.21) with the series of minimum problem:

$$\text{find } \mathbf{f}_\varepsilon \in \mathsf{F} \text{ such that } \mathcal{J}_\varepsilon(\mathbf{f}_\varepsilon) \leq \mathcal{J}_\varepsilon(\mathbf{g}) \ \forall \mathbf{g} \in \mathsf{F} \tag{2.23}$$

where $\mathcal{J}_\varepsilon(\mathbf{g}) := \frac{\varepsilon}{2}\|\mathbf{g}\|^2_{\mathsf{F}} + \frac{1}{2}\|\mathcal{M}\mathbf{g} - \mathbf{h}\|^2_{\mathsf{H}}$.
The convergence of the sequence of solutions of these regularized problems to the Best Approximation Solution as $\varepsilon \to 0$ is guaranteed under suitable hypothesis (see [26] for the details).
A still missing fundamental ingredient of our picture is the *noise* that can influence the data in our posses. Since the noise is unavoidable in real world measurements, it is unreasonable to take the coefficient ε as small as possible in practical computations since the theory sketched above does not encompass the presence of uncertain data (note that $\mathbf{h} \in \mathsf{H}$ is supposed to be exact in the discussion above). In fact, the convergence of the regularized solution to the Best Approximation Solution (as $\varepsilon \to 0$) is not guaranteed when the noise does not vanish. The question that arises now is how to choose an 'optimal' value of the parameter ε to get a reliable solution, extracting all the possible information from the given noisy data.
In the most general case, since the only information are the measurements $\mathbf{h}$ and possibly also an estimate of the noise level , say $\nu \in \mathbb{R}^+$, a *parameter choice rule* can be written (slightly abusing the notations) as a map $(\mathbf{h}, \nu) \mapsto \varepsilon(\mathbf{h}, \nu) : \mathsf{H} \times \mathbb{R}^+ \to \mathbb{R}^+$. The latter selects an optimal value of ε, in the sense sketched before, given the measurements and an estimate of the noise level [26].
A suitable theorem of convergence to the Best Approximation Solution, accounting for the presence of noise, could be obtained when considering the slightly simpler parameter choice rule $\nu \mapsto \varepsilon(\nu)$ [¶] (see [26]):

[¶] we stress that this parameter selection rule depends only on the estimate of noise level and not on the set of data $\mathbf{h}$

Theorem 2.19. *Set* $\mathbf{f}_\varepsilon^\nu$ *the solution of* (2.23) *when* ν *is the noise level (i.e.* $\|\mathbf{h}-\mathbf{h}^\diamondsuit\|_H \leq \nu$*, being* $\mathbf{h}^\diamondsuit \in \mathsf{ran}\mathcal{M}$ *the 'true' data whereas* $\mathbf{h}$ *are the measured ones). If:*

$$\lim_{\nu\to 0} \varepsilon(\nu) = 0 \text{ and } \lim_{\nu\to 0} \frac{\nu^2}{\varepsilon(\nu)} = 0$$

then:

$$\lim_{\nu\to 0} \mathbf{f}_{\varepsilon(\nu)}^\nu = \mathcal{M}^\dagger \mathbf{h}^\diamondsuit$$

To make things short, we cite only one parameter choice criterium, namely the L–Curve rule [26, 71]. This method states that an 'optimal' value of ε can be found at the corner of the presumed L-shaped curve

$$\|\mathbf{f}_\varepsilon\|_{\mathsf{F}} \mapsto \|\mathcal{M}\mathbf{f}_\varepsilon - \mathbf{h}\|_{\mathsf{H}}$$

having $\varepsilon > 0$ as a parameter. Following [71], the optimal ε_{opt} is the argument that minimizes the curvature of the aforementioned L–curve (thus, giving a precise meaning of corner). The curvature κ can be expressed, when using the Tichonov regularization shown in (2.23), as [71]:

$$\kappa(\varepsilon) := -\frac{R(\varepsilon)S(\varepsilon)(\varepsilon R(\varepsilon) + \varepsilon^2 S(\varepsilon)) + \frac{(R(\varepsilon)S(\varepsilon))^2}{S'(\varepsilon)}}{(R(\varepsilon)^2 + \varepsilon^2 S(\varepsilon)^2)^{3/2}} \tag{2.24}$$

where $S : \varepsilon \mapsto \|\mathbf{f}_\varepsilon\|_{\mathsf{F}}$ and $R : \varepsilon \mapsto \|\mathcal{M}\mathbf{f}_\varepsilon - \mathbf{h}\|_{\mathsf{H}}$.
It has been noted that sometimes the L–curve criterion may not satisfy the hypothesis on the parameter selection rule in the Theorem 2.19, see for example [71]. However, the L–curve strategy is very easy to implement and turns out to be very effective, at least in our application (see the Third Chapter of this Part).

2.3.3 Optimal Control Problems

The problem (2.23) (for fixed ε) is well known in the Optimal Control literature. The additional difficulty arising here is the fact that the operator $\mathcal{M}$ is not immediately evaluable. In fact, in Optimal Control as well as in the case we are going to present during this work, (2.23) usually comes from a constrained minimization problem, viz:

$$\begin{cases} \text{minimize } \mathcal{J} : (\mathbf{u}, \mathbf{g}) \mapsto \frac{\varepsilon}{2}\|\mathbf{g}\|_{\mathsf{F}}^2 + \frac{1}{2}\|\mathcal{O}\mathbf{u} - \mathbf{h}\|_{\mathsf{H}}^2 \\ \text{subjected to } \mathcal{A}\mathbf{u} = \mathbf{f} \end{cases}$$

where $\mathcal{O} : \mathsf{U} \to \mathsf{H}$ and $\mathcal{A} : \mathsf{U} \to \mathsf{F}$ are linear operators. Note that in this case we have $\mathcal{M} = \mathcal{O}\mathcal{A}^{-1}$.
Also, the terminology used in the Optimal Control literature refers to the field $\mathbf{f}$ as the *control* of the above set of equations. It is clear that, in general, the inversion of an infinite dimensional operator is not a trivial task. The problem above is usually solved introducing the adjoint state $\mathbf{p}$, formally defined as:

$$\mathcal{A}^T\mathbf{p} = \mathcal{O}^T(\mathcal{O}\mathbf{u} - \mathbf{h}).$$

Using the Euler equation for $\mathbf{g} \mapsto \mathcal{J} \circ (\mathcal{A}^{-1}\mathbf{g}, \mathbf{g}) : \mathsf{F} \to \mathbb{R}$ which writes

$$\varepsilon\mathbf{g} + \mathcal{A}^{-T}\mathcal{O}^T(\mathcal{O}\mathcal{A}^{-1}\mathbf{g} - \mathbf{h}) = 0,$$

and gluing together all the previous equations one finds the coupled set of functional equations:

$$\begin{cases} \mathcal{A}\mathbf{u} & = -\frac{1}{\varepsilon}\mathbf{p} \\ \mathcal{A}^T\mathbf{p} & = \mathcal{O}^T(\mathcal{O}\mathbf{u} - \mathbf{h}) \end{cases}$$

The above system of equations is usually solvable in practice, at least when $\mathcal{A}$ is a linear differential operator [40].

Chapter 3

Analytical Results

Force Traction Microscopy is an inversion method that allows to obtain the stress field applied by a living cell on the environment on the basis of a pointwise knowledge of the displacement produced by the cell itself. This classical biophysical problem, usually addressed in terms of Green functions, can be alternatively tackled using a variational framework and then a finite elements discretization. In such a case, a variation of the error functional under suitable regularization is operated in view of its minimization. This setting naturally suggests the introduction of a new equation, based on the adjoint operator of the elasticity problem. In this Chapter, we illustrate the rigorous theory of the two–dimensional and three dimensional problems, involving in the former case a distributed control and in the latter case a surface control. The pointwise observations require to exploit the theory of elasticity extended to forcing terms that are Borel measures.

3.1 General Issues

This Sections introduces the mathematical aspects of the Force Traction Microscopy problem. Here, we will see the previously introduced concepts and tools applied to our specific issues.

3.1.1 Forward Problem

The forward problem considered for our applications is the one of linear elasticity, introduced in the previous chapter in (2.19). In the following, we denote as $\mathbf{f} \in \mathsf{F}$ (F is a suitable Hilbert space) the so called control field (i.e. the right hand side of (2.20)):

$$\mathbf{f} := \mathbf{v} \mapsto \int_{\Omega} \mathbf{b} \cdot \mathbf{v} + \int_{\Gamma_N} \mathbf{c} \cdot \mathbf{v} \tag{3.1}$$

for all suitable test fields $\mathbf{v}$. We also denote by U the Hilbert space containing the displacement field $\mathbf{u}$.
The main definition of this section is:

Definition 3.1. *We define* Solution Operator $\mathcal{S} : \mathsf{F} \to \mathsf{U}$*, the map that, for a given control* $\mathbf{f}$ *on the right hand side of* (2.19) *or* (2.20) *(see the* (3.1) *above), assigns the*

displacement field $\mathbf{u}$ *that solves the problem. More specifically, we study the following two cases* [*] *:*

- *Distributed control:* $\mathcal{S}\mathbf{u} = \mathbf{b}$ *if (2.19) or (2.20) hold, with* $\mathbf{c} = 0$ *;*
- *Boundary Control:* $\mathcal{S}\mathbf{u} = \mathbf{c}$ *if (2.19) or (2.20) hold, with* $\mathbf{b} = 0$.

In this section we assume that F and U are tuned in such a way that [†]:

$$\mathcal{S} \in \mathsf{Lin}(\mathsf{F}, \mathsf{U}). \tag{3.2}$$

The rigorous proof of this fact is given in the following Sections.

3.1.2 The Inverse Problem

In this work, the term at the right hand side of equation (2.20) is to be interpreted as a control, so that the traction at the boundary $\mathbf{c}$ or the volume force $\mathbf{b}$ are formally an unknown of the problem. As declared above, such a control will be generically indicated as $\mathbf{f} \in \mathsf{F}$ according to the Eqn. (2.20).
We introduce below another operator that will turn useful for the applications to be discussed in the following.
In this work, in fact, we are interested in pointwise observation of the state. Typically, in cellular traction microscopy some beads are seeded into the elastic matrigel and their displacement is recorded during the motion of the cell. Mathematically, the observation operator is therefore defined as a list of Dirac Delta distributions [‡]:

Definition 3.2. *The* Observation Operator *is intended to be the map that assigns to a continuous field the list of the values that assumes at some given points* $\mathbf{x}_1, \dots, \mathbf{x}_N$*, i.e.:*

$$\mathcal{O} := (\delta_{\mathbf{x}_1}, \dots, \delta_{\mathbf{x}_N})$$

It can be easily shown that this operator is continuous in the functional spaces of our interest if $\Omega \subset \mathbb{R}^n$, $n \leq 3$. In fact (see [61]):

Proposition 3.3. $\mathcal{O}$ *is a linear and continuous form on* $C^0(\mathsf{cl}\Omega)$ *if* $\Omega \subset \mathbb{R}^n$ *(*$n = 1, 2, 3$*).*

Under suitable regularity of the control $\mathbf{f}$, in the following section we will prove that

$$\mathcal{O} \in \mathsf{Lin}(\mathsf{U}, \mathbb{R}^{Nn}). \tag{3.3}$$

Let also:

⋆ $\mathsf{F}_{\mathrm{adm}}$ be the admissible force space, a closed subspace of F;

⋆ $\mathsf{X} := \mathbb{R}^{Nn}$, where N is the number of beads and $n \leq 3$ as before (we denote with the bullet $\bullet$ the scalar product in X);

⋆ $u_0 = (\mathbf{u}_0^1, \dots, \mathbf{u}_0^N) \in \mathsf{X}$ is the list of the measured displacements, supposed known;

[*] For simplicity, we restrict ourselves in the case where only the control appears as a forcing term. The more general case in which the forces in (2.19) or in (2.20) are sum of known fields and the control is analogous but technically more cumbersome, since the solution operator $\mathcal{S}$ is affine (see [40]).

[†] We recall that $\mathsf{Lin}(\mathsf{U}, \mathcal{V})$ is the space of linear and continuous functional from U to $\mathcal{V}$.

[‡] a Dirac Delta distribution is a linear form $\delta_{\mathbf{x}} : \mathsf{Lin}(C^0(\mathsf{cl}\Omega, \mathcal{V}), \mathcal{V})$ such that $\delta_{\mathbf{x}}\mathbf{u} = \mathbf{u}(\mathbf{x})$.

Since we want to use the tool presented above as an Inverse method rather than an Optimal Control one, it is worthwhile to recall some basic definition and properties of Inverse and Ill–Posed problems and their regularization. As a basic reference for this matter one can consider [26] an the brief introduction given in the previous chapter. Here the discussion is taken at a minimum level of complexity and, hence, of rigor. Let us focus on our basic problem, i.e. find the force producing exactly the displacement measured which writes in formulas (cfr. with (2.21)):

$$\text{find } \mathbf{f} \in \mathsf{F}_{\text{adm}} \text{ such that } \mathcal{OS}\mathbf{f} = u_0. \tag{3.4}$$

Since it is not guaranteed the existence (since the data u_0 can be affected by noise) and the uniqueness (since $\mathcal{O}$ maps an infinite dimensional space into a finite one, i.e. data are few) of the solution of the problem above, it is convenient to deal with the mollified notion of solution introduced in Section 2.3. Since the range of the operator $\mathcal{OS}$ ($\mathsf{ran}(\mathcal{OS})$) is a subspace of $\mathbb{R}^{3N}$ we can apply the the Theorem 2.18 to state:

Proposition 3.4. *The $\mathbf{f}_{BAS}$, as defined above, exists unique and the operator $(\mathcal{OS})^\dagger$ is continuous.*

3.1.3 Regularization and Optimal Control Strategy

We now discuss the regularization of the problem in (3.4) giving the convergence results and discussing the its solvability properties.

Penalty Functional

Following Chapter 2, we introduce the Tichonov Regularization of the problem in (3.4) fixing the penalization parameter $\varepsilon > 0$. We introduce a definition analogous the one given in the Eqn. (2.23) [§]:

Definition 3.5. *The penalty functional $\mathcal{J} : \mathsf{F} \to \mathbb{R}^+$ is defined as:*

$$\mathcal{J}(\mathbf{g}) = \frac{1}{2}\|\mathcal{OS}\mathbf{g} - u_0\|^2_{\mathsf{X}} + \frac{\varepsilon}{2}\|\mathbf{g}\|^2_{\mathsf{F}}. \tag{3.5}$$

Our goal is to minimize the functional $\mathcal{J}$ on F_{adm}. If the forward problem (2.19) has the properties stated in the previous section, the existence and uniqueness of a global minimum for the functional $\mathcal{J}$ above can be readily obtained. We first state (see [40]):

Proposition 3.6. *The penalty functional $\mathcal{J}$ in (3.5) is coercive and convex. Moreover, if* (3.2) *and* (3.3) *hold, it is also continuous.*

Proof.
After some manipulations, we can rewrite the penalty functional as follows:

$$\mathcal{J}(\mathbf{g}) = \frac{\varepsilon}{2}\|\mathbf{g}\|^2_{\mathsf{F}} + \frac{1}{2}\|\mathcal{OS}\mathbf{g}\|^2_{\mathsf{X}} - \mathcal{OS}\mathbf{g} \bullet u_0 + \frac{1}{2}\|u_0\|^2_{\mathsf{X}},$$

⋆ $\mathcal{J}$ is *convex*: it is obvious since it is quadratic;

⋆ $\mathcal{J}$ is *coercive*: $2\mathcal{J}(\mathbf{g}) \geq \varepsilon\|\mathbf{g}\|^2_{\mathsf{F}} - 2\mathcal{OS}\mathbf{f} \bullet u_0 \to \infty$ if $\|\mathbf{g}\|_{\mathsf{F}} \to \infty$ since ε is fixed positive;

[§] We drop the subscript ε on $\mathcal{J}$ in order to have lighter notations.

⋆ $\mathcal{J}$ is *continuous*: given $\mathbf{f}$, $\mathbf{g}$ in F

$$\begin{aligned}
|\mathcal{J}(\mathbf{g}) - \mathcal{J}(\mathbf{f})| &= \frac{\varepsilon}{2}(\|\mathbf{g}\|_{\mathsf{F}}^2 - \|\mathbf{f}\|_{\mathsf{F}}^2) + \frac{1}{2}(\|\mathcal{OS}\mathbf{g}\|_{\mathsf{X}}^2 - \|\mathcal{OS}\mathbf{f}\|_{\mathsf{X}}^2) - u_0 \bullet \mathcal{OS}[\mathbf{g} - \mathbf{f}], \\
&= \frac{\varepsilon}{2}(\|\mathbf{g}\|_{\mathsf{F}} + \|\mathbf{f}\|_{\mathsf{F}})\Big|\|\mathbf{g}\|_{\mathsf{F}} - \|\mathbf{f}\|_{\mathsf{F}}\Big| + \\
&\quad + \frac{1}{2}\left(\|\mathcal{OS}\mathbf{g}\|_{\mathsf{X}} + \|\mathcal{OS}\mathbf{f}\|_{\mathsf{X}}\right)\Big|\|\mathcal{OS}\mathbf{g}\|_{\mathsf{X}} - \|\mathcal{OS}\mathbf{f}\|_{\mathsf{X}}\Big| + \\
&\quad - u_0 \bullet \mathcal{OS}(\mathbf{g} - \mathbf{f}), \\
&\leq \frac{1}{2}\Big[\left(\varepsilon + \|\mathcal{O}\|_{\mathsf{Lin}(\mathsf{U},\mathsf{X})}\|\mathcal{S}\|_{\mathsf{Lin}(\mathsf{F},\mathsf{U})}\right)\left(1 + \|\mathcal{O}\|_{\mathsf{Lin}(\mathsf{U},\mathsf{X})}\|\mathcal{S}\|_{\mathsf{Lin}(\mathsf{F},\mathsf{U})}\right)(\|\mathbf{g}\|_{\mathsf{F}} + \|\mathbf{f}\|_{\mathsf{F}}) + \\
&\quad + 2\|u_0\|_X\|\mathcal{O}\|_{\mathsf{Lin}(\mathsf{U},\mathsf{X})}\|\mathcal{S}\|_{\mathsf{Lin}(\mathsf{F},\mathsf{U})}\Big]\|\mathbf{g} - \mathbf{f}\|_{\mathsf{F}},
\end{aligned}$$

where we have used continuity of the norms and the hypothesis on $\mathcal{O}$ and $\mathcal{S}$ (Eqs. (3.2), (3.3)).

□

According to the Theorem 2.9 of the previous Chapter a unique minimum point of $\mathcal{J}$ exists, say $\mathbf{f}$. Now we can characterize it using the Euler equation associated to $\mathcal{J}$. We must show that:

Proposition 3.7. *If* (3.2) *and* (3.3) *hold, then* $\mathcal{J}$ *is differentiable.*

Proof.
The proof is a direct calculation of the functional derivative $\mathcal{J}' : \mathsf{F} \to \mathsf{F}^*$. Set $o(\mathbf{h})$ any function such that $\lim_{\|\mathbf{h}\|_{\mathsf{F}} \to 0} \dfrac{o(\mathbf{h})}{\|\mathbf{h}\|_{\mathsf{F}}} = 0$. Then it holds

$$\begin{aligned}
\mathcal{J}'(\mathbf{g})[\mathbf{h}] + o(\mathbf{h}) &= \mathcal{J}(\mathbf{g} + \mathbf{h}) - \mathcal{J}(\mathbf{g}) \\
&= \varepsilon\left((\mathbf{g}|\mathbf{h})_{\mathsf{F}} + \frac{1}{2}(\mathbf{h}|\mathbf{h})_{\mathsf{F}}\right) + \mathcal{OS}\mathbf{g} \bullet \mathcal{OS}\mathbf{h} - u_0 \bullet \mathcal{OS}\mathbf{h} + \frac{1}{2}\mathcal{OS}\mathbf{h} \bullet \mathcal{OS}\mathbf{h} \\
&= \varepsilon(\mathbf{g}|\mathbf{h})_{\mathsf{F}} + (\mathcal{OS}\mathbf{g} - u_0) \bullet \mathcal{OS}\mathbf{h} + o(\mathbf{h}),
\end{aligned}$$

since $\mathcal{OS}$ is continuous we have $\mathcal{OS}\mathbf{h} \bullet \mathcal{OS}\mathbf{h} = o(\mathbf{h})$ and the result follows.

□

Remarkably, the theorem above gives:

$$\mathcal{J}'(\mathbf{g})[\mathbf{h}] = \varepsilon(\mathbf{g}|\mathbf{h})_{\mathsf{F}} + (\mathcal{OS}\mathbf{g} - u_0) \bullet \mathcal{OS}\mathbf{h} \tag{3.6}$$

The following statement resumes the results obtained in this section. From Theorem 2.9 and 2.11 of Chapter 2 we have:

Proposition 3.8. *Let* F *be an Hilbert space,* $\mathcal{J} : \mathsf{F}_{\mathrm{adm}} \subset \mathsf{F} \to \mathbb{R}^+$ *defined as in* (3.5) *and* $\mathsf{F}_{\mathrm{adm}}$ *being a closed subspace of* F. *Let the hypothesis* (3.2), (3.3) *on* $\mathcal{S}$ *and* $\mathcal{O}$ *hold. Then, a unique minimum point of* $\mathcal{J}$ *exists, say* $\mathbf{f} \in \mathsf{F}_{\mathrm{adm}}$ *and it solves:*

$$\mathcal{P}\mathcal{J}'(\mathbf{f}) = 0.$$

where $\mathcal{P} \in \mathsf{LinF}$ *is the projection onto* $\mathsf{F}_{\mathrm{adm}}$.

Applying the Tichonov regularization procedure to the operator $(\mathcal{OS})^\dagger$ we end up with the minimum problem for the family, with respect to the parameter ε, of penalty functional in (3.5). Actually, the Theorem 2.19 confirms us that:

Proposition 3.9. *If the noise level ν tends to 0 and the parameter choice rule $\nu \mapsto \varepsilon(\nu)$ satisfies the hypothesis of Theorem 2.19, the sequence of minimum of $\mathcal{J}$ strongly converges to $\mathbf{f}_{BAS}$.*

Adjoint State

Since the functional $\mathcal{J}$ admits a unique global minimum in a closed subspace $\mathsf{F}_{\text{adm}} \subset \mathsf{F}$ and it is differentiable, from (3.6) and the Proposition 3.8 it follows that the minimum control $\mathbf{f} \in \mathsf{F}_{\text{adm}}$ satisfies

$$\mathcal{P}\mathcal{J}'(\mathbf{f}) = 0 \;\Leftrightarrow\; \varepsilon\mathbf{f} + \mathcal{P}(\mathcal{OS})^T(\mathcal{OS}\mathbf{f} - u_0) = 0, \tag{3.7}$$

where $\mathcal{P} \in \mathsf{LinF}$ is the projection onto F_{adm}.
To avoid the evaluation of the operator $\mathcal{S}$ in equation (3.7), we introduce the so called adjoint state [40]. The proof of well posedness of the following problem will be given in the following sections for the specific contexts. Let $\mathbf{p} \in \mathsf{P}$ be formally defined as:

$$\mathcal{A}^T\mathbf{p} = \mathcal{O}^T(\mathcal{O}\mathbf{u} - u_0), \tag{3.8}$$

where P is a suitable functional space and $\mathcal{A}^T : \mathsf{P} \to \mathsf{U}^*$ an operator to be assigned. Roughly speaking, $\mathcal{A}$ should be taken such that the operator $\mathcal{SA}$ will be easy to handle. For example, in Section 2, we will find that $\mathcal{SA}$ is the identity map. Differently to most of the literature on the subject (e.g. [40]), we strictly need to make a distinction between $\mathcal{A}$ and $\mathcal{S}^{-1}$ as we shall see in Section 3. Now, plugging Equation (3.8) into (3.7), we obtain:

$$\varepsilon\mathbf{f} + \mathcal{P}\mathcal{S}^T\mathcal{A}^T\mathbf{p} = 0. \tag{3.9}$$

The choice of the operator $\mathcal{A}$ and the analysis of its continuity property is the main goal of the paper. We deal with this issue in the following section, discussing the control of Dirichlet and Neumann problems.

3.2 The Dirichlet Problem with Distributed Control

In this section we introduce and analyse an inverse problem which arises in cellular traction microscopy on flat substrates. We provide well–posedness results for the problem formally stated in [2], [3] in the plane. Results still hold for a Dirichlet problem in $\mathbb{R}^3$ with almost no modifications.

3.2.1 Forward Problem

Let $\Omega \subset \mathbb{R}^2$ be a regular set, where the Dirichlet problem of Linear Elasticity applies. For this section we consider $\Gamma_D = \partial\Omega$, $\mathsf{F} = L^2(\Omega)$, $\mathsf{U} = H^2(\Omega) \cap H^1_0(\Omega)$, $\mathbf{c} = 0$ and $\mathbf{b} := \mathbf{f}$. The problem (2.19) or (2.20) with the above hypothesis reads:

$$\text{given } \mathbf{f} \in L^2(\Omega), \text{ find } \mathbf{u} \in H^2 \cap H^1_0(\Omega) \text{ s.t. } \forall \mathbf{v} \in H^1_0(\Omega):$$

$$\int_\Omega \nabla\mathbf{u} \cdot \mathbb{C}[\nabla\mathbf{v}] = \int_\Omega \mathbf{f} \cdot \mathbf{v}. \tag{3.10}$$

According to the notation introduced in the previous section, if $\mathbf{u}$ and $\mathbf{f}$ satisfy (3.10), then we say that $\mathcal{S}\mathbf{f} = \mathbf{u}$. If $\mathbf{f} \in L^2(\Omega)$ is known, the problem (3.10) is well–posed from Theorem 2.14 and, thanks to Theorem 2.15, its solution satisfies:

$$\|\mathcal{S}\mathbf{f}\|_{H^2(\Omega)} \leq k\|\mathbf{f}\|_{L^2(\Omega)}, \quad k > 0, \tag{3.11}$$

which is the continuity estimate requested in (3.2) for the solution operator.

Admissible Force Space

Let $\Omega_c \subset \Omega$ be the Lebesgue–measurable set where the cell lays and $\mathbf{f} \in \mathsf{F} = L^2(\Omega)$ the force density per unit surface exerted by the cell. Since neither external forces nor constraints apply on the cell and inertia is negligible, we can argue that its force field $\mathbf{f}$ must have null average and null average momentum, so that it belongs to [¶]:

$$\mathsf{F}_{\text{adm}} := \left\{ \mathbf{g} \in \mathsf{F} = L^2(\Omega) \middle| \int_{\Omega_c} \mathbf{f} = 0, \ \int_{\Omega_c} \mathbf{r} \times \mathbf{f} = 0, \ \mathbf{f} = 0 \text{ a.e. on } \Omega \setminus \Omega_c \right\}. \tag{3.12}$$

We can easily prove the following characterization of F_{adm}.

Proposition 3.10. F_{adm}, *as defined in* (3.12), *is a closed subspace of* F.

Proof.

- F_{adm} has the structure of a linear space.
- Since Ω has finite measure, $L^2(\Omega) \hookrightarrow L^1(\Omega)$ (via Hölder inequality, Theorem 2.4) and therefore the forms $\mathbf{f} \mapsto \int_\Omega \mathbf{f}$ and $\mathbf{f} \mapsto \int_\Omega \mathbf{r} \times \mathbf{f}$ are continuous in $L^2(\Omega)$.

[¶]To define the wedge product in $\mathbb{R}^2$, we proceed in this way. Fix $\mathbf{J} \in \mathsf{Skw}(\mathbb{R}^2) \cap \mathsf{Ort}(\mathbb{R}^2)$ one among the two perpendicular turn in $\mathbb{R}^2$ [51]. Define: $\mathbf{h} \times \mathbf{g} = \mathbf{J}\mathbf{h} \cdot \mathbf{g}$ for all vectors $\mathbf{g}$,$\mathbf{h}$ of $\mathbb{R}^2$.
Moreover we have defined $\mathbf{r}(\mathbf{x}) := \mathbf{x} - \mathbf{o}$ where $\mathbf{o} \in \mathbb{R}^3$ is a given point.

- Eventually, set $(\mathbf{f}_n)_{n=1}^{\infty} \subset \mathsf{F}_{\mathrm{adm}}$ such that: $\mathbf{f}_n \to \mathbf{f} \in \mathsf{F}$, $\mathbf{f}_n \neq 0$ on $\Xi_n \subset \Omega \setminus \Omega_c$ and $\mathsf{meas}(\Xi_n) = 0$ for all $n \in \mathbb{N}$, where the symbol meas indicates the Lebesgue measure of a set. Then, by continuity of measures, $\mathsf{meas}(\cup_{n\in\mathbb{N}}\Xi_n) \leq \Sigma_{n\in\mathbb{N}}\mathsf{meas}(\Xi_n) = 0$; this means that the limit function $\mathbf{f}$ equals to 0 almost everywhere in $\Omega \setminus \Omega_c$.

□

3.2.2 Optimal Control

Penalty Functional

Our goal is to determine $\mathbf{f}$ minimizing the penalty functional in (3.5) and belonging to a closed subspace $\mathsf{F}_{\mathrm{adm}} \subset \mathsf{F}$. In the previous sections, we have proved (see inequality (3.11)) that the suitable choice of U and F done at the beginning of this section yields a continuous solution operator $\mathcal{S}$ (i.e. satisfying (3.2)). Since the solution $\mathbf{u}$ belongs to $H^2(\Omega)$, the observation map $\mathcal{O}$ is also continuous. In fact, by the Sobolev Theorem 2.6, $H^2(\Omega) \hookrightarrow C^0(\mathsf{cl}\Omega)$ when $n = 2, 3$ and, thanks to Proposition 3.3, the condition (3.3) is clearly satisfied. We can then apply Theorem 3.8 and find that, in this case, our functional $\mathcal{J}$ admits a unique minimum point and it is differentiable therein.

Adjoint State

In this section we explicitly assign the operator $\mathcal{A}$ appearing, in abstract form, in equation (3.8) and we prove some of its properties. Taking $\mathcal{A} = \mathcal{S}^{-1}$, we argue that Problem (3.8) rewrites as follows (cfr. with [19]): [‖]:

$$\text{find } \mathbf{p} \in W_0^{1,s}(\Omega) \text{ s.t. } \forall \mathbf{q} \in W_0^{1,s'}(\Omega):$$

$$\int_\Omega \nabla\mathbf{p} \cdot \mathbb{C}[\nabla\mathbf{q}] = (\mathcal{O}\mathbf{u} - u_0) \bullet \mathcal{O}\mathbf{q}. \tag{3.13}$$

The next step is to prove the well–posedness of the above equation.

Proposition 3.11. *The problem in* (3.13) *is well–posed when* $s \in [1, \frac{n}{n-1})$, s' *is conjugate to* s, Ω *is a bounded domain with* C^2-*boundary and* $n = 2, 3$.

Proof:
As a consequence of the Prop. 3.3, $\mathcal{O}^T(\mathcal{O}\mathbf{u} - u_0)$ is a Borel measure (having fixed $\mathbf{u} \in H^1_{0,\Gamma_D}(\Omega) \cap H^2(\Omega) \hookrightarrow C^0(\mathsf{cl}\Omega)$ as noted before).
We also observe that, by Sobolev embedding Theorem:

$$\mathbf{q} \in W^{1,s'}(\Omega) \hookrightarrow C^0(\mathsf{cl}\Omega) \text{ if } s' > n \Leftrightarrow s \in \Big[1, \frac{n}{n-1}\Big).$$

Then, we can apply Theorem 2.16 with $s \in [1, \frac{n}{n-1})$ and $n = 2, 3$ to prove the thesis.

□

Using Sobolev embedding Theorem 2.6 it can be proved that:

$$\mathbf{p} \in W^{1,s}(\Omega) \hookrightarrow L^2(\Omega) \text{ if } s \geq \frac{2n}{n+2} \Leftrightarrow s' \in \Big[1, \frac{2n}{n-2}\Big).$$

[‖] $W_0^{1,s}(\Omega)$ is the subspace of $W^{1,s}(\Omega)$ of functions having zero trace on $\partial\Omega$, see [49] and [1].

Moreover, let $\mathbf{q} = \mathcal{S}\mathbf{h}$ ($\mathbf{h} \in L^2(\Omega)$): one has from (3.11) that $\mathbf{q} \in H^2(\Omega) \cap H_0^1$.
Using again the Sobolev embedding Theorem 2.6, one has:

$$H^2(\Omega) \hookrightarrow W^{1,s'}(\Omega) \text{ if } s' \in \left[1, \frac{2n}{n-2}\right] \Leftrightarrow s \geq \frac{2n}{n+2}.$$

Collecting the latter results, the following equation is thus well defined granted $s \in \left[\frac{2n}{n+2}, \frac{n}{n-1}\right)$:

$$\int_\Omega \nabla \mathbf{p} \cdot \mathbb{C}[\nabla \mathcal{S}\mathbf{h}] = \int_\Omega \mathbf{h} \cdot \mathbf{p}.$$

We observe that the equality above follows from the definition of $\mathcal{S}$ (as in the forward problem (3.10)) and the symmetry of $\mathbb{C}$ (see Eq. (2.16)).

Characterization of the optimal control

The optimal control $\mathbf{f}$ satisfies, as stated in (3.9), $\mathbf{f} = -\frac{1}{\varepsilon}\mathcal{P}\mathbf{p}$. We now wish to characterize the projection operator $\mathcal{P} : \mathsf{F} \to \mathsf{F}_{\mathrm{adm}} \subset \mathsf{F}$. Equation (3.9) here takes the following meaning:

$$(\varepsilon \mathbf{f} + \mathbf{p}|\mathbf{h})_{L^2(\Omega)} = 0, \qquad \forall \mathbf{h} \in \mathsf{F}_{\mathrm{adm}}. \tag{3.14}$$

Since any test function $\mathbf{h}$ is equal to zero in measure on $\Omega \setminus \Omega_c$, equation (3.14) reduces to:

$$\varepsilon(\mathbf{f}|\mathbf{h})_{L^2(\Omega_c)} + (\mathbf{p}|\mathbf{h})_{L^2(\Omega_c)} = 0, \qquad \forall \mathbf{h} \in \mathsf{F}_{\mathrm{adm}c}, \tag{3.15}$$

where $\mathsf{F}_{\mathrm{adm}c} := \{L^2(\Omega_c) | \int_{\Omega_c} \mathbf{f} = 0, \int_{\Omega_c} \mathbf{r} \times \mathbf{f} = 0\}$.
Then $\mathbf{f} = -\frac{1}{\varepsilon}\chi_c \mathbf{p} + \mathbf{f}^\perp$, where $\mathbf{f}^\perp \in \mathsf{F}_{\mathrm{adm}c}^{\ \perp}$ and χ_c is the characteristic function of Ω_c.
To determine $\mathbf{f}^\perp$ we note that (from the Theorem on the dimension of range and kernel [51]):

Theorem 3.12. *Let $\mathcal{H} \in \mathsf{Lin}(\mathsf{Y}, \mathbb{R}^n)$, Y a (possibly infinite dimensional) Hilbert space, $n \in \mathbb{N}$. Then $\mathsf{dim}(\mathsf{ker}\mathcal{H})^\perp \leq n$.*

In $\mathbb{R}^2$, if we set $\mathcal{H} = \left[\mathbf{f} \in L^2(\Omega_c) \mapsto \left(\int_{\Omega_c} \mathbf{f}, \int_{\Omega_c} \mathbf{r} \times \mathbf{f}\right) \in \mathbb{R}^3\right]$, then we have $\mathsf{dim}\mathsf{F}_{\mathrm{adm}c}^{\ \perp} \leq 3$. Moreover one can readily find a 3−dimensional basis, say $\{\mathbf{e}_i\}_{i=1}^3$ for this space. Set $\{\mathbf{e}_1, \mathbf{e}_2\}$ as two constant, linearly independent–valued mappings. Obviously, if $\mathbf{h} \in \mathsf{F}_{\mathrm{adm}c}$:

$$(\mathbf{e}_i|\mathbf{h})_{L^2(\Omega_c)} = \int_{\Omega_c} \mathbf{e}_i \cdot \mathbf{h} = \mathbf{e}_i \cdot \int_{\Omega_c} \mathbf{h} = 0,$$

for $i = 1, 2$. Evidently $\{\mathbf{e}_1, \mathbf{e}_2\} \subset \mathsf{F}_{\mathrm{adm}c}^{\ \perp}$. Next, let $\mathbf{J} \in \mathsf{Skw}(\mathbb{R}^2) \cap \mathsf{Ort}(\mathbb{R}^2)$ the chosen perpendicular turn in $\mathbb{R}^2$, as in footnote ¶ (the same calculation in $\mathbb{R}^3$ would require a slightly different technique). Choose $\mathbf{e}_3(\mathbf{x}) = \mathbf{J}\mathbf{x}$, then:

$$(\mathbf{e}_3|\mathbf{h})_{L^2(\Omega_c)} = (\mathbf{J}\mathbf{r}|\mathbf{h})_{L^2(\Omega_c)} = \int_{\Omega_c} \mathbf{J}\mathbf{r} \cdot \mathbf{h} = \int_{\Omega_c} \mathbf{r} \times \mathbf{h} = 0.$$

Eventually, given $\{\mathbf{e}_i\}_{i=1}^3$ as above, $\mathbf{f} \in \mathsf{F}_{\mathrm{adm}}$ turns out to be:

$$\mathbf{f} = -\frac{1}{\varepsilon}\chi_c \mathbf{p} + \sum_{i=1}^{3} l_i \mathbf{e}_i, \tag{3.16}$$

where $(l_i)_{i=1}^3 \in \mathbb{R}^3$ are the Lagrangian multiplier associated to the constraint of null net force and torque (see the definition of $\mathsf{F}_{\mathrm{adm}c}$ above) and so they are unknowns of the problems.

3.2.3 System of equations

Below we resume the results of the present section, pointing out the system of differential equations, in weak form, that one may want to solve in practice.

$$\text{find } \mathbf{u} \in H^2(\Omega) \cap H_0^1(\Omega),\ \mathbf{p} \in W_0^{1,s}(\Omega),\ (l_i)_{i=1}^3 \in \mathbb{R}^3,\ s \in [\tfrac{2n}{n+2}, \tfrac{n}{n-1})$$
$$\text{such that } \forall \mathbf{q} \in W_0^{1,s'}(\Omega),\ \forall \mathbf{v} \in H_0^1(\Omega):$$

$$\begin{cases} \displaystyle\int_\Omega \mathbb{C}\nabla\mathbf{u} \cdot \nabla\mathbf{v} + \int_\Omega \mathbf{f} \cdot \mathbf{v} & = 0, \\ \displaystyle\int_\Omega \mathbb{C}\nabla\mathbf{p} \cdot \nabla\mathbf{q} + \sum_{j=1}^N \delta_{\mathbf{x}_j}\mathbf{u} \cdot \delta_{\mathbf{x}_j}\mathbf{q} & = \displaystyle\sum_{j=1}^N u_{0_j} \cdot \delta_{\mathbf{x}_j}\mathbf{q}, \\ \mathbf{f} + \dfrac{1}{\varepsilon}\mathbf{p} - \displaystyle\sum_{i=1}^3 l_i \mathbf{e}_i & = 0, \\ \displaystyle\int_\Omega \mathbf{f} & = 0, \\ \displaystyle\int_\Omega \mathbf{r} \times \mathbf{f} & = 0. \end{cases} \tag{3.17}$$

3.3 Boundary Control with Neumann or Mixed Conditions

While traction force microscopy on flat surfaces is nowadays a well established technique for cells moving on flat surfaces, the challenging goal is currently to obtain a good reconstruction of the stress exerted by a cell in its physiological three dimensional migration environment. In a typical experimental setup, a cell is immersed in a matrigel box as in Fig. 3.1 and exerts a stress on the inner boundary of the gel, the traction at the inner surface plays here the role of the unknown of the problem. Homogeneous Dirichlet or Neumann conditions can be considered for the outer boundary, i.e. the walls of the box..

3.3.1 Forward Problem

Let $\Omega \subset \mathbb{R}^3$ be an open bounded domain with C^2-regular border, as in fig.3.1. The boundary conditions characterize a mixed problem in Linear Elasticity and, in this section, we consider $\mathsf{U} = H^1_{0,\Gamma_D}(\Omega) \cap H^2(\Omega)$, $\mathsf{F} = H^{\frac{1}{2}}(\Gamma_N)$, $\mathbf{c} := \mathbf{f}$ and $\mathbf{b} = 0$. The forward problem (2.19) or (2.20) now reads:

given $\mathbf{f} \in H^{\frac{1}{2}}(\Gamma_N)$, find $\mathbf{u} \in H^1_{0,\Gamma_D}(\Omega) \cap H^2(\Omega)$ such that for all $\mathbf{v} \in H^1_{0,\Gamma_D}(\Omega)$:

$$\int_\Omega \nabla \mathbf{u} \cdot \mathbb{C}[\nabla \mathbf{v}] = \int_{\Gamma_N} \mathbf{f} \cdot \mathbf{v}. \tag{3.18}$$

The above problem admits a unique solution in $H^1(\Omega)$ thanks to the Lax–Milgram lemma (Theorem 2.14). If we consider the setup as in fig.3.1, where $\Gamma_D \neq \emptyset$ and $\mathsf{cl}(\Gamma_N) \cap \mathsf{cl}(\Gamma_D) = \emptyset$, we can apply the Theorem 2.15 to obtain the estimate:

$$\|\mathcal{S}\mathbf{f}\|_{H^2(\Omega)} \leq k \|\mathbf{f}\|_{H^{\frac{1}{2}}(\Gamma_N)}, \qquad k > 0, \tag{3.19}$$

where $\mathcal{S}\mathbf{f} = \mathbf{u}$ if (3.18) is satisfied. For a pure Neumann problem ($\Gamma_N = \partial\Omega$), the same results hold, but the solution $\mathbf{u}$ is unique up to a rigid motion (see [21]).

Admissible Force Space

As in the case of distributed control of the previous section, since neither force nor constraint act on the cell, we define the admissible force space as:

$$\mathsf{F}_{\text{adm}} := \left\{ \mathbf{g} \in \mathsf{F} = H^{\frac{1}{2}}(\Gamma_N) \middle| \int_{\Gamma_N} \mathbf{f} = 0, \ \int_{\Gamma_N} \mathbf{r} \times \mathbf{f} = 0 \right\}. \tag{3.20}$$

This is a closed subspace of $L^2(\Gamma_N)$ and therefore also of $\mathsf{F} = H^{\frac{1}{2}}(\Gamma_N)$ since $H^{\frac{1}{2}}(\Gamma_N) \hookrightarrow L^2(\Gamma_N)$, the proof being the same as the one given in the previous section (it is sufficient to exchange Ω with Γ_N, noting that also Γ_N has a finite measure).

3.3.2 Optimal Control

Penalty Functional

We search for $\mathbf{f} \in \mathsf{F}_{\text{adm}}$ which minimizes the functional in (3.5). The discussion below is very similar to the one in the previous Section and some details are omitted.
We have proved in (3.19) that the choice of U, F done in this section provides a continuous solution operator $\mathcal{S}$. Since the solution $\mathbf{u}$ belongs to $H^2(\Omega)$ also the observation map

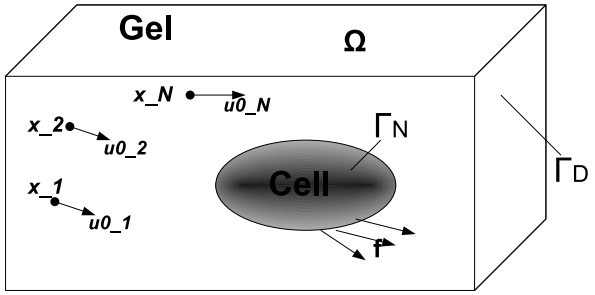

Figure 3.1: A pictorial representation of the experimental setup: the outer boundary of the domain Ω is Γ_D, the inner boundary is Γ_N where the traction of the cell applies.

$\mathcal{O}$ is continuous. In fact, by Sobolev Theorem 2.6, $H^2(\Omega) \hookrightarrow C^0(\mathsf{cl}\Omega)$ when $n = 2, 3$ and, thanks to Proposition 3.3, (3.3) is clearly satisfied. We can then apply Theorem 3.8 to see that in this case our functional $\mathcal{J}$ admits a unique minimum point and it is differentiable therein.

Adjoint State

In the following, we explicitly characterize the operator $\mathcal{A}$ that appears in (3.8) and prove some of its properties. In this case $\mathcal{A} \neq \mathcal{S}^{-1}$, in fact we state the following counterpart of (3.8) (cfr. with [20]):

$$\text{find } \mathbf{p} \in W^{1,s}_{0,\Gamma_D}(\Omega) \text{ s.t. } \forall \mathbf{q} \in W^{1,s'}_{0,\Gamma_D}(\Omega):$$

$$\int_\Omega \nabla \mathbf{p} \cdot \mathbb{C}[\nabla \mathbf{q}] = (\mathcal{O}\mathbf{u} - u_0) \bullet \mathcal{O}\mathbf{q}. \tag{3.21}$$

We now state the well posedness of the above equation, the proof being identical to the one of the Prop. 3.11.

Proposition 3.13. *The problem in* (3.21) *is well posed when* $s \in [1, \frac{n}{n-1})$, s' *is conjugate to* s, Ω *is a bounded domain with* C^2-*boundary and* $n \leq 3$.

It happens that $\mathcal{T}_{\Gamma_N}\mathbf{p} \in L^s(\Gamma_N)$ because from the Trace Theorem 2.5 :

$$W^{1,s}(\Omega) \hookrightarrow L^s(\partial\Omega) \text{ if } s < n.$$

Moreover, let $\mathbf{q} = \mathcal{S}\mathbf{h}$ ($\mathbf{h} \in H^{\frac{1}{2}}(\Gamma_N)$); one has, according to (3.11), that $\mathbf{q} \in H^1_{0,\Gamma_D} \cap H^2(O)$.
Using again the Sobolev embedding Theorem 2.6, we find that:

$$H^2(\Omega) \hookrightarrow W^{1,s'}(\Omega) \text{ if } s' \in \left[1, \frac{2n}{n-2}\right] \Leftrightarrow s \geq \frac{2n}{n+2}.$$

Since, by virtue of Trace Theorem 2.5, one has $H^1(\Omega) \hookrightarrow H^{\frac{1}{2}}(\Gamma_N)$ then it is worth to point out the following embedding:

$$H^1(\Omega) \hookrightarrow L^{s'}(\partial\Omega) \text{ if } s' \in \left[1, \frac{2n-2}{n-2}\right] \Leftrightarrow s \geq \frac{2n-2}{n}.$$

that guarantees $\mathbf{h} \in L^{s'}(\partial\Omega)$.
According to the above results, the following equation is thus well defined, granted $s \in [\frac{2n-2}{n}, \frac{n}{n-1}]$:

$$\int_\Omega \nabla\mathbf{p} \cdot \mathbb{C}[\nabla\mathcal{S}\mathbf{h}] = \int_{\Gamma_N} \mathcal{T}_{\Gamma_N}\mathbf{p} \cdot \mathbf{h}, \tag{3.22}$$

We observe that the equality above follows from the definition of $\mathcal{S}$ (as in the forward problem (3.18)) and the symmetry of $\mathbb{C}$ (see Eq. (2.16)).

Remark 3.14. *Similar arguments hold for a pure Neumann problem, excepts for minor details.*

Remark 3.15. *A proof of the well–posedness of a pure Neumann problem when* $\mathsf{supp}\mathcal{O} \subset \partial\Omega$ *is given in [25] using the potential theory (suitable for the boundary elements numerical method). Here we do not constrain the support of the observation operator.*

Characterization of the optimal control

The optimal $\mathbf{f}$, as stated in (3.9), satisfies $\mathbf{f} = -\frac{1}{\varepsilon}\mathcal{P}\mathcal{S}^T\mathcal{A}\mathbf{p}$. It can be useful to recall that Equation (3.9) here takes the following meaning (see (3.22)):

$$\varepsilon(\mathbf{f}|\mathbf{h})_{H^{\frac{1}{2}}(\Gamma_N)} + \int_{\Gamma_N} \mathbf{p} \cdot \mathbf{h} = 0, \qquad \forall\mathbf{h} \in \mathsf{F}_{\mathrm{adm}}. \tag{3.23}$$

Given $\mathbf{p} \in W^{1,s}(\Omega)$, thanks to Riesz theorem (see [8]), a unique solution $\mathbf{f} \in H^{\frac{1}{2}}(\Gamma_N)$ of this problem exists since $\mathbf{h} \in H^{\frac{1}{2}}(\Gamma_N) \mapsto \int_{\Gamma_N} \mathbf{p} \cdot \mathbf{h}$ is a linear and continuous functional on $H^{\frac{1}{2}}(\Gamma_N)$. Unfortunately, Equation (3.23) cannot be approximated by standard FEM tools, even when $\mathsf{F}_{\mathrm{adm}} = \mathsf{F}$, since they do usually not deal with non–integer Sobolev spaces. A reasonable and computationally cheap way to overcome these difficulties is addressed in the next paragraph.

An hypothesis on the Observation Operator and its consequences

We note that, according to Theorem 2.5, the trace of an element of $W^{1,s}(\Omega)$ (s as before) does not necessarily belongs to $H^{\frac{1}{2}}(\Gamma_N)$. Nevertheless, if we add an additional hypothesis, we can achieve a greater regularity for the adjoint state.

Hypothesis 3.16. *The support of the observation operator* $\mathcal{O}$ *is an open set contained in* Ω' *which is such that* $\mathsf{cl}\Omega' \subsetneq \Omega$.

Using the hypothesis 3.16, we are able to state (see [38] for the proof):

Proposition 3.17. *Let* $\Omega" \subset \Omega \setminus \Omega'$ *strictly. Then* $\mathbf{p}|_{\Omega"}$ *belongs to* $H^1(\Omega")$.

Since, by the above hypothesis 3.16, $\mathsf{dist}(\Gamma_N, \Omega') > 0$ we can surely choose a set $\Omega" \subset \Omega \setminus \Omega'$ such that $\Gamma_N \subset \Omega"$. Then, by (3.17), $\mathbf{p}|_{\Omega"}$ belongs to $H^1(\Omega")$ and, by the Trace Theorem 2.5, $\mathcal{T}_{\Gamma_N}\mathbf{p}$ belongs to $H^{\frac{1}{2}}(\Gamma_N)$. According to [20], the adjoint variable $\mathbf{p}$, solution of (3.21), actually solves:

$$\int_\Omega \mathbf{p} \cdot (\mathrm{div}(\mathbb{C}\nabla\mathbf{q})) + (\mathbf{p}|(\mathbb{C}\nabla\mathbf{q})\mathbf{n})_{H^{\frac{1}{2}}(\Gamma_N)} = (\mathcal{O}\mathbf{u} - u_0) \bullet \mathcal{O}\mathbf{q}. \tag{3.24}$$

If we put the last equation inside Eq. (3.9) with $\mathbf{q} = \mathcal{S}\mathbf{h}$ ($\mathbf{h}$ is any function in $H^{\frac{1}{2}}(\Gamma_N)$, as before), we find that:

$$\mathbf{f} = -\frac{1}{\varepsilon}\mathcal{P}\mathbf{p},$$

which is a purely algebraic equation in the non–constrained case (i.e., when $\mathcal{P}$ is the identity). The constrained case can be treated as above, as we shall see during the next paragraph.

Remark 3.18. *Remarkably, thanks to the hypothesis 3.16, the problem is also well posed choosing* $\mathsf{F} = L^2(\Gamma_N)$. *The incoming paragraph takes a great advantage of this comment, as we shall see.*

The Space $\mathsf{F}_{\mathrm{adm}}{}^{\perp}$

In the constrained case the latter equation can be exploited as in Section 2, and

$$\mathbf{f} = -\frac{1}{\varepsilon}\mathcal{T}_{\Gamma_N}\mathbf{p} + \mathbf{f}^{\perp}$$

with $\mathbf{f}^{\perp} \in \mathsf{F}_{\mathrm{adm}}{}^{\perp}$. As noted in the Remark 3.18, we can consider $\mathsf{F}_{\mathrm{adm}}$ as in the definition (3.20) but with $\mathsf{F} = L^2(\Gamma_N)$. The actual calculation of a basis for its orthogonal $\mathsf{F}_{\mathrm{adm}}{}^{\perp}$ can be performed exactly in the same way as we have done in Section 2 (the little difference, purely algebraic, is due to the fact that we are working in three dimension). Actually, by the theorem of range and kernel (Theorem 3.12 of Section 2) we argue that $\mathsf{dim}(\mathsf{F}_{\mathrm{adm}}{}^{\perp}) \leq 6$, since we are now in $\mathbb{R}^3$. But one can readily find a $6-$dimensional basis for $\mathsf{F}_{\mathrm{adm}}{}^{\perp}$ letting $(\mathbf{e}_i)_{i=1}^3$ be three constant–linear independent–valued mappings and $\mathbf{e}_{i+3} = \mathbf{r} \times \mathbf{e}_i$, $i = 1, 2, 3$. The conclusion of the proof follows exactly the same calculations and reasoning of the discussions done for the analogous problem in Section 2.

Another observation that is worth to be done is the following: the null total moment of force constraint can be a little tricky to implement. For this reason, and only in this paragraph, we deal with the following admissible force space:

$$\mathsf{F}_{\mathrm{adm}} := \left\{ \mathbf{g} \in \mathsf{F} = L^2(\Gamma_N) \middle| \int_{\Gamma_N} \mathbf{f} = 0 \right\}.$$

Loosely speaking, we do not enforce the equilibrium of momentum and we just constraint the force field to have null resultant only. This choice of $\mathsf{F}_{\mathrm{adm}}$, as the reader may easily verify, does not affect the well–posedness results previously found. In such a case, we find that the set of equations (where $(l_i)_{i=1}^3$ is the set of Lagrangian multiplier associated with the constraint):

$$\begin{aligned} \mathbf{f} &= -\frac{1}{\varepsilon}\mathcal{T}_{\Gamma_N}\mathbf{p} + \sum_{i=1}^{3} l_i \mathbf{e}_i \\ \int_{\Gamma_N} \mathbf{f} &= 0 \end{aligned}$$

can be solved explicitly thanks to the fact that the basis $(\mathbf{e}_i)_{i=1}^3$ assume constant values. The above equation is thus equivalent to:

$$\mathbf{f} = \frac{1}{\varepsilon}\left(\frac{1}{\mathsf{meas}\Gamma_N} \int_{\Gamma_N} \mathbf{p} \; - \mathcal{T}\mathbf{p} \right)$$

being $\mathsf{meas}\Gamma_N$ the $(n-1)$-measure of Γ_N. Of course, this kind of reasoning can be repeated when treating the problem discussed in Section 2.

3.3.3 System of equations

Below we resume the results of the Section, pointing out the system of differential equations in weak form that one may want to solve in practice. Here we consider the assumption made in section 3.18, i.e. we only consider the null total force constraint, that give us a considerably simpler set of equations.

$$\begin{gathered}\text{find } \mathbf{u} \in H^1_{0,\Gamma_D}(\Omega) \cap H^2(\Omega),\ \mathbf{p} \in W^{1,s}_{0,\Gamma_D}(\Omega),\ s \in [\tfrac{2n-2}{n}, \tfrac{n}{n-1}] \\ \text{such that } \forall \mathbf{q} \in W^{1,s'}_{0,\Gamma_D}(\Omega),\ \forall \mathbf{v} \in H^1_{0,\Gamma_D}(\Omega):\end{gathered}$$

$$\begin{cases} \displaystyle\int_\Omega \mathbb{C}\nabla\mathbf{u}\cdot\nabla\mathbf{v} + \int_{\Gamma_N} \mathbf{f}\cdot\mathbf{v} & = 0, \\ \displaystyle\int_\Omega \mathbb{C}\nabla\mathbf{p}\cdot\nabla\mathbf{q} + \sum_{j=1}^N \delta_{\mathbf{x}_j}\mathbf{u}\cdot\delta_{\mathbf{x}_j}\mathbf{q} & = \displaystyle\sum_{j=1}^N u_{0_j}\cdot\delta_{\mathbf{x}_j}\mathbf{q}, \\ \mathbf{f} = \dfrac{1}{\varepsilon}\left(\dfrac{1}{\mathsf{meas}\Gamma_N}\displaystyle\int_{\Gamma_N}\mathbf{p} - \mathcal{T}_{\Gamma_N}\mathbf{p}\right), & \end{cases} \tag{3.25}$$

We are now in the position to step back to the original biological problem and recover the physical interpretation of equations (3.25). This reintepretation may become more apparent when assuming that the elastic gel is isotropic, so that the elasticity tensor takes a particularly simple form, depending just on two material parameters (μ and λ, the usual Lamé moduli). In this case equations (3.25) rewrite **

$$\begin{cases} \displaystyle\int_\Omega (\mu\nabla\mathbf{u}\cdot\nabla\mathbf{v} + \lambda(\mathrm{div}\mathbf{u})(\mathrm{div}\mathbf{v})) - \frac{1}{\varepsilon}\left(\int_{\Gamma_N}\mathbf{p}\cdot\mathbf{v} - \frac{1}{\mathsf{meas}\Gamma_N}\int_{\Gamma_N}\mathbf{p}\cdot\int_{\Gamma_N}\mathbf{v}\right) = 0, \\ \displaystyle\int_\Omega (\mu\nabla\mathbf{p}\cdot\nabla\mathbf{q} + \lambda(\mathrm{div}\mathbf{p})(\mathrm{div}\mathbf{q})) + \sum_{j=1}^N \delta_{\mathbf{x}_j}\mathbf{u}\cdot\delta_{\mathbf{x}_j}\mathbf{q} = \sum_{j=1}^N u_{0_j}\cdot\delta_{\mathbf{x}_j}\mathbf{q}, \end{cases} \tag{3.26}$$

The differential system in the weak form (3.26) eventually has the following meaning. Given an isotropic elastic material (like polyacrilamide), with known elastic moduli λ and μ, deformed by a living cell embedded in it, we have experimentally measured pointwise displacements $\mathbf{u}$ in the positions $\mathbf{x}_j$. The force field that produces such a displacement, in the sense of the one minimizing the penalty functional (3.5), is the traction field $\mathbf{f}$ solution of the system (3.26), defined on the boundary Γ_N where the gel and the cell are in contact. The traction $\mathbf{f}$ is simply proportional to the solution of the adjoint equation $\mathbf{p}$, up to a correction due to the null–average constrain. The two differential equations are coupled by linear non–differential terms, of surface or volumetric type. In this respect, one can pictorially say that the discrepancy between the measured and the calculated displacement the right hand side of equation (3.26.b) is the volumetric source for the adjoint field $\mathbf{p}$, its value at the interface being basically the cell traction we are looking for.

**This sentence translates in formula as (see [21]):

$$\mathbb{C} = 3\lambda\,\mathsf{sph} + 2\mu\,\mathsf{sym},$$

where sph denotes the projection onto $\mathsf{Sph}(\mathbb{R}^3)$ (spherical tensors) and sym is the projection onto $\mathsf{Sym}(\mathbb{R}^3)$.

Chapter 4

Numerical Approximation

The main goal of this chapter is to ascertain the accuracy and robustness of an inversion method of force traction microscopy in 3D. This biophysical target rewrites, in mathematical terms, in solving numerically the differential problem (3.26) by a finite element discretization on an unstructured grid. In this section we illustrate and discuss numerical results of the numerical model on a specific test case: a three dimensional boundary control of the linear elasticity problem with mixed boundary conditions. To best of our knowledge, numerical simulations of this type have not yet appeared in the literature, with a notable exception [39] where the three dimensional cellular traction problem is tackled using Green functions. However, no details are provided on the mathematical well–posedness. In addition, the finite element reconstruction using Green functions seems not really efficient and not appealing for generalization.

Several methods for solving optimization problems are known in the literature. Following [2] and [43], we chose the approach that in optimal control is called *first optimize then discretize* method [33]. In a few words, we first write down the optimality condition and then we solve numerically the two resulting coupled PDEs. In our case, this corresponds to take the coupled system of equations (3.26), approximating the unknowns ($\mathbf{u}$,$\mathbf{p}$) and the corresponding test fields ($\mathbf{v}$,$\mathbf{q}$) with their counterpart finite element function ($\mathbf{u}_h$, $\mathbf{p}_h$) etc. The numerical approximation of the problem (3.25) is obtained discretizing the trial fields $\mathbf{u}$ and $\mathbf{p}$ and the associated test fields $\mathbf{v}$ and $\mathbf{q}$ with Lagrange P1 elements. The integration of the forms is done using a Gauss formula, exact on polynomials of fifth degree. This is done in practice using the code `Free-FEM v.3.11`, see [31] for the details.

The following validation algorithm is adopted according to [63, 39]:

- Set $\mathbf{f}_{\text{given}}$ and evaluate the displacement solving numerically $\mathbf{u}_{\text{given}} = \mathcal{S}\mathbf{f}_{\text{given}}$ (the linear elliptic elasticity problem).
- Observe the displacement $u_0 = \mathcal{O}\mathbf{u}_{\text{given}}$ (possibly perturbed by artificial noise).
- Solve the Optimal Control Problem (for a range of ε): given u_0 and the model parameters, obtain $\mathbf{u}$ and $\mathbf{f}$.

- Evaluate the errors such as $\|\mathbf{f} - \mathbf{f}_{\text{given}}\|_2$ etc. and discuss the results.

4.1 A Comparison with the Green Function Approach

We now explain the reasons why we believe that the method exposed in this work, borrowed from Inverse and Optimal Control Theory, is more efficient from the computational point of view than its Green function counterpart, as exposed in [39]. Set:

- $\mathcal{N}$ the number of degrees of freedom of the computational mesh.
- $\mathcal{M}$ the number of degrees of freedom associated to the boundary traction at the border Γ_N.

Starting the analysis considering our approach, the unknown of our problem (see (3.25)) are the displacement $\mathbf{u}$ and the adjoint state $\mathbf{p}$ which will be easily discretized in a $2 \cdot 3 \cdot \mathcal{N}$ vector. The system obtained can be efficiently solved using an iterative method for sparse matrix at an average cost proportional to the dimension of the matrix (in this case, $2 \cdot 3 \cdot \mathcal{N}$ evidently). Thus, the cost of one run of our algorithm is proportional to $\mathcal{N}$, whatever the value of N (number of beads) or $\mathcal{M}$ we choose.

We now sketch what kind of operations involves the algorithm of Legant, Chen et al. [39]. First, they calculate numerically the operator we call $\mathcal{OS}$ which relates the boundary traction $\mathbf{f}$ to the displacements u_0 measured on the beads at $\mathbf{x}_1, \ldots, \mathbf{x}_N$ (Γ, in their notations) using Finite Elements. In order to do so, they have to solve numerically the Eqn. (2.20) for every element of the Finite Element basis whose support belongs to Γ_N; since the problem is linear, this is enough to evaluate the operator $\mathcal{OS}$. Having done so they can evaluate the displacement (i.e. the solution of the problem (2.20)) at the observation points.
Since the number of base elements having support on Γ_N is $3 \cdot \mathcal{M}$ the cost of such an operation scales as $\mathcal{M} \cdot \mathcal{N}$, since we consider, as before, that a FEM run costs as the number of degrees freedom of the grid. After this first passage, they use such a discretized operator $\mathcal{OS}$ (let us call it G, which is a $3N \times 3\mathcal{M}$ matrix) to solve the discrete minimum problem:

$$\text{find the minimum of } F \mapsto \left(|\mathrm{G}\, F - u_0|^2 + \varepsilon |F|^2\right)$$

where F is the $3\mathcal{M}-$vector containing the values of the discrete boundary traction. Such a problem will lead to a $3\mathcal{M}$ dimensional linear system. The latter is presumably attacked using an iterative method, which costs (as we have said before) about $\mathcal{M}$ flops.
The overall cost of the inverting procedure advocated by Legant, Chen et al. [39] scale thus as $\mathcal{M} \cdot \mathcal{N}$. If we do the estimate (as could roughly be expected) $\mathcal{M} \sim \mathcal{N}^{1/2}$, then the cost of the Green function method would be proportional to $\mathcal{N}^{3/2}$.
The procedure advocated by the latter authors has thus a considerably higher cost than what can be obtained using a variational framework.

Remark 4.1. *When analyzing the Legant, Chen et al. [39] approach to the force traction microscopy, the reader should be persuaded by the fact that their calculations are absolutely not generalizable to a genuine non–linear case since the assumption of linearity of $\mathcal{OS}$ is crucial if one wants to evaluate it numerically in the way described before.*

4.2 Numerical Setup

In this work all the equations are written in dimensional form, so that the reader interested in the specific biophysical application can easily appreciate that the order of magnitude of forces and spatial dimensions match the ones typically observed in the experiments.

The reference setup that we use for the simulations has a computational domain, a $100^3 \mu m^3$ cube, with a $20 \times 10 \times 10 \mu m^3$ ellipsoidal hole, representing the cell. In the reference case we have used 300 beads (i.e., the "observation points") with mean distance $17.88 \mu m$ from the origin. The mesh is characterized by a tethraedron aspect ratio ranging between $0.6 \mu m$ (near the ellipsoid) and $10 \mu m$ (near the external border). The number of degrees of freedom is 7392. In Fig. 4.1 are reported a picture of the computational mesh and of the position of the beads. In Section 5 we explore the behavior of the inverse method when the listed numerical parameters change in suitable ranges.

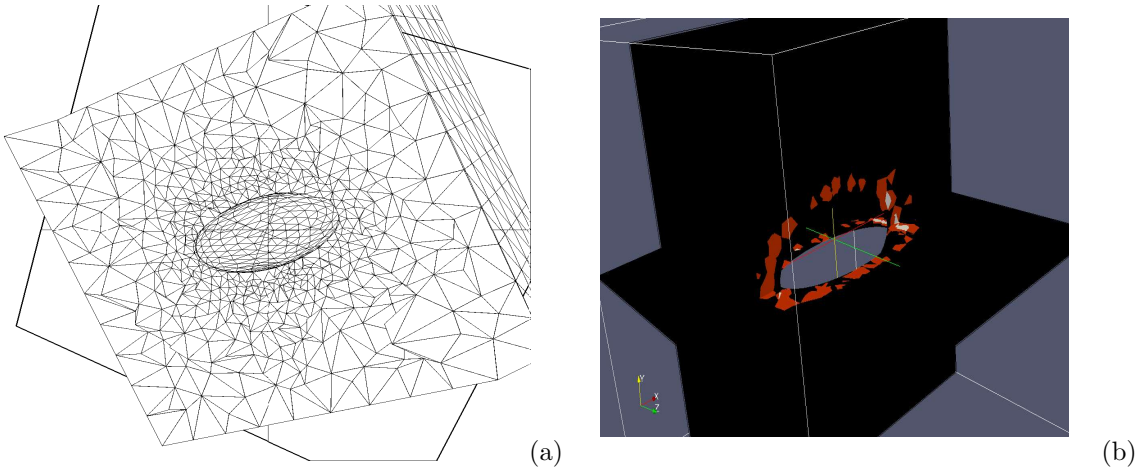

(a) (b)

Figure 4.1: The computational mesh (a) and the location of the beads (b)

In the calculations that follow we use the standard value of the elastic moduli [2, 3, 24] $\lambda = 4150 \frac{pN}{\mu m^2}$, $\mu = 2100 \frac{pN}{\mu m^2}$.

The observed displacement field is first produced, once for all, solving the direct problem using the following given dipole–like force (see Fig. 4.2):

$$\mathbf{f}_{\text{given}} := 10^3 \begin{cases} (x, y, z) & x > 15 \\ (\alpha_x x, \alpha_y y, \alpha_z z) & x < 0 \end{cases} \quad \frac{pN}{\mu m^2} \tag{4.1}$$

The origin of the axis is put at the geometrical center of the computational setup. We have chosen Cartesian coordinates, with the x axis coincident with the semi–major axis of the ellipsoid. We have defined $\alpha_\xi := \dfrac{\int_{\Gamma_N} \chi_{(x>15)}\, \xi}{\int_{\Gamma_N} \chi_{(x<0)}\, \xi}$ (for $\xi = x, y, z$) and χ is the characteristic function of a set ($\chi_\Sigma(x) = 1$ if $x \in \Sigma$ and 0 elsewhere). The given force and the resulting displacement are graphically represented in Figure 4.2.

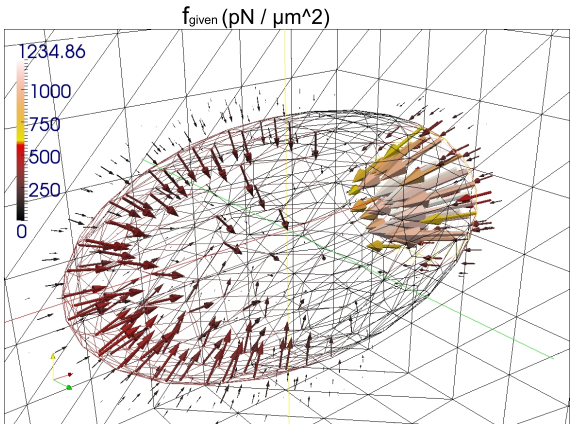

a

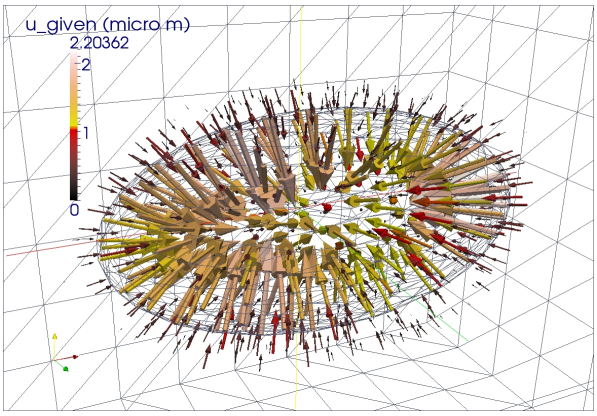

b

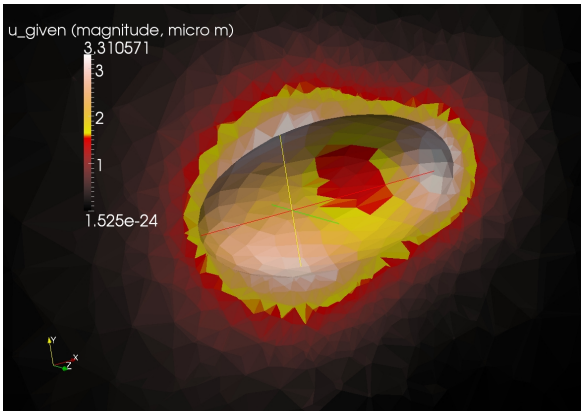

c

Figure 4.2: The given traction $\mathbf{f}_{\text{given}}$ in picoNewton per micron square (a) and the given displacement $\mathbf{u}_{\text{given}} = \mathcal{S}\mathbf{f}_{\text{given}}$ in microns (b) are plotted at the cell–gel surface. A colour map of the magnitude of $\mathbf{u}_{\text{given}}$ in some points is in figure c.

4.3 Numerical results

The main aim of the present work is to evaluate the ability of the inversion method to recover the true force produced by a cell on the basis of pointwise measures of the displacement. In other words, we aim controlling and possibly minimizing the error in calculating $\mathbf{f}$ according to the proposed inversion procedure. Different error measures can be applied, depending on the physical meaning and on the expected level of regularity of an unknown (see the analytical results collected in section 3.3). It is therefore useful

to introduce here the following concise notations:

$$e_2(\mathbf{f}) := \frac{||\mathbf{f}-\mathbf{f}_{\text{given}}||_2}{||\mathbf{f}_{\text{given}}||_2} := \frac{\left(\int_{\Gamma_N}|\mathbf{f}-\mathbf{f}_{\text{given}}|^2\right)^{1/2}}{\left(\int_{\Gamma_N}|\mathbf{f}_{\text{given}}|^2\right)^{1/2}} \tag{4.2}$$

$$e_2(\mathbf{u}) := \frac{||\mathbf{u}-\mathbf{u}_{\text{given}}||_2}{||\mathbf{u}_{\text{given}}||_2} := \frac{\left(\int_{\Omega}|\mathbf{u}-\mathbf{u}_{\text{given}}|^2\right)^{1/2}}{\left|\int_{\Omega}|\mathbf{u}_{\text{given}}|^2\right|^{1/2}} \tag{4.3}$$

$$e_2(\mathcal{O}\mathbf{u}) := \frac{|\mathcal{O}\mathbf{u}-\mathbf{u}_0|_2}{|u_0|_2} := \frac{\left(\sum_{i=1}^{N}|\mathbf{u}(\mathbf{x}_i)-\mathbf{u}_{\text{given}}(\mathbf{x}_i)|^2\right)^{1/2}}{\left(\sum_{i=1}^{N}|\mathbf{u}_{\text{given}}(\mathbf{x}_i)|^2\right)^{1/2}} \tag{4.4}$$

$$e_\infty(\mathbf{u}) := \frac{\max_{\mathbf{x}\in\Omega}|\mathbf{u}(\mathbf{x})-\mathbf{u}_{\text{given}}(\mathbf{x})|}{\max_{\mathbf{x}\in\Omega}|\mathbf{u}_{\text{given}}(\mathbf{x})|} \tag{4.5}$$

We observe that a stronger norm (as the infinity norm) for the force field $\mathbf{f}$ is not allowed in this framework as, in general, such a force field might not have the needed regularity. In fact, in section 3.3.2, we have found that $\mathbf{f} \in H^{\frac{1}{2}}(\Gamma_N)$.

4.3.1 Noise and regularization

In this Section we report numerical results obtained from data u_0 either exact and affected by noise. As a matter of fact, experimental measures are always affected by noise. In order to estimate the stability of the inversion method to small perturbations in the data we introduce a list of independent and isotropic Uniform Random Functions with zero mean and amplitude $\nu = 0.4\mu m$. The same numerical simulations are then carried out with the data $u_0 = (\mathbf{u}_0^1, \ldots, \mathbf{u}_0^N)$ perturbed as follows:

$$\mathbf{u}_0^i \cdot \mathbf{w} = \mathbf{u}_{\text{given}}(\mathbf{x}_i)\cdot\mathbf{w} + \nu\,\mathsf{Unf}\Big(-\frac{1}{2},\frac{1}{2}\Big),$$

for all unitary vectors $\mathbf{w}$. The symbol $\mathsf{Unf}(a,b)$ denotes the uniform probability distribution in the interval $]a,b[$. The above expression is referred in the literature [71] as a semistochastic semidiscrete linear data model with additive noise.

The amplitude of the noise is comparable to what is found in practice [39]: here ν is greater than the sum of the uncertainty in the placement of the beads (declared to be $0.210\mu m$) and the error of cell surface reconstruction (which is estimated at $0.176\mu m$). Notwithstanding the common agreement that the errors introduced by a measure apparatus follow a Normal Probability Distribution, here we use a Uniform one (easier to implement in our code), while aware that we possibly overestimate the actual noise. Figures 4.3 and 4.4 compare the errors when data are affected or not by noise

A major issue in inversion algorithms is the determination of the optimal value of the regularization parameter ε and the analysis of the sensitivity of such a value to the numerical and physical data. Figures 4.3 and 4.4 show the relative error in force and displacement, as defined in (4.2,4.3,4.4,4.5), depending on the regularization parameter ε.

The error approaches 100% when ε is large both in the noisy and in the non–noisy case. As far as ε decreases, the error becomes smaller up to a minimum. When data are not perturbed by noise, the numerical method becomes unstable below a critical value

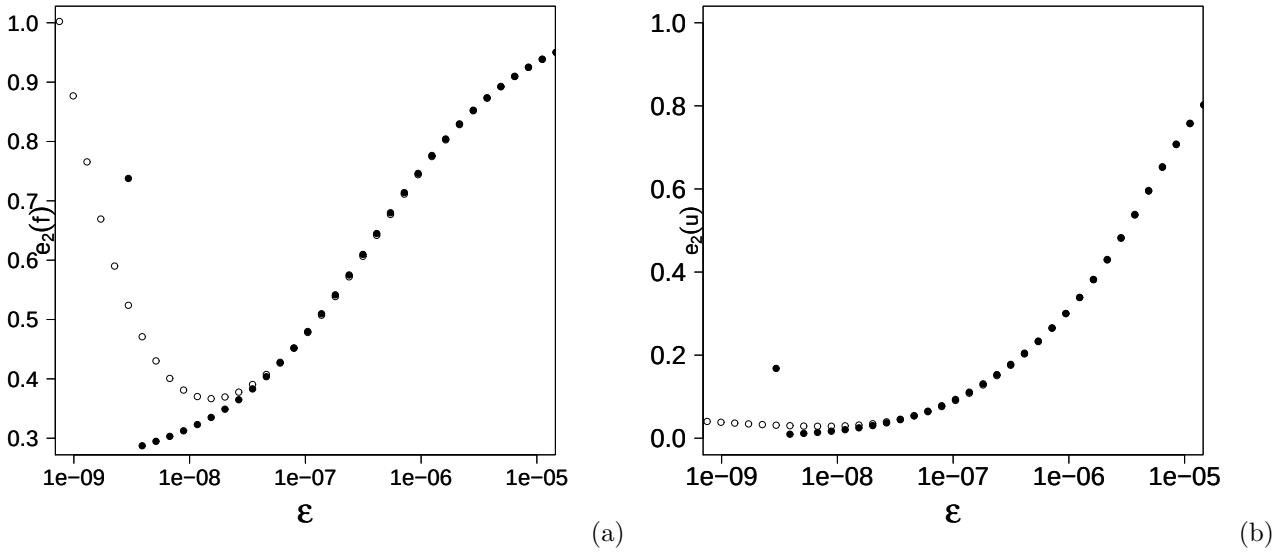

(a) (b)

Figure 4.3: Error in the traction field, $e_2(\mathbf{f})$ *vs* ε (figure a) and error in the displacement field, $e_2(\mathbf{u})$ *vs* ε(figure b). Empty circles refer to noisy data, filled ones refer to non–noisy data. In the ideal case of measures not affected by errors, a minimum (non–null) reconstruction error of $\mathbf{f}$ can be achieved. Below this optimal ε, the error abruptly grows.

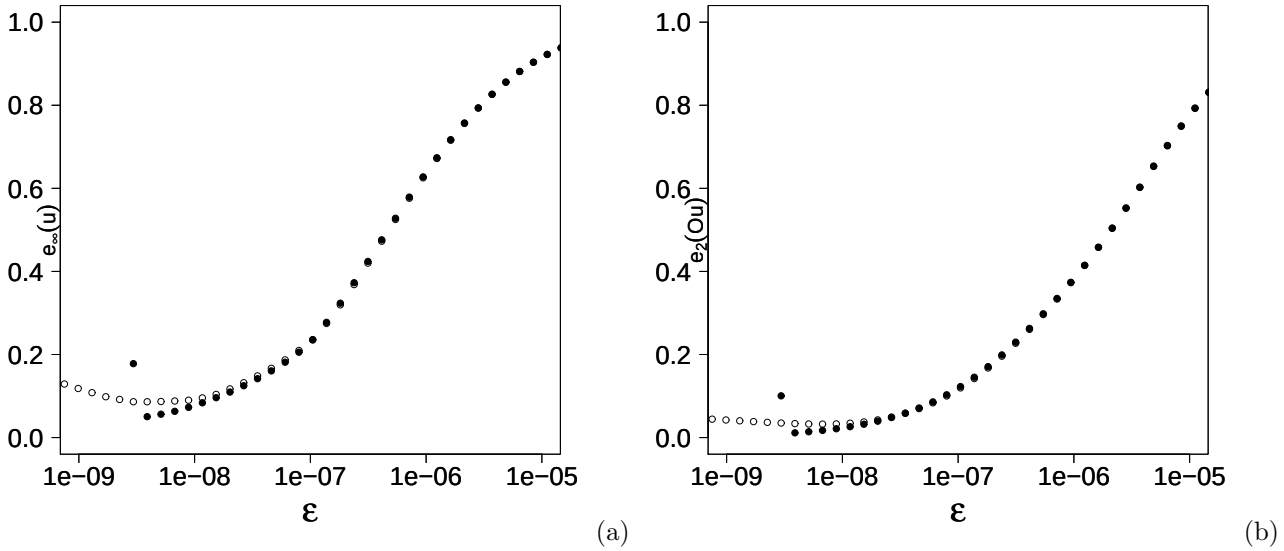

(a) (b)

Figure 4.4: Error in the displacement field. Figure (a) reports $e_\infty(\mathbf{u})$ *vs* ε, Figure (b) shows $e_2(\mathcal{O}\mathbf{u})$ *vs* ε. Empty circles refer to noisy data, filled ones refer to non–noisy data.

of the regularization parameter. The best possible approximation for the traction, the quantity of our main interest, has an apparently uneliminable 30% error, attained when exact data are inverted.

The behavior of the error vs. ε is very similar for noisy data: in particular, the optimal stabilization parameter grows with the noise. The main difference is in the minimum error in traction that one can hopefully obtain (now of the order of 40 %) and the somehow counter–intuitive stabilization of the numerical algorithm for very small ε.

Remark 4.2. *We observe that the stability of the inversion method with respect to noise actually comes from the continuity of the generalized (Moon–Penrose) inverse of the operator $\mathcal{OS}$ (see the Proposition 3.4 for the proof and the introductory matter in section 2.3 for the general theoretical setting, in particular the Theorem 2.18).*

4.3.2 Optimal choice of the regularization parameter

As anticipated in Section 2.3, here we consider a method to estimate an (in some sense) optimal value of the regularization parameter ε that does not require knowledge of the exact force field in a very analogue problem. This method is known as the L–curve criterion, and it is briefly described at page 24.

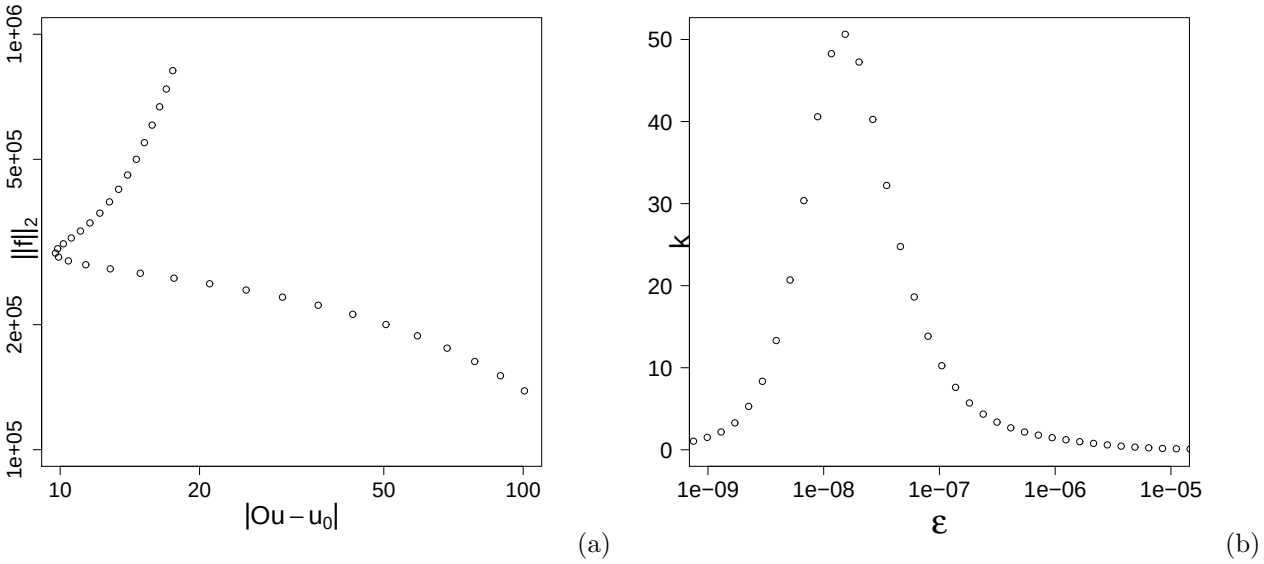

Figure 4.5: Left: the L-curve, i.e. $|\mathcal{O}\mathbf{u}-\mathbf{u}_0|_2$ *vs* $\|\mathbf{f}\|_2$. Right: the curvature of the L-curve κ as a function of ε.

The L–curve criterion states that the optimal value of ε lies in the corner of the curve plotting the magnitude of $\mathbf{f}$ versus the discrepancy between measured and calculated displacement, viz $|\mathcal{O}\mathbf{u} - u_0|_2$ (Fig. 4.5a). In figure 4.5b the curvature κ is plotted as a function of ε; the corner of the L-curve corresponds to the value of ε that maximizes the curvature κ. Such a curvature can be evaluated as a function of ε referring to the Eqn. (2.24). However, we have found that the following approximation of Eqn. (2.24) works

well, since the outcome of our simulation shows $\varepsilon\frac{S(\varepsilon)}{R(\varepsilon)} \ll 1$ for small ε (*data omitted*):

$$\kappa(\varepsilon) \approx \frac{S(\varepsilon)}{R(\varepsilon)}\left(\frac{S(\varepsilon)}{S'(\varepsilon)} + \varepsilon\right).$$

Following this approach, we find that the optimal value of the regularization parameter for the reference problem is $\varepsilon_{opt} = 1.5347 \cdot 10^{-8}$. The L-curve turns out to be an effective criterium: the value of ε that actually provides the minimum error $e_2(\mathbf{f})$ is exactly the same.

We are now in the position to state a reference inversion set up of the parameters for our problem:

- regularization parameter $\varepsilon = \varepsilon_{opt} = 1.5347 \cdot 10^{-8}$,
- number of observation points $N = 300$,
- average distance of observation points from origin $17,88\mu m$,
- noise level $\nu = 0.4\mu m$.

The three dimensional plots shown in Fig. 4.6 report the numerical solution obtained using such values.

4.4 Sensitivity analysis

In this Section we perform simulations varying some numerical and physical parameters, one by one, with respect to the reference test. The sensitivity analysis aims to test the robustness and reliability of the inversion technique. In particular, we explore the accuracy of the reconstruction provided by the inversion tool when

- varying the number of observation,
- perturbing the ellipsoidal shape of the boundary Γ_N,
- refining and coarsening the computational mesh,
- changing the beads-to-cell distance.

All the simulations are performed for noisy data as, in practice, data are always affected by noise. Moreover, this choice allows us to compare the optimal value of ε in the L-curve sense.

4.4.1 Number of observation points

In Figure 4.7 we compare the results obtained by the reference simulation traction and displacement computed using 150 and 450 beads, *ceteris paribus*. In particular, the mean distance from the origin (i.e. the center of the ellipsoid) is $17.95\mu m$ when using 150 beads and $17.87\mu m$ when using 450 beads, values that are close to the mean distance in our standard simulation.

Increasing the number of observations, one obtains a small improvement in the minimum error, both on the force and on displacement fields. More remarkably, also the slope

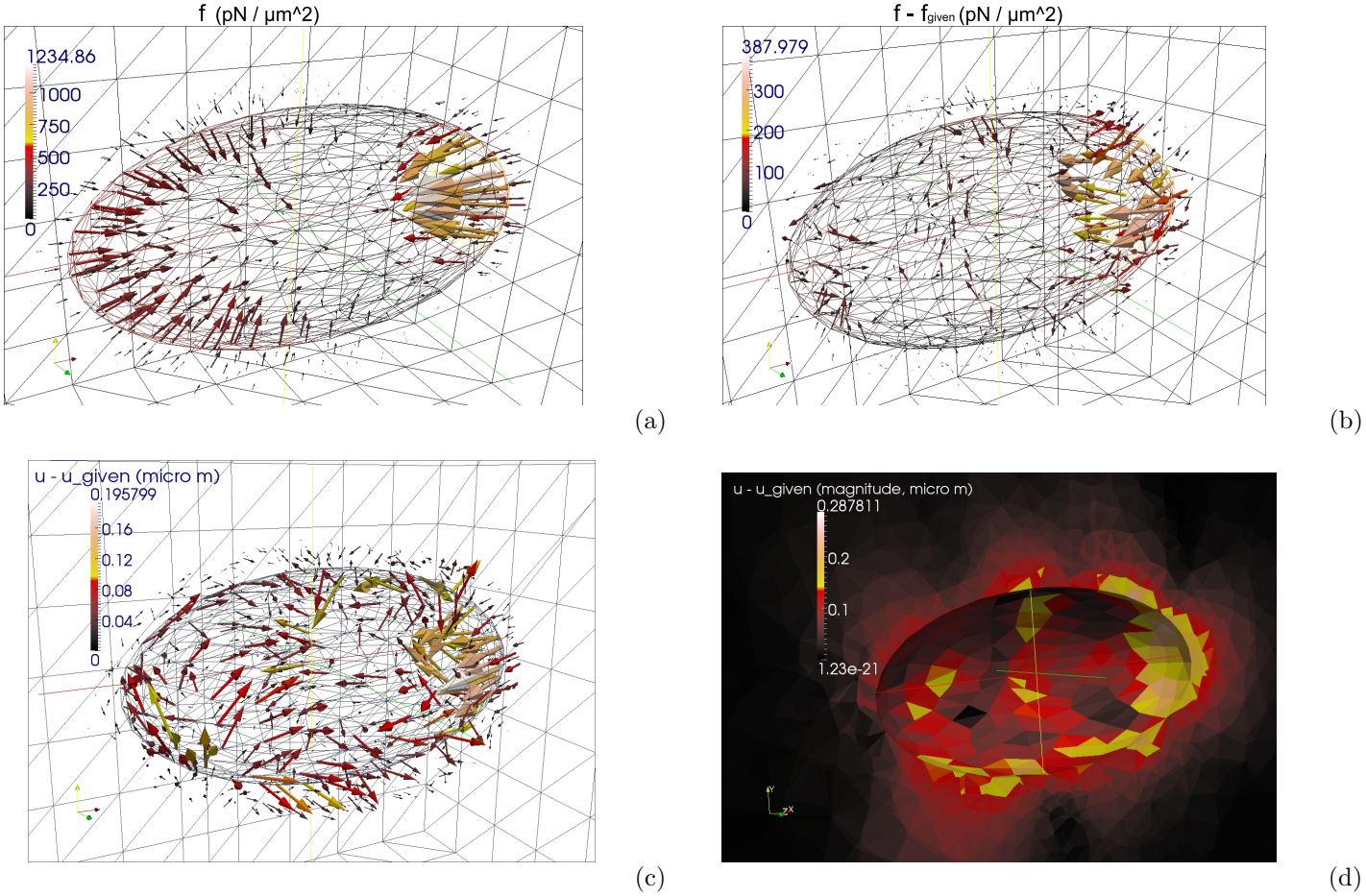

Figure 4.6: Force reconstructed using our inversion method (a). Error between given and reconstructed force (i.e. $\mathbf{f} - \mathbf{f}_{\text{given}}$) (b). Error between given and reconstructed displacement on the cell boundary (i.e. $(\mathbf{u} - \mathbf{u}_{\text{given}})|_{\Gamma_N}$) (c). Magnitude of the local error in displacement (d).

of the curve diminishes, thus representing a smaller sensitivity of the error on ε. The optimal ε (see Figure 4.7) has the same value for 300 and 450 beads, thus suggesting that a plateau is reached, while only the curvature of the L curve changes. It therefore appears that adding more than 300 beads does not increase the information on the system.

4.4.2 Shape of the boundary

A geometrical characterization of traction force microscopy that might influence the accuracy of the inversion method is the regularity of the boundary *. We therefore perturb the shape of the smooth ellipsoid as shown in Fig. 4.8. The same numerical experiments carried out above are now performed in the less regular domain.

*Here, the terms *regular* and *smooth* should not be intended in their topological meaning. As will become clear in a while, we are always working with C^2 boundaries. What we want to analyze here is the sensitivity of the method with respect to the shape of the boundary, an aspect of little mathematical importance but very relevant when dealing with applications.

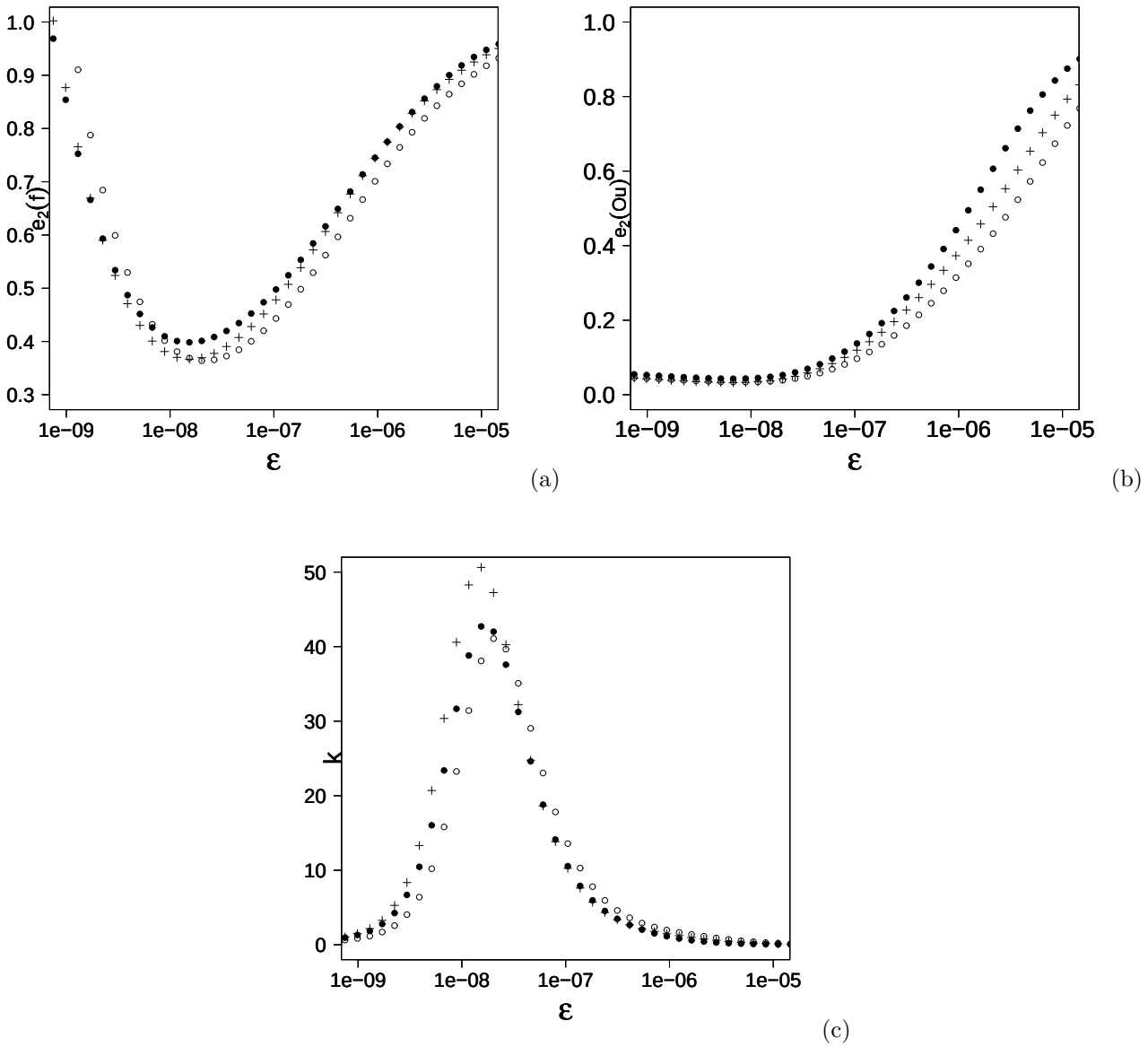

Figure 4.7: Plot of the error in traction $e_2(\mathbf{f})$ *vs* ε (figure a), the displacement field evaluated at beads $e_2(\mathcal{O}\mathbf{u})$ *vs* ε (figure b) and curvature of the L-curve κ as a function of ε (figure c). The curves refer to 150 beads (filled circles), 300 beads (plus signs) and 450 beads (empty circles).

The results are to be compared with the reference solution, although here the mesh is slightly finer then in the computations above, to prevent sharp corners with few elements. The average distance of the beads from the center of the ellipsoid is now $17.492\mu m$. The analytical expression for the force is the same as above in Eqn. (4.1).

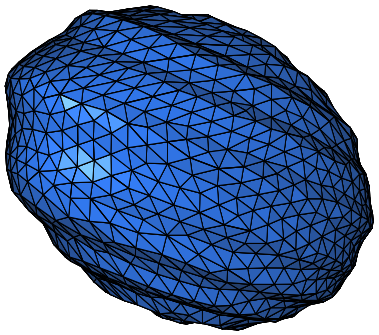

Figure 4.8: The irregular shaped cell, i.e. Γ_N.

Results of the numerical inversion in the perturbed geometry are reported in Figure 4.9. The error increases a bit, when compared with the reference results. In this specific case, an error of 40% in the reconstruction of $\mathbf{f}$ is found. Moreover, the optimal ε (see Figure 4.9) increases for the case of shape perturbed ellipsoid: this behavior is qualitatively similar, although conceptually different, to an addition of noise to the reference setup. The optimal value of the regularization parameter in the case of perturbed ellipsoid, in the sense of the L-curve, turns out to be $\varepsilon_{opt} = 2.657 \cdot 10^{-8}$. The value of ε that actually gives the minimal discrepancy in the force field is, instead, $3.496 \cdot 10^{-8}$. In Figure 4.10 are shown calculations for $\varepsilon = \varepsilon_{opt}$.

4.4.3 Mesh Refinement

All the errors quantified in the present work are numerically calculated; therefore, they depend not only on the inversion method, but also on the discretization scheme too (mesh size, finite element basis, numerical algorithm...). Let ξ be any quantity of interest and ξ^h its discrete counterpart. Using the triangular inequality we get:

$$\|\xi - \xi_{given}\| \leq \|\xi^h - \xi^h_{given}\| + \|\xi - \xi^h\| + \|\xi_{given} - \xi^h_{given}\| \leq \|\xi^h - \xi^h_{given}\| + O(h^p) \quad (4.6)$$

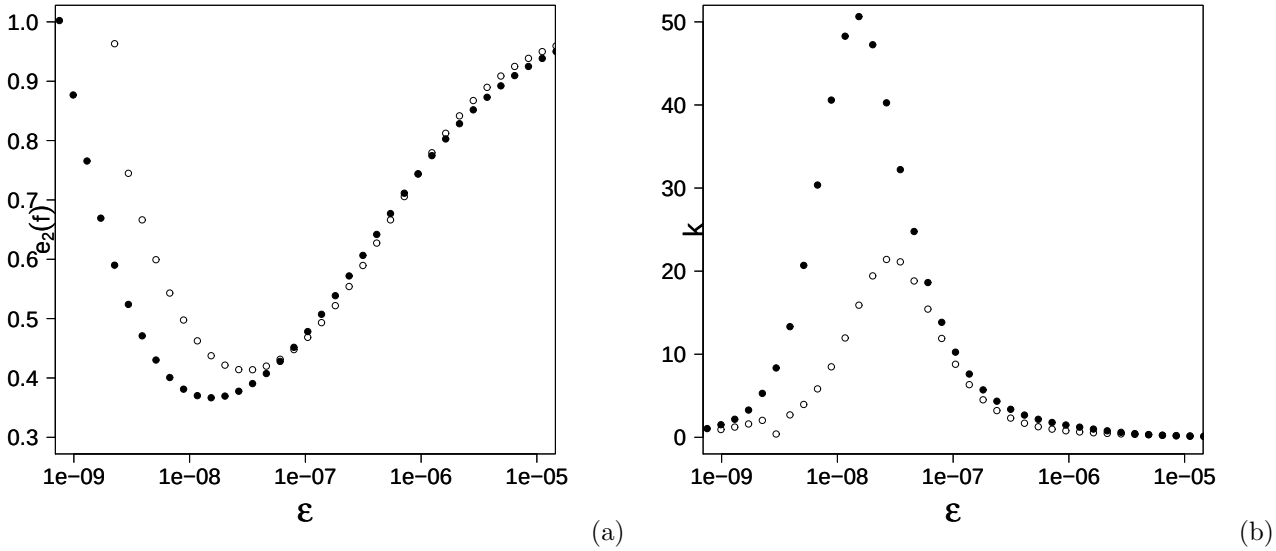

(a) (b)

Figure 4.9: Plot of the error in traction $e_2(\mathbf{f})$ *vs* ε (figure a) and curvature of the L-curve κ as a function of ε (figure b). The curves refer to the smooth ellipsoid (filled circles) and the perturbed ellipsoid (empty circles).

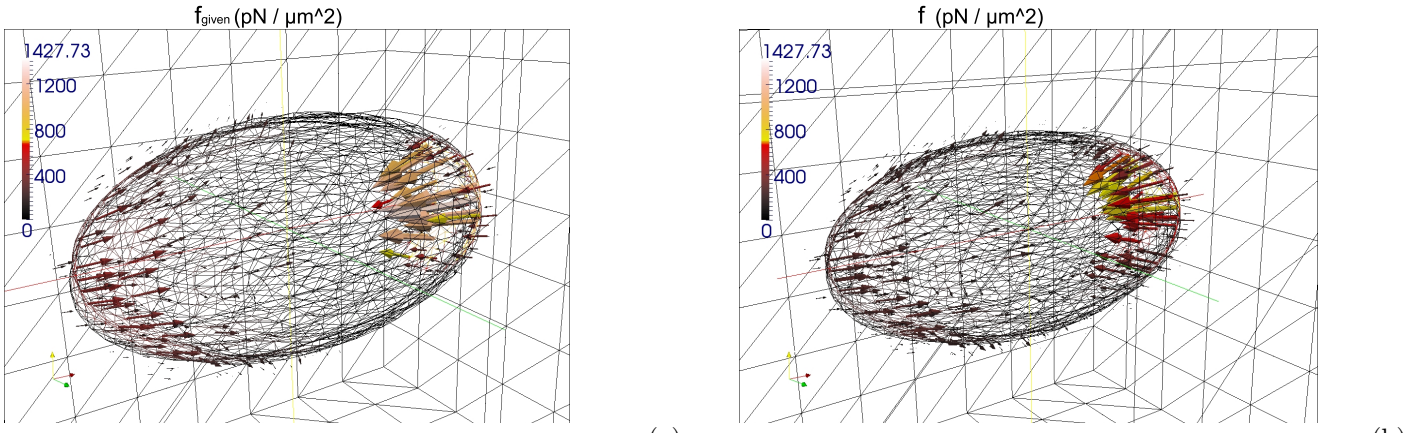

(a) (b)

Figure 4.10: Comparison between given (a) and reconstructed (b) force field for an irregularly shaped ellipsoid.

where ξ^h and ξ^h_{given} are the approximate values of the exact and the inverted ξ, respectively. The first term at the right hand side of (4.6) is the inversion error, the second one represents the numerical one, i.e. the one due to the projection of the solution (ξ, ξ_{given}) onto the finite element space of interest.
For $h \to 0$ the second term at the right hand side tends to zero, but the same comment does not apply to the first one. The inversion errors is therefore underestimated on coarse numerical grids, since the ratio between number of observations and degrees of freedom of the finite element basis is high. This is the reason why, for a fixed number of observation points, the inversion error actually grows for smaller h.

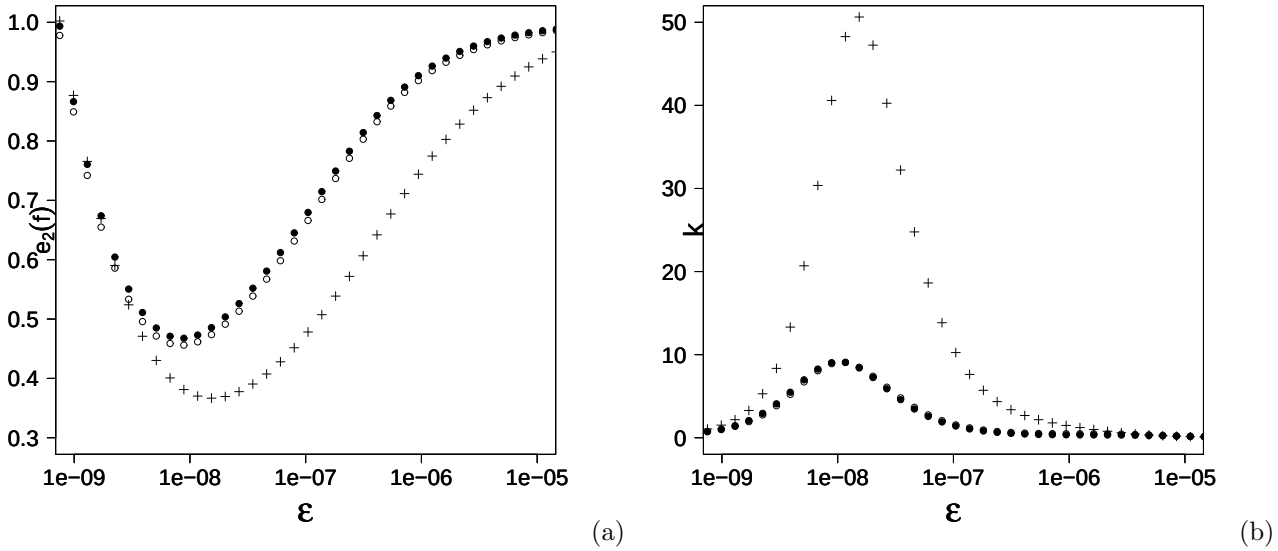

Figure 4.11: Error $e_2(\mathbf{f})$ vs ε calculated on different grids (a). Curvature of the L-curve κ vs ε: note that the values labeled with empty and filled circles are nearly superposed (b). Filled Circles: Grid 2 (Finest grid). Empty Circles: Grid 1. Plus signs: Grid 0 (Standard Grid).

In Figure 4.11 the error in $\mathbf{f}$ are plotted as a function of ε using three numerical grids:

- Grid 0: the reference one described in Section 3.
- Grid 1 has 14331 degrees of freedom, the tethraedron aspect ratio ranges between $0.5\mu m$ (near the ellipsoid) and $10\mu m$ (near the external border). The mean distance of the beads from the origin is $17.43\mu m$
- Grid 2 has 21758 degrees of freedom and the tethraedron aspect ratio ranges between $0.4\mu m$ (near the ellipsoid) and $10\mu m$ (near the external border). The mean distance of the beads from the origin is $17.48\mu m$.

The noise level, the number and position of the observation points are the reference ones. According to Figure 4.11, the error reaches to its mesh–independent value in grid 1, while the optimal ε decreases as the grid becomes fine enough. This is mainly due to the fact that, using finer grids, the true displacement u_0 calculated from the force field $\mathbf{f}_{\text{given}}$ in

(4.1) is actually more accurate, leading to a greater signal to noise ratio (having the same noise level per bead). Despite of this fact, the curvature of the L-curves takes smaller values as the grid gets finer.

4.4.4 Location of the beads

Numerical simulations have been performed applying a variation in the positions of the beads, while keeping all the other parameters in their reference values. The results are reported in Fig. 4.12, where the mean distance of the beads from the center of the ellipsoid center is denoted by ϱ.

As intuitively expected, the error in all fields increases as far as the distance of the beads increases (see Figure 4.12). Conversely, the optimal value of ε decreases with ϱ. The maximum value of the curvature of the L-curve also decreases with distance. Therefore the distance between the beads and the Neumann border Γ_N happens to be a crucial parameter to be taken into account (see also the remarks by Legant, Chen et al. [39]).

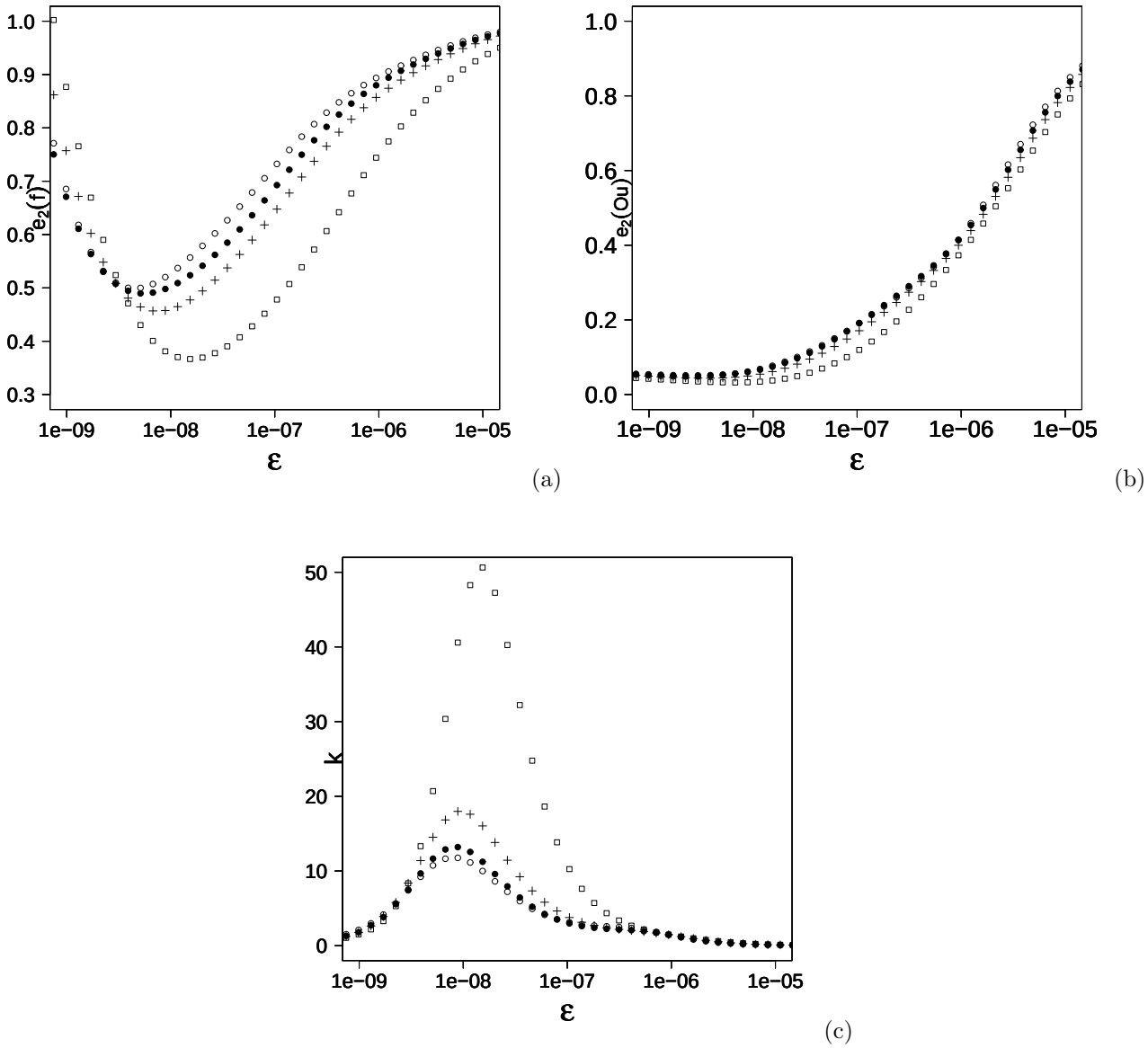

Figure 4.12: L^2 error in the reconstruction of the traction field vs ε for different bead distributions (a) errors on displacement calculated at beads vs ε (b), and curvature of the L-curve κ vs ε (c). The mean distance of the observation points from the origin is $\varrho = 17.88\mu m$ (squares), $\varrho = 19.63\mu m$ (plus signs), $\varrho = 20.52\mu m$ (filled circles), and $\varrho = 21.41\mu m$ (empty circles).

Chapter 5

Final Remarks

A inverse problem inspired by biophysical practice has been address in terms of formal and rigorous statements. The specific characteristics of this problem is to assume pointwise observations: they call for a generalization of the classical elasticity theory to forcing terms (for the adjoint problem) that are Borel measures.

The results exposed in this Part are not a theoretical advancement in optimal control theory *per se*. Our main aim here is the correct statement of the set of equations that can be adopted to address traction force microscopy in a three dimensional environment, a challenging question in cell biology. The mathematical theory largely stands on known results, while the novelty of this contribution is in the specific form system of equations (3.25) and their well posedness for the application at hand. Now, on this basis, the reader interested in biological applications can step forward to the numerical approximation of these two elliptic partial differential equations, coupled by the boundary conditions. It may be worth to recall that force traction microscopy in three dimensions is still in its infancy; just in very recent years imaging techniques have revealed detail of the patterns of the mechanical strain produced by the cells in their movement. Early attempts of quantitative inversion have been carried out [39], but a precise analysis of the methods seems to be still missing.

The content of this work provides now the basis for a mathematically precise application of the inversion method to real biophysical questions.

The inversion method has been here implemented using Finite Element Method and applied to a prototype system. Before running the inversion code, we assign an explicit force field and numerically solve the direct elasticity problem only. Such a tension at the boundary and the resulting deformation are then taken as *true* values. The efficacy of the inversion code is then evaluated in terms of its ability to recover the *true* fields on the basis of the provided data. The numerical simulations yields the following conclusions.

- Even in the best possible configurations, the relative error in the recovered force is never below 30%. For small variations of the parameters of the problem around such an optimal setting, the error remains below 40%. The pattern of the reconstructed force has, however, a fairly good agreement with the given one.
- The location of the observation points is crucial: they should stay as near as possible to the cell-gel interface.

- The results are obviously dependent on the value of the regularization parameter ε; an almost–optimal choice of its value is provided by the L-criterion.
- The quality of the inverted data depends poorly on the noise in data and on the regularity of the contour of the cell, at least for the range of variations numerically explored.
- The solution depends weakly on the number of observation points, provided that a minimum number of bead locations is registered.

Part II

Mathematical Model of Cell Adhesion in Tissues

Chapter 6

Motivation

Starting from the paper [16], in the last ten years several multiphase models have been developed and applied with success to describe tumour growth. As reviewed in [4, 5, 11, 27, 46, 57, 67], most of the models use fluid-like constitutive equations for the cellular constituents. However, this is only an approximation, because tumors and multicellular spheroids, as most tissues, are more complex, showing solid-like properties associated with the adhesive characteristics of cells. Only recently some attention has been paid to such adhesive interactions between cells and between cells and ECM [6, 7, 22, 32, 44, 45] and how these mechanisms influence the behaviour of cell aggregates and therefore the detachment of metastases. All the models above, including the one presented here, work at a mesoscopic tissue level, though the experiments studying adhesions are performed at a molecular scale. In fact, what is usually measured is the strength of single or clustered adhesion bonds formed by a cell (see, for instance, [9, 17, 55, 66]). The typical experiment is done using an atomic force microscopy cantilever with a tip that can be possibly functionalised with proper adhesion molecules to check the specific interaction of the cell adhesion molecules with those placed on the tip of the cantilever. After putting the tip in contact with the cell for some time, either the cantilever or the plate with the cell are pulled away at a constant speed, typically in the range 0.2–5 μm/sec. If the tip of the cantilever does not attach to the cell, when the cell is moved away, the cantilever does not deflect. This behaviour is experimentally obtained, for instance, by the addition of an antibody attaching to the external domain of the adhesion molecule [9], or by interfering with the links between the adhesion molecules and the cell cytoskeleton [17], or by disrupting the actin cytoskeleton [66]. Otherwise, adhesion gives rise to the deflection of the cantilever that can be related to the stretching force exerted by the cell. Of course, the distance between the cell and the cantilever increases with time, increasing the deflection angle and the stretching force. It is then observed that, after some time, one or more adhesive bonds break causing a characteristic jump in the deflection of the cantilever that tends to return to its undeformed configuration. In this way it is possible to evaluate the maximum force exerted by an adhesion bond before breaking.

Baumgardner et al. [9] found that the mean strength of the adhesion bonds is in the range 35–55 pN, giving a distribution function of the critical unbinding force like the one shown in Fig.6.1a.

Similar results were obtained by Canetta et al. [17], and Sun et al. [66] (see Fig.

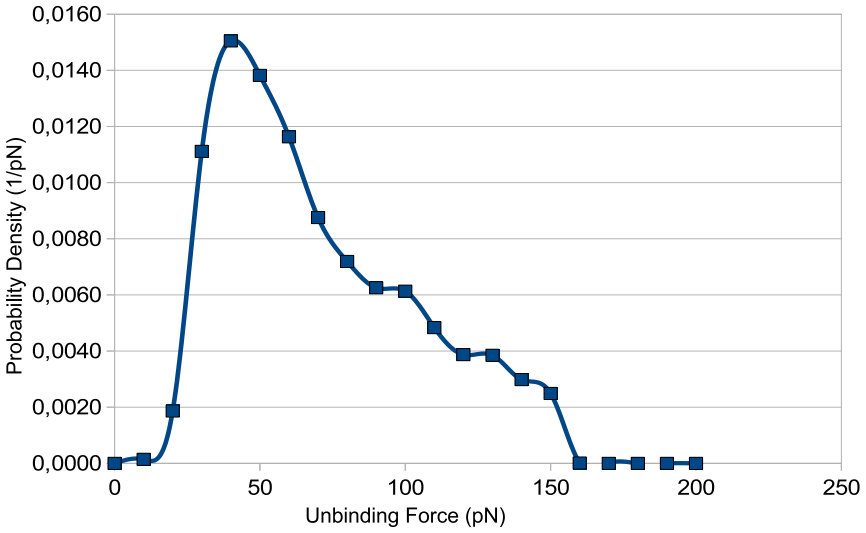

(a)

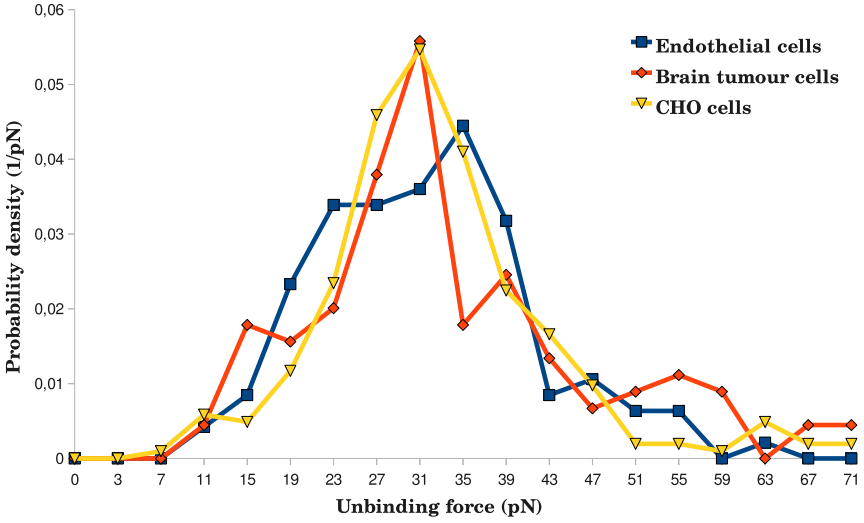

(b)

Figure 6.1: Distribution function of the force of unbinding events (a) when a single bond is acting (Data from [9]) and (b) for different types of cells (Data from [66]).

1b). In particular, Sun et al. [66] did not functionalize the microsphere and allowed a longer resting period on the cell surface, ranging from 2 to 30 seconds. Again, pulling away the cantilever at a constant speed in the range 3–5 μm/sec caused the rupture of one or more adhesive bonds. They used different cell types (Chinese hamster ovary cells, endothelial cells and human brain tumour cells), all showing a mean adhesive strength of a single bond slightly below 30 pN (see Fig.6.1b).

Panorchan et al. [55] attach to the cantilever a cadherin-expressing cell, similar to the cell attached to the substratum. The time of contact is short, in order to have the formation of a very limited number of adhesion bonds. The rupture force is found to increase with the loading rate and it is much smaller when N-cadherin bonds are involved (up to 40 pN) rather than E-cadherin bonds (up to 73 pN for a loading rate of 1000 pN/s and 157 pN for a loading rate of 10000 pN/s).

In order to utilize these data in a multiphase (PDE) model like the one used in this Part, one needs to upscale the results of the above experiments to the macroscopic scale. Specifically, one needs to describe how the attachment/detachment behaviour of the ensemble of adhesion sites linking the cells with the surrounding ECM influence the constitutive equation related to the interaction force between the cellular and the extracellular constituent present in the multiphase model. When describing the behaviour of the actin cytoskeleton, Ölz and Schmeiser [52, 53, 54] faced a similar problem because they needed to relate the link between the adhesion of the single actin filaments to the behaviour of the whole cytoskeleton. Using some of their ideas we here solve the problem in a multiphase framework. According to the rules used to describe the detachment phenomena depending on the type of cells, we find different relationships for the interaction force, that might correspond to the different migration behaviours of the cell populations. First of all, we distinguish between a Darcy–like contribution, related to the tortuosity and the porosity of the extracellular matrix (ECM), and a contribution due to the adhesion of cells on the ECM, related to microscopic quantities like the probability of bond rupture, the density of adhesive molecules on the membrane, the rate of bond formation, the possible continuous renewal of bonds due to spontaneous internalisation and externalisation, the strength of the single bonds. The dynamics generated by such laws presents similarities with the transition from epithelial to mesenhymal cells or from mesenchymal to ameboid motion, and viceversa, though the chemical cues triggering such transitions, that at least as a first approximation influence such microscopic parameters, are out of the scopes of this Part.

The plan of this Part is the following. After an introductory Chapter concerning some aspects of Continuum Mixture Theory, Sections 8.1 and 8.2 deal with the interaction force between different constituents for which adhesion plays a relevant role. In particular we focus on cells and ECM. In Section 8.3 some examples of macroscopic interaction laws are deduced analytically.

Chapter 9 briefly presents few possible developments.

Chapter 7

Basic Mixture Theory

In this Chapter we provide the basic notions of the mechanical *Theory of Continuum Mixtures* that will be instrumental for modeling some gross features of biological tissues and aggregates. A *Virtual Work* format is used to derive balance equations, as done when dealing with the single component theory in Part I. In fact, some notions introduced in the previous part are recalled in this Chapter. Constitutive admissible laws are derived explicitly using *frame invariance* arguments and a *Clausius–Duhem* like inequality. Thus, our approach follows mainly the *Configurational* one adopted in [60]. The slightly different framework we stick to will eventually allow to introduce the notion of *adhesion*, discussed in greater details during the next chapters.

7.1 Kinematics

Consider two *continuous bodies* * $\mathcal{B}^\alpha, \mathcal{B}^\beta$ of the mixture and their *motion* maps χ^α, χ^β defined as (see [13], [14], [36], [56])

$$\chi^\alpha(\cdot, \tau) : \mathcal{B}^\alpha \to \mathcal{B}^\alpha_\tau \subset \mathcal{A}\,, \qquad \tau \in [0, T)\,, \tag{7.1}$$

where $\mathcal{B}^\alpha_\tau$ is the configuration of the $\alpha-$body manifold at time τ, embedded in the affine space $\mathcal{A}$, with translation space $\mathcal{V}$. The definition of χ^β is obviously similar. Let assume that whenever introducing the definition for the constituent α, a similar definition holds in the following also for the constituent β.

We consider the mixture manifold as the Cartesian product of the two body manifolds considered $\mathcal{B}^\alpha, \mathcal{B}^\beta$. Any field $\mathfrak{f}$ defined on such a mixture is, in the most general case, a mapping

$$\mathfrak{f} : \left(X^\alpha \in \mathcal{B}^\alpha, X^\beta \in \mathcal{B}^\beta, t \in [0, T)\right) \mapsto \mathfrak{f}(X^\alpha, X^\beta, t)\,.$$

Other descriptions, such as the Eulerian one in the current configuration at the current time t, can be obtained straightforwardly using the motion definition in (7.1) (see [13], [14], [36]). Moreover we indicate with a superposed dot ($\dot{\square}$) the derivation with respect

*we restrict ourselves to a binary mixture, the generalization to a $n-$component one is straightforward, although cumbersome.

to time and with the nabla (∇) the derivation with respect to space [†] .
We defined, analogously to Part I, the $\alpha-$*Deformation Gradient*

$$\mathbf{F}^\alpha(X^\alpha,t) := \nabla\chi^\alpha(\cdot,t)(X^\alpha) \in \mathsf{Lin}\left(\mathbb{T}_{X^\alpha}\mathcal{B}^\alpha,\mathcal{V}\right) ,$$

The tensor $\mathbf{F}^\alpha$ maps the set of all vectors tangent to $\mathcal{B}^\alpha$ in X^α (say, in $\mathbb{T}_{X^\alpha}\mathcal{B}^\alpha$) onto $\mathcal{V}$. Since some smoothness is assumed for χ^α, a three-dimensional region of the reference configuration cannot collapse under the $\alpha-$motion: loosely speaking, no cracks or compenetration are allowed. We define the spatial *velocity* of a constituent α as

$$\mathbf{v}^\alpha(\cdot,t) := x \in \mathcal{B}_t^\alpha \mapsto \dot{\chi^\alpha}\left(\chi^{\alpha-1}(x,t),\cdot\right)(t) \in \mathcal{V} ,$$

when, clearly, $x \in \mathcal{B}_t^\alpha$. The spatial $\alpha-$*Velocity Gradient* is, as customary:

$$\mathbf{L}^\alpha := \nabla\mathbf{v}^\alpha : [0,T)\times\mathcal{B}_t^\alpha \to \mathsf{Lin}\mathcal{V} .$$

7.2 Dynamics

In this Section we describe the procedure to obtain balance equations and invariance requirements for the mixture at hand. As mentioned before, a standard Virtual Power setting is used. We restrict, for the sake of simplicity, to a first gradient theory.

7.2.1 Virtual Power

We introduce the *momentum exchange vector* and the *Cauchy stress tensor* spatial fields (one for each constituent), respectively:

- $\mathbf{s}^\alpha : [0,T)\times\mathcal{B}_t^\alpha\times\mathcal{B}_t^\beta \to \mathcal{V}$,
- $\mathbf{T}^\alpha : [0,T)\times\mathcal{B}_t^\alpha \to \mathsf{Lin}\mathcal{V}$.

Note that the domain of the Cauchy stress tensor field is, as usual, the body it is referred to. The domain of momentum exchange vector field is the Cartesian product of both bodies. This slight generalization would take into account long range forces between constituents. Obviously, analogous definitions hold for the β constituent.
A key quantity of interest is the *internal power* of the mixture, which we define as (cfr. with Part 1):

$$w^{int} := \int_{\mathcal{B}_t^\alpha\times\mathcal{B}_t^\beta} \left(\mathbf{s}^\alpha\cdot\mathbf{v}^\alpha + \mathbf{s}^\beta\cdot\mathbf{v}^\beta + \mathbf{T}^\alpha\cdot\mathbf{L}^\alpha + \mathbf{T}^\beta\cdot\mathbf{L}^\beta\right) \tag{7.2}$$

where $\mathbf{v}^\alpha : \mathcal{B}_t^\alpha \to \mathcal{V}$, $\mathbf{v}^\beta : \mathcal{B}_t^\beta \to \mathcal{V}$ have the role of arbitrary *test velocity fields*.
We also postulate the power expended by external actions as:

$$w^{ext} := \int_{\mathcal{B}_t^\alpha\times\mathcal{B}_t^\beta} \left(\mathbf{b}^\alpha\cdot\mathbf{v}^\alpha + \mathbf{b}^\beta\cdot\mathbf{v}^\beta\right) + \int_{\partial\left(\mathcal{B}_t^\alpha\times\mathcal{B}_t^\beta\right)} \left(\mathbf{f}^\alpha\cdot\mathbf{v}^\alpha + \mathbf{f}^\beta\cdot\mathbf{v}^\beta\right) \tag{7.3}$$

With respect to the theory outlined in [60], one may note that the virtual powers defined in (7.2) and (7.3) are actually considered as measures defined on the Cartesian product $\mathcal{B}_t^\alpha\times\mathcal{B}_t^\beta$, instead of $\mathcal{B}_t^\alpha\cap\mathcal{B}_t^\beta \subset \mathcal{A}$. Remarkably, our kind of choice of the power does not depend on the existence of the embedding $\mathcal{B}_t^\alpha$, $\mathcal{B}_t^\beta \subset \mathcal{A}$. Such an embedding is, however, sometimes advocated during this work for rendering the discussion more understandable.

[†] We choose not to overload the notations with several "gradient like" symbols, as happens in treatise on Continuum Mechanics. The reader should pay attention to the domain of the field involved in the derivation (the material manifold rather than the current configuration) and interpret the ∇ consistently.

7.2.2 Frame Indifference

A *change of reference frame* is introduced as done in Part 1 (see the footnote at page 14). The map χ^α changes, after such a change of frame, as:

$$\chi^{\alpha *} = o + \mathbf{c} + \mathbf{Q}(\chi^\alpha - o), \tag{7.4}$$

where o, $\mathbf{c}$ and $\mathbf{Q}$ are defined as in the footnote at page 14. Deriving in time the above expression:

$$\mathbf{v}^{\alpha *}(x,\cdot) = \dot{o} + \dot{\mathbf{c}} + \dot{\mathbf{Q}}(x-o) + \mathbf{Q}(\mathbf{v}^\alpha(x,\cdot) - \dot{o}).$$

Then, after the change of frame resumed above, the internal power becomes:

$$\begin{aligned} w^{int\,*} &= \int_{\mathcal{B}_t^\alpha \times \mathcal{B}_t^\beta} \left(\mathbf{s}^{\alpha\,*} \cdot \mathbf{v}^{\alpha *} + \mathbf{s}^{\beta\,*} \cdot \mathbf{v}^{\beta *} + \mathbf{T}^{\alpha\,*} \cdot \mathbf{L}^{\alpha\,*} + \mathbf{T}^{\beta\,*} \cdot \mathbf{L}^{\beta\,*} \right) \\ &= \int_{\mathcal{B}_t^\alpha \times \mathcal{B}_t^\beta} \Big[\mathbf{s}^{\alpha\,*} \cdot \left(\mathbf{w} + \dot{\mathbf{Q}}(p-o) + \mathbf{Q}\mathbf{v}^\alpha \right) + \\ &\qquad \mathbf{s}^{\beta\,*} \cdot \left(\mathbf{w} + \dot{\mathbf{Q}}(q-o) + \mathbf{Q}\mathbf{v}^\beta \right) + \\ &\qquad \mathbf{T}^{\alpha\,*} \cdot \left(\mathbf{Q}\mathbf{L}^\alpha\mathbf{Q}^T + \dot{\mathbf{Q}}\mathbf{Q}^T \right) + \\ &\qquad \mathbf{T}^{\beta\,*} \cdot \left(\mathbf{Q}\mathbf{L}^\beta\mathbf{Q}^T + \dot{\mathbf{Q}}\mathbf{Q}^T \right) \Big]. \end{aligned} \tag{7.5}$$

where $\mathbf{w} := \dot{o} + \dot{\mathbf{c}} - \mathbf{Q}\dot{o}$. For clarity, we have defined:

$$p : (x \in \mathcal{B}_t^\alpha, y \in \mathcal{B}_t^\beta, t \in [0,T)) \mapsto x \in \mathcal{A},$$

$$q : (x \in \mathcal{B}_t^\alpha, y \in \mathcal{B}_t^\beta, t \in [0,T)) \mapsto y \in \mathcal{A}.$$

According to Part I the invariance of the internal power, as stated in the Axiom 2.1, allows us to deduce the following interesting consequences (cfr. with [60]).

(i) Let $\mathbf{w} \in \mathcal{V}$ be arbitrary, with $\dot{\mathbf{Q}} = 0$ and $\mathbf{v}^\alpha = \mathbf{v}^\beta = 0$.
From (7.2) we have $w^{int} = 0$ and Eqn. (7.4) gives $w^{int\,*} = \int_{\mathcal{B}_t^\alpha \times \mathcal{B}_t^\beta} (\mathbf{s}^{\alpha\,*} + \mathbf{s}^{\beta\,*}) \cdot \mathbf{w}$.
From the Axiom 2.1 it turns out, after localizing, that: $\mathbf{s}^{\alpha\,*} + \mathbf{s}^{\beta\,*} = 0$. The latter equation can be interpreted as a balance law for the momentum exchange vectors.

(ii) Let $\mathbf{Q} \in \mathsf{Ort}\mathcal{V}$ be arbitrary, with $\dot{\mathbf{Q}} = 0$ and $\mathbf{v}^\alpha$, $\mathbf{v}^\beta$ arbitrary homogeneous fields.
The equality in Axiom 2.1, looking at the expressions of the internal powers in (7.2, 7.5) and using the result obtained in `(i)`, implies:

$$\int_{\mathcal{B}_t^\alpha \times \mathcal{B}_t^\beta} \left(\mathbf{s}^\alpha \cdot \mathbf{v}^\alpha + \mathbf{s}^\beta \cdot \mathbf{v}^\beta \right) = \int_{\mathcal{B}_t^\alpha \times \mathcal{B}_t^\beta} \left(\mathbf{s}^{\alpha\,*} \cdot \mathbf{Q}\mathbf{v}^\alpha + \mathbf{s}^{\beta\,*} \cdot \mathbf{Q}\mathbf{v}^\beta \right).$$

taking $\mathbf{v}^\beta = 0$ in the latter and localizing we find $\mathbf{s}^{\alpha\,*} = \mathbf{Q}\mathbf{s}^\alpha$. Conversely, taking $\mathbf{v}^\alpha = 0$, we obtain $\mathbf{s}^{\beta\,*} = \mathbf{Q}\mathbf{s}^\beta$. Taking into account the item `(i)`, one also has $\mathbf{s}^\alpha = -\mathbf{s}^\beta$. Thus, from now on we call $\mathbf{s} := \mathbf{s}^\alpha = -\mathbf{s}^\beta$.

(iii) Let $\mathbf{Q} \in \mathsf{Ort}\mathcal{V}$ be arbitrary, with $\dot{\mathbf{Q}} = 0$ and $\mathbf{v}^\alpha$, $\mathbf{v}^\beta$ arbitrary.
The equality in Axiom 2.1, together with the previous result in items `(i)-(ii)`

and Eqns. (7.2), (7.5), implies:

$$\int_{\mathcal{B}_t^\alpha \times \mathcal{B}_t^\beta} \left(\mathbf{T}^\alpha \cdot \mathbf{L}^\alpha + \mathbf{T}^\beta \cdot \mathbf{L}^\beta\right) = \int_{\mathcal{B}_t^\alpha \times \mathcal{B}_t^\beta} \mathbf{T}^{\alpha\,*} \cdot \left(\mathbf{Q}\mathbf{L}^\alpha\mathbf{Q}^T\right) + \mathbf{T}^{\beta\,*} \cdot \left(\mathbf{Q}\mathbf{L}^\beta\mathbf{Q}^T\right).$$

from which, as customary: $\mathbf{T}^{\alpha\,*} = \mathbf{Q}\mathbf{T}^\alpha\mathbf{Q}^T$.

(iv) Eventually, consider $\mathbf{Q} \in \mathsf{Ort}\mathcal{V}$ and $\dot{\mathbf{Q}}\mathbf{Q}^T \in \mathsf{Skw}\mathcal{V}$ arbitrary.
The equality in Axiom 2.1, together with the previous results in items `(i)-(ii)-(iii)` and Eqns. (7.2), (7.5), implies:

$$\begin{aligned} 0 &= \int_{\mathcal{B}_t^\alpha \times \mathcal{B}_t^\beta} \left(\mathbf{s}^* \cdot \dot{\mathbf{Q}}(p-q) + (\mathbf{T}^{\alpha\,*} + \mathbf{T}^{\beta\,*}) \cdot \dot{\mathbf{Q}}\mathbf{Q}^T\right) \\ &= \int_{\mathcal{B}_t^\alpha \times \mathcal{B}_t^\beta} \left(\mathbf{T}^\alpha + \mathbf{T}^\beta + \mathbf{s} \otimes (p-q)\right) \cdot \mathbf{Q}^T\dot{\mathbf{Q}}. \end{aligned}$$

from which (since $\mathbf{Q}^T\dot{\mathbf{Q}}$ is an arbitrary skew tensor):

$$\mathsf{skw}\left(\mathbf{T}^\alpha + \mathbf{T}^\beta + \mathbf{s} \otimes (p-q)\right) = 0.$$

In the classical literature adopting a balance law approach rather than a configurational one, the equations obtained above in `(i)` and `(iv)` are better known as the balance of momentum exchange [56] and of the moment of momentum respectively [14, 56]. The equations obtained in `(ii)` and in `(iii)` represent the usual invariance requirements for the momentum exchange and for the Cauchy stress respectively [14].

7.2.3 Balance Laws

Fundamental balance laws can be derived from the balance of virtual power, as stated in [29] and briefly sketched in the Part I of this dissertation. Their derivation consists in a standard application of Stokes–Gauss theorem [12] and localization arguments, granted the arbitrarity of the test velocity fields. If we substitute the expressions (7.2) and (7.3) in the statement of Axiom 2.2, if we incorporate the results contained in the items `(i)` and `(ii)` of the previous Section, we eventually get:

$$\begin{aligned} &\int_{\mathcal{B}_t^\alpha \times \mathcal{B}_t^\beta} \left(\mathbf{s} \cdot (\mathbf{v}^\alpha - \mathbf{v}^\beta) + \mathbf{T}^\alpha \cdot \mathbf{L}^\alpha + \mathbf{T}^\beta \cdot \mathbf{L}^\beta\right) = \\ &\int_{\mathcal{B}_t^\alpha \times \mathcal{B}_t^\beta} \left(\mathbf{b}^\alpha \cdot \mathbf{v}^\alpha + \mathbf{b}^\beta \cdot \mathbf{v}^\beta\right) + \int_{\partial\left(\mathcal{B}_t^\alpha \times \mathcal{B}_t^\beta\right)} \left(\mathbf{f}^\alpha \cdot \mathbf{v}^\alpha + \mathbf{f}^\beta \cdot \mathbf{v}^\beta\right) \end{aligned} \tag{7.6}$$

Since $\mathbf{L}^\alpha = \nabla\mathbf{v}^\alpha$, using Gauss theorem we can rewrite:

$$\int_{\mathcal{B}_t^\alpha \times \mathcal{B}_t^\beta} \mathbf{T}^\alpha \cdot \mathbf{L}^\alpha = \int_{\mathcal{B}_t^\alpha \times \mathcal{B}_t^\beta} -\mathrm{div}\,\mathbf{T}^\alpha \cdot \mathbf{v}^\alpha + \int_{\partial\mathcal{B}_t^\alpha \times \mathcal{B}_t^\beta} \mathbf{T}^\alpha\mathbf{n}^\alpha \cdot \mathbf{v}^\alpha$$

where $\mathbf{n}^\alpha$ is the normal vector to the material surface $\partial\mathcal{B}_t^\alpha$. The momentum balance equations for the α constituent can be obtained choosing a $\mathbf{v}^\alpha$ field vanishing at the

boundary $\partial\mathcal{B}_t^\alpha$ and taking $\mathbf{v}^\beta = 0$. Using eqn. (7.6), the above consequence of Gauss theorem and remembering that $\mathbf{T}^\alpha$ and $\mathbf{v}^\alpha$ actually depend only on $\mathcal{B}_t^\alpha$:

$$\int_{\mathcal{B}_t^\alpha} \mathbf{v}^\alpha \cdot \left(-(\mathsf{meas}\,\mathcal{B}_t^\beta)\,\mathrm{div}\mathbf{T}^\alpha + \int_{\mathcal{B}_t^\beta} \mathbf{s} \right) = (\mathsf{meas}\,\mathcal{B}_t^\beta) \int_{\mathcal{B}_t^\alpha} \mathbf{v}^\alpha \cdot \mathbf{b}^\alpha.$$

After a standard localization argument on $\mathcal{B}_t^\alpha$, the latter gives:

$$-\,\mathrm{div}\mathbf{T}^\alpha + \mathbf{m}^\alpha = \mathbf{b}^\alpha \quad \text{on } \mathcal{B}_t^\alpha \tag{7.7}$$

where $\mathbf{m}^\alpha := \dfrac{1}{\mathsf{meas}\,\mathcal{B}_t^\beta} \displaystyle\int_{\mathcal{B}_t^\beta} \mathbf{s}$. This equation is the balance of the momentum of the species α at the net of external actions, either due to the other constituent β or due to the environment. The equation for the β constituent is similarly obtained reversing the role of $\mathbf{v}^\alpha$ and $\mathbf{v}^\beta$.

Boundary conditions appears to be trivial with this approach (cfr. with [60]). Playing with the Stokes–Gauss Theorem when substituting the expressions (7.2) and (7.3) in the Axiom 2.2, using the balance equation (7.7) one easily finds:

$$\int_{\partial\mathcal{B}_t^\alpha \times \mathcal{B}_t^\beta} \mathbf{T}^\alpha \mathbf{n}^\alpha \cdot \mathbf{v}^\alpha + \int_{\partial\mathcal{B}_t^\beta \times \mathcal{B}_t^\alpha} \mathbf{T}^\beta \mathbf{n}^\beta \cdot \mathbf{v}^\beta = \int_{\partial\left(\mathcal{B}_t^\alpha \times \mathcal{B}_t^\beta\right)} \left(\mathbf{f}^\alpha \cdot \mathbf{v}^\alpha + \mathbf{f}^\beta \cdot \mathbf{v}^\beta \right).$$

Next, using the Leibniz rule $\partial(\mathcal{B}_t^\alpha \times \mathcal{B}_t^\beta) = (\partial\mathcal{B}_t^\alpha \times \mathcal{B}_t^\beta) \cup (\partial\mathcal{B}_t^\beta \times \mathcal{B}_t^\alpha)$ and letting $\mathbf{v}^\beta = 0$, it can be reached:

$$\mathbf{T}^\alpha \mathbf{n}^\alpha = \mathbf{f}^\alpha.$$

The analogous boundary conditions for the β constituent are similarly obtained reversing the role of $\mathbf{v}^\alpha$ and $\mathbf{v}^\beta$. Since the latter are of little importance for our scope, we skip the discussion on this controversial subject [41].

7.3 Constitutive Issues

We now sketch some notions of the *constitutive theory* for the mixture at hand.
A *constitutive field* c will be here provided with a *constitutive mapping* $\hat{c}$ such that

$$c(X^\alpha, X^\beta, t) = \hat{c}(\chi^\alpha, \chi^\beta; X^\alpha, X^\beta)$$

The constitutive dependence on the motions only follows from the choice of dealing with a purely mechanical theory. Since we aim to keep the theory at the minimum level of complexity, we choose to work with $c = \left(\psi, \mathbf{T}^\alpha, \mathbf{T}^\beta, \mathbf{s}\right)$, ψ being the so-called *free energy*. The existence of the latter is, as a matter of fact, postulated [42].

We then restrict the constitutive map form by the use of the objectivity principle. Moreover, via an entropy–like inequality, we exploit the relationship between stress tensors, momentum exchange vectors and the free energy postulated before.

7.3.1 The Free Energy

We define the free energy in a material description, this only because the dissipation inequality would be easier to exploit. The latter is presumed to be an additive scalar–valued continuous measure, reading:

$$\Psi := \int_{\mathcal{B}^\alpha \times \mathcal{B}^\beta} \psi,$$

where $\psi : [0,T) \times \mathcal{B}^\alpha \times \mathcal{B}^\beta \to \mathbb{R}$ is the free energy density (also called free energy in the following, for brevity). The constitutive map $\hat{\psi}$ associated to ψ, is supposed to be objective, i.e.:

$$\hat{\psi}(\chi^\alpha, \chi^\beta) = \hat{\psi}(\chi^{\alpha *}, \chi^{\beta *})$$

Such a condition leads to the following considerations (please refer, for the definitions to the footnote at page 14 and to (7.4)):

(i) set $\mathbf{Q} = \mathbf{1}$ and $\mathbf{c}$ arbitrary:

$$\hat{\psi}(\chi^\alpha, \chi^\beta) - \hat{\psi}(\chi^\alpha + \mathbf{c}, \chi^\beta + \mathbf{c}) = 0$$

if we assume regularity, for small $\mathbf{c}$ [‡]:

$$\Big((\partial_1 + \partial_2)\hat{\psi}\Big)\,\mathbf{c} = 0$$

which is a hyperbolic differential equation whose well-known general solution is:

$$\psi = \hat{\psi}(\chi^\alpha - \chi^\beta)$$

(ii) set $\mathbf{Q}$ arbitrary:

$$\hat{\psi}(\chi^\alpha - \chi^\beta) = \hat{\psi}(\mathbf{Q}(\chi^\alpha - \chi^\beta))$$

that means that $\hat{\psi}$ is an isotropic scalar function, see [42].

The considerations given in the two item above are, to the best of our knowledge, not found in the literature although quite simple to obtain. Such a line of reasoning gives the important result:

$$\psi = \hat{\psi}(|\chi^\alpha - \chi^\beta|).$$

7.3.2 Dissipation Principle

A simplified Thermodynamic framework is now introduced. For later convenience, we introduce a material description for the fields, according to the identity:

$$\mathfrak{f}(X^\alpha, X^\beta, t) = \mathfrak{f}(\chi^{\alpha\,-1}(x,t), \chi^{\beta\,-1}(y,t), t)$$

for any $x = \chi^\alpha(X^\alpha, t) \in \mathcal{B}_t^\alpha$, $y = \chi^\beta(X^\beta, t) \in \mathcal{B}_t^\beta$. From here to the end of the Section we consider a material description of the fields $(\mathbf{v}^\alpha, \mathbf{v}^\beta, \mathbf{L}^\alpha, \mathbf{L}^\beta, \mathbf{T}^\alpha, \mathbf{T}^\beta)$ without changing their name, thus abusing the notations slightly as customary in Continuum Mechanics. A Clausius–Duhem type of inequality is assumed as a dissipation principle [60] (in the material manifold):

$$\dot{\Psi} \leq w^{ext}.$$

Using the Axiom 2.2 and the expression of the internal power (7.2), the above inequality rewrites:

$$\dot{\Psi} - \int_{\mathcal{B}_t^\alpha \times \mathcal{B}_t^\beta} \left(\mathbf{s} \cdot (\mathbf{v}^\alpha - \mathbf{v}^\beta) + \mathbf{T}^\alpha \cdot \mathbf{L}^\alpha + \mathbf{T}^\beta \cdot \mathbf{L}^\beta\right) \leq 0 \tag{7.8}$$

[‡]We recall that ∂_i means the derivative of the function at hand with respect to the $i-$th argument.

Under this assumption, we can localize Eqn. (7.8) in order to get:

$$\dot{\psi} - \mathbf{s} \cdot (\mathbf{v}^\alpha - \mathbf{v}^\beta) - \mathbf{T}^\alpha \cdot \mathbf{L}^\alpha - \mathbf{T}^\beta \cdot \mathbf{L}^\beta \leq 0. \tag{7.9}$$

Then, we postulate a *simple material behavior* [42]. This writes in mathematical terms as:

$$\begin{aligned}&\psi(X^a, X^b, t) = \\ &\hat{\psi}(\left|\chi^\alpha(X^\alpha, t) - \chi^\beta(X^\beta, t)\right|, \left|\mathbf{v}^\alpha(X^\alpha, t) - \mathbf{v}^\beta(X^\beta, t)\right|, \mathbf{F}^\alpha(X^\alpha, t), \mathbf{F}^\beta(X^\beta, t)).\end{aligned}$$

Taking into account the above relations, we can follow the usual *Coleman–Noll* exploitation of (7.9) (see [13], [29]):

$$\begin{aligned}&(\partial_1\hat{\psi})\frac{\chi^\alpha - \chi^\beta}{|\chi^\alpha - \chi^\beta|} \cdot (\mathbf{v}^\alpha - \mathbf{v}^\beta) + (\partial_2\hat{\psi})\frac{\mathbf{v}^\alpha - \mathbf{v}^\beta}{|\mathbf{v}^\alpha - \mathbf{v}^\beta|} \cdot (\dot{\mathbf{v}^\alpha} - \dot{\mathbf{v}^\beta}) \\ &+ (\partial_3\hat{\psi}) \cdot \dot{\mathbf{F}}^\alpha + (\partial_4\hat{\psi}) \cdot \dot{\mathbf{F}}^\beta - \mathbf{s} \cdot (\mathbf{v}^\alpha - \mathbf{v}^\beta) - \mathbf{T}^\alpha \cdot \mathbf{L}^\alpha - \mathbf{T}^\beta \cdot \mathbf{L}^\beta \leq 0.\end{aligned}$$

The latter, using the standard argument of arbitrary and independent prescription of the fields $\left|\chi^\alpha(X^\alpha, t) - \chi^\beta(X^\beta, t)\right|, \left|\mathbf{v}^\alpha(X^\alpha, t) - \mathbf{v}^\beta(X^\beta, t)\right|, \mathbf{F}^\alpha(X^\alpha, t), \mathbf{F}^\beta(X^\beta, t)$ (cfr. e.g. with [28]), leads to:

$$\begin{cases}\partial_2\hat{\psi} &= 0, \\ \hat{\mathbf{s}} &= (\partial_1\hat{\psi})\frac{\chi^\alpha - \chi^\beta}{|\chi^\alpha - \chi^\beta|} + \mathbf{s}_+, \\ \hat{\mathbf{T}}^\alpha &= (\partial_3\hat{\psi})\mathbf{F}^{\alpha\,T}, \\ \hat{\mathbf{T}}^\beta &= (\partial_4\hat{\psi})\mathbf{F}^{\beta\,T}\end{cases} \tag{7.10}$$

where the additional term with the subscript '+' satisfies the residual inequality:

$$\mathbf{s}_+ \cdot (\mathbf{v}^\alpha - \mathbf{v}^\beta) \leq 0\,. \tag{7.11}$$

7.4 Further Discussions

The constitutive restrictions (7.10) and (7.11) are quite standard, see [13, 56].

The first equation in (7.10) state the independency of the free energy from the velocity fields.

Moreover, the Cauchy stress tensors can be prescribed exactly in the same way as for a single component theory, as stated in the third and fourth equations in (7.10). A useful remark is that, since $\mathbf{T}^\alpha$ (resp. $\mathbf{T}^\beta$) is a field defined only on $\mathcal{B}_t^\alpha(\mathcal{B}_t^\beta)$ (as defined in Section 7.2), then it can constitutively depend only on $\mathbf{F}^\alpha$ (resp. $\mathbf{F}^\beta$). The latter sentence means $\mathbf{T}^\alpha = \hat{\mathbf{T}}^\alpha(\mathbf{F}^\alpha)$ (resp. $\mathbf{T}^\beta = \hat{\mathbf{T}}^\beta(\mathbf{F}^\beta)$). From the third and the fourth relationship in (7.10), following the above reasoning:

$$\partial_3\partial_4\hat{\psi} = \partial_1\partial_3\hat{\psi} = \partial_1\partial_4\hat{\psi} = 0.$$

Including the result encapsulated in the first equation in (7.10), one can deduce the important splitting of the free energy:

$$\psi(X^\alpha, X^\beta, t) = \hat{\psi}_{\mathbf{s}}\left(\left|\chi^\alpha(X^\alpha, t) - \chi^\beta(X^\beta, t)\right|\right) + \hat{\psi}_\alpha\left(\mathbf{F}^\alpha(X^\alpha, t)\right) + \hat{\psi}_\beta\left(\mathbf{F}^\beta(X^\beta, t)\right).$$

The three addenda on the r.h.s. above take into account the energy associated with links between material points of different constituents ($\hat{\psi}_{\mathbf{s}}$), the potential energy of the internal stress for the constituent α ($\hat{\psi}_{\alpha}$) and β ($\hat{\psi}_{\beta}$), respectively.

The second equation of the system (7.10), together with the residual inequality (7.11), restricts the possible form of the momentum exchange vector. Apart from its dissipative part $\mathbf{s}_+$, the latter can essentially take into account spring–like type of links between material points [56]. Interestingly, such energetic–type forces are directed along the vector connecting the material points in exam. The dissipative part of the momentum exchange vector can be taken, for example:

$$\mathbf{s}_+(x,y) = \mathbf{M}(|x-y|)\big(\mathbf{v}^{\alpha}(x) - \mathbf{v}^{\beta}(y)\big).$$

With $\mathbf{M}$ a positive–definite tensor. When $\mathbf{s}_+$ satisfies the equation above for $x = y$ (x and y viewed as elements of $\mathcal{A}$) and, if $\mathbf{s}_+$ is supposed to vanish when $x \neq y$, one has the so-called Darcy law [14]. In view of the definition of $\mathbf{m}^{\alpha}$ appearing in Eqn. (7.7), if we (constitutively) demand a suitable measure on $\mathcal{B}^{\beta}$ concentrated on the set $\{(x,y) \in \mathcal{A}^2 \; s.t. \; x = y\}$ we find:

$$\mathbf{m}^{a}(x) = \mathbf{M}\big(\mathbf{v}^{\alpha}(x) - \mathbf{v}^{\beta}(x)\big).$$

The latter is a short range constitutive map largely used to model solid–fluid friction in porous media [36]. Remarkably, in the case of Darcy law, the balance of momentum exchange found in the items `(i)` and `(ii)` at page 67 implies $\mathbf{m}^{\alpha} = \mathbf{m}^{\beta}$.

We now turn into the discussion of an invariance requirement in which the momentum exchange vector enters in a substantial way. In the item `(iv)` of the Section 2.2 we have found:

$$\mathsf{skw}\left(\mathbf{T}^{\alpha}(x) + \mathbf{T}^{\beta}(y) + \mathbf{s}(x,y) \otimes (x-y)\right) = 0.$$

In view of the first equation in (7.10) the latter is equivalent to:

$$\mathsf{skw}\left(\mathbf{T}^{\alpha}(x) + \mathbf{T}^{\beta}(y)\right) = \mathsf{skw}\left(\mathbf{s}_+(x,y) \otimes (y-x)\right).$$

In the case we assume a Darcy law of friction for $\mathbf{s}_+$, this further simplifies to:

$$\mathsf{skw}\left(\mathbf{T}^{\alpha}(x) + \mathbf{T}^{\beta}(y)\right) = 0.$$

Since the latter holds whatever $x \in \mathcal{B}_t^{\alpha}$ and $y \in \mathcal{B}_t^{\beta}$ are, it implies:

$$\mathbf{T}^{\alpha} \in \mathsf{Sym}(\mathcal{V}) \text{ and } \mathbf{T}^{\beta} \in \mathsf{Sym}(\mathcal{V}).$$

This point renders our theory slightly different in predictions than those contained in [60] and classical theories [13, 56, 68]. All those theories end up with the weaker requirement $\mathsf{skw}\left(\mathbf{T}^{\alpha}(x) + \mathbf{T}^{\beta}(x)\right) = 0$.

Chapter 8

Mixture Theory Modeling Adhesion

This chapter is entirely devoted to the introduction of the notion of *adhesion* and to the related discussions, as advocated in the introduction. The first section introduces a simplified kinematics with respect to the one sketched in the previous Chapter. As shown in the other two sections of this Chapter, this slight simplification still allows to describe mathematically the adhesive bonds in a mixture framework in a more straightforward way.

8.1 Reduced Kinematics

In this section, we are going to describe a special type of mixture, in which the fields are allowed to depend on the point of the bodies that were superposed somewhere in time, for instance, because of the formation of some adhesive bonds. In such a way, we avoid the complication induced by the introduction of fields that depend on points belonging to both bodies. As a paradigmatic example, think to the momentum exchange vector $\mathbf{s}$ defined in Chapter 7.
As sketched in Fig. 8.1, let then $\chi^\beta(X^\beta, t-a) = \chi^\alpha(X^\alpha, t-a) = \xi$. We will state for every field $\mathfrak{f}$ that

$$\mathfrak{f}(X^\alpha, X^\beta, t) = \tilde{\mathfrak{f}}(\xi, t)\,. \tag{8.1}$$

It is also useful to introduce the quantity

$$\mathbf{r}^{\alpha\beta}(X^\alpha, X^\beta, t) := \chi^\alpha(X^\alpha, t) - \chi^\beta(X^\beta, t)\,. \tag{8.2}$$

Referring to Fig.8.1, since the body points X^α and X^β were superposed at time $t-a$, we remark that

$$X^\beta = \chi^{\beta^{-1}}(\xi, t-a) = \chi^{\beta^{-1}}(\chi^\alpha(X^\alpha, t-a), t-a)\,. \tag{8.3}$$

The vector field $\mathbf{r}^{\alpha\beta}$ can then be written as

$$\mathbf{r}^{\alpha\beta}(X^\alpha, X^\beta, t) = \chi^\alpha(X^\alpha, t) - \chi^\beta(\chi^{\beta^{-1}}(\chi^\alpha(X^\alpha, t-a), t-a), t)\,. \tag{8.4}$$

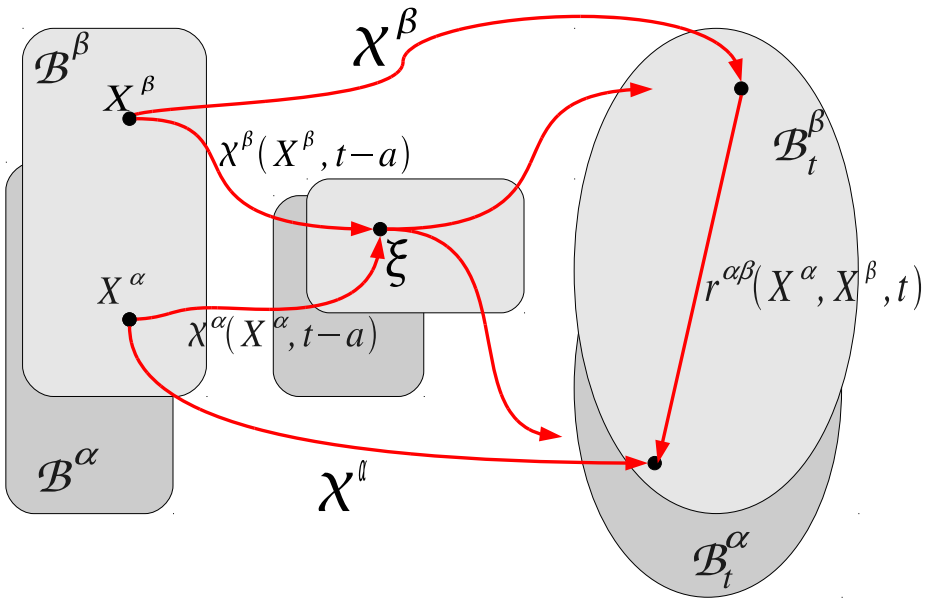

Figure 8.1: Superposition of material points of different bodies.

Remark 8.1. *It is worth to stress again some facts. In this special kind of mixture, any field can be described uniquely by prescribing the $\alpha-$point X^α and the time lapse a measuring the time passed from the superposition. It means that, instead of a product of two body manifolds (as done in the general treatment in Chapter 7), we can refer to the $4-$dimensional manifold $\mathcal{B}^\alpha \times [0,t)$. This kind of mixtures requires, roughly speaking, an additional scalar coordinate to fully specify a field (in contrast with all previous theories, see [13], [14], [15], [36], [56]). So,by a field $\mathfrak{f}$ on the mixture, we shall intend the mapping*

$$\mathfrak{f}: (X^\alpha \in \mathcal{B}^\alpha, a \in [0,+\infty), t \in [0,+\infty)) \mapsto \mathfrak{f}(X^\alpha, a, t)\,.$$

From now to the end of the chapter we intend that any field is of the above type, if not explicitly stated in a different way.

We point out that the material derivative, using the type of description suggested in the remark above, is well defined as

$$\dot{\mathfrak{f}}(X^\alpha, a, t) := \lim_{h\to 0} \frac{\mathfrak{f}(X^\alpha, a+h, t+h) - \mathfrak{f}(X^\alpha, a, t)}{h} \equiv \mathfrak{f}'(X^\alpha, a, \cdot)(t) + \mathfrak{f}'(X^\alpha, \cdot, t)(a)\,, \tag{8.5}$$

that holds constant the time of superposition $t-a$. For fields declared to be independent from a: $\dot{\mathfrak{f}}(X^\alpha, t) \equiv \mathfrak{f}'(X^\alpha, a, \cdot)(t)$.

It is interesting for future developments to compare here the typical lifetime of a bond A with the characteristic time T related to cell motion, that can be related to the cell size L and the characteristic velocity of cell motion V through $T = L/V$. T is then the time needed by a cell to move across a cell length, that using physiological values is at least of the order of few minutes. On the other hand, due to the fast trafficking of adhesion molecules coming back and forth from the membrane A is of the order of few seconds (see, for instance, [9, 69, 72]). This behaviour, that from the biological

viewpoint is understood to lead to cell plasticity, from the mathematical viewpoint leads to the existence of a small parameter $\epsilon = A/T$, that allows to study the limit $\epsilon \ll 1$ that in dimensional terms corresponds to what we will denote with the dimensional limit $a \to 0$.

Defining $x := \chi^\alpha(X^\alpha, t)$, for small a one has

$$\chi^\alpha(X^\alpha, t-a) \simeq x - a\frac{\partial}{\partial t}\chi^\alpha(X^\alpha, t), \qquad a \to 0. \tag{8.6}$$

Next we consider

$$\begin{aligned}
&\chi^{\beta^{-1}}\left(x - a\frac{\partial}{\partial t}\chi^\alpha(X^\alpha, t), t-a\right)\\
&\simeq \chi^{\beta^{-1}}(x,t) - a\frac{\partial}{\partial t}(\chi^{\beta^{-1}})(x,t) - a\,\nabla(\chi^{\beta^{-1}})(x,t)\,[\mathbf{v}^\alpha(X^\alpha,t)] \qquad (8.7)\\
&= \chi^{\beta^{-1}}(x,t) + a\,(\mathbf{F}^\beta)^{-1}(x,t)\left[\mathbf{v}^\beta(\chi^{\beta^{-1}}(x,t),t)\right] - a\,(\mathbf{F}^\beta)^{-1}(x,t)\,[\mathbf{v}^\alpha(X^\alpha,t)], \qquad a \to 0\,,
\end{aligned}$$

where, as in the previous Chapter, we stress that ∇ means the differentiation respect to the first argument of the function at hand (i.e, it is a derivation in space). Remarkably, in the calculations above, we used the fact that

$$\frac{\partial}{\partial t}\chi^{\beta^{-1}}(x,t) = -\mathbf{F}^{\beta^{-1}}\left[\mathbf{v}^\beta(\chi^{\beta^{-1}}(x,t),t)\right], \tag{8.8}$$

and

$$\nabla\,\chi^{\beta^{-1}}(x,t) = \mathbf{F}^{\beta^{-1}}(x,t)\,. \tag{8.9}$$

Using (8.6) and (8.7), we can approximate (8.4) as

$$\begin{aligned}
\mathbf{r}^{\alpha\beta} &\simeq x - \chi^\beta\Bigg(\chi^{\beta^{-1}}(x,t) +\\
&+ a\,\mathbf{F}^{\beta^{-1}}(x,t)\frac{\partial}{\partial\tau}\chi^\beta\left(\chi^{\beta^{-1}}(x,t),\tau\right)\Big|_{\tau=t} - a\,\mathbf{F}^{\beta^{-1}}(x,t)\frac{\partial}{\partial t}\chi^\alpha(X^\alpha,t)\;,\;t\Bigg)\\
&\simeq -a\,\nabla\chi^\beta(\cdot,t)\Big|_{\chi^{\beta^{-1}}(x,t)}\mathbf{F}^{\beta^{-1}}(x,t)\left[\frac{\partial}{\partial\tau}\chi^\beta\left(\chi^{\beta^{-1}}(x,t),\tau\right)\Big|_{\tau=t} - \frac{\partial}{\partial t}\chi^\alpha(X^\alpha,t)\right]
\end{aligned}$$

for $a \to 0$. Therefore, since $\nabla\chi^\beta(\cdot,t)(\chi^{\beta^{-1}}(x,t)) = \mathbf{F}^\beta(\chi^{\beta^{-1}}(x,t),t)$

$$\begin{aligned}
\mathbf{r}^{\alpha\beta}(x,t) &\simeq -a\left[\frac{\partial}{\partial\tau}\chi^\beta\left(\chi^{\beta^{-1}}(x,t),\tau\right)\Big|_{\tau=t} - \frac{\partial}{\partial t}\chi^\alpha(X^\alpha,t)\right]\\
&\simeq a\,\left(\mathbf{v}^\alpha(x,t) - \mathbf{v}^\beta(x,t)\right), \qquad a \to 0\,,
\end{aligned} \tag{8.10}$$

where the Eulerian description of velocities is used. In other words, (8.10) means

$$\mathbf{r}^{\alpha\beta\prime}(x,\cdot,t)(0) = \mathbf{v}^\alpha(x,t) - \mathbf{v}^\beta(x,t)\,. \tag{8.11}$$

8.2 Iteraction Force between Constituents

Equation (7.7) of Chapter 7 represents the momentum balance for a constituent of the mixture. For convenience we now recall it:

$$-\mathrm{div}\mathbf{T}^\alpha + \mathbf{m}^\alpha = \mathbf{b}^\alpha \quad \text{on } \mathcal{B}_t^\alpha,$$

where $\mathbf{T}_\alpha$ is the Cauchy partial stress tensor, $\mathbf{m}_\alpha = (1/\mathsf{meas}\,\mathcal{B}_t^\beta)\int_{\mathcal{B}_t^\beta}\mathbf{s}$ and $\mathbf{s}$ is the so–called momentum exchange. In this Section we will focus on this last term. The vector field $\mathbf{m}^\alpha$ only measures the forces acting on the α-constituent due to its interactions with the other constituents of the mixture. It is also worth recalling that the momentum exchange $\mathbf{s}$ is intrinsically defined on the whole mixture manifold, while other quantities, like stress tensors and densities, are defined only on the single body and no meaningful extension exists out of this manifold. Also balance equations are defined on the body *per se*, but the presence of interaction forces constitutes a link among the bodies.

For sake of clarity, the reader may think of the indices α and β as those referring respectively to the cell population and to the extracellular matrix, though the argument has a wider generality and can be, for instance, applied to cells of different type. When dealing with cell-ECM interactions, we distinguish in $\mathbf{m}^\alpha$ two types of contributions: the first is related to the tortuosity of the extracellular matrix and therefore to the fact that the cells must move to an intricate network of fibers. Hence, even in absence of adhesive interactions the ensemble of cells move in a porous-like medium so that the interaction force can be modeled by the classical term leading to Darcy's law (see the last section of chapter 7)

$$\mathbf{m}_D^\alpha(x,t) = \mathbf{M}(\mathbf{v}^\alpha(x,t) - \mathbf{v}^\beta(x,t)) \tag{8.12}$$

where the spatial description of the fields is used, since Darcy's law is a local type interaction between point superposed in the current configuration. The second is related to the adhesion between the constituents. Therefore, even if cells were in a straight channel in the ECM and the force were aligned to it, the ensemble of cells would still experience a traction force $\mathbf{m}_{ad}^\alpha$ due to the adhesive interaction with the ECM.

In further detail, we call *microscopic force* $\mathbf{F}_{mic}^\alpha(X^\alpha, X^\beta, t)$ the part of momentum exchange (called $\mathbf{s}$ above and in Chapter 7) due to the adhesive interaction between $X^\beta \in \mathcal{B}^\beta$ and $X^\alpha \in \mathcal{B}^\alpha$. The total momentum exchanged in X^α with the manifold $\mathcal{B}^\beta$ due to adhesion forces, according to the definition of $\mathbf{m}^\alpha$ after the (7.7), reads:

$$\mathbf{m}_{ad}^\alpha(X^\alpha, t) := \int_{\mathcal{B}^\beta} \mathbf{F}_{mic}^{\alpha\beta}(X^\alpha, Y, t)\, dY. \tag{8.13}$$

Using the hypothesis in (8.1) we have the nice formula

$$\mathbf{m}_{ad}^\alpha(X^\alpha, t) = \int_0^{+\infty} \mathbf{F}_{mic}^{\alpha\beta}(X^\alpha, a, t)\mu(da)\,. \tag{8.14}$$

where $\mu(da)$ is a measure to be *a priori* given. For reasons that will become apparent later, we define the dummy a in the Eq. (8.14) as the *age of the bond* between the two considered material points. The range of the integration with respect to the latter spans from 0 (adhesion bonds born at current time) to ∞ (adhesion bonds formed at the

"beginning"). Clarifying examples will be exploited in the following section. In view of the items (i) and (ii) at page 67:

$$\mathbf{F}^{\alpha\beta}_{mic}(X^\alpha, X^\beta, t) + \mathbf{F}^{\beta\alpha}_{mic}(X^\beta, X^\alpha, t) = 0, \qquad \forall\, X^\alpha \in \mathcal{B}^\alpha, X^\beta \in \mathcal{B}^\beta. \tag{8.15}$$

As advocated in Chapter 7, we take as *basic fields* only the motions χ^α, χ^β as defined in (2.1) since we want to keep the discussion at the minimum level of complexity.
Then, taking adhesion into account, we introduce the scalar internal variable $f^{\alpha\beta}$ related to the probability of forming an adhesion bond between an $\alpha-$material point and a $\beta-$material point.

Using the field hypothesis (8.1), the number density of bonds formed at time t is

$$N^{\alpha\beta}(X^\alpha, t) = \int_0^{+\infty} f^{\alpha\beta}(X^\alpha, a, t)\, da\,. \tag{8.16}$$

This internal variable has its own balance equation suggested by population dynamics theory [34] or kinetic theory [10]

$$\dot{f}^{\alpha\beta} := \frac{\partial f^{\alpha\beta}}{\partial t} + \frac{\partial f^{\alpha\beta}}{\partial a} = -\eta^{\alpha\beta}, \tag{8.17}$$

where $\eta^{\alpha\beta}$ has the role of describing detachment processes.

The internal variable $f^{\alpha\beta}$ is also used to specify the measure $\mu(da)$ that is taken to be absolutely continuous and proportional to the bond density $\mu(da) = f^{\alpha\beta}(X^\alpha, a, t)da$.

We now discuss the constitutive maps for the microscopic force $\mathbf{F}^{\alpha\beta}_{mic}$ and the detachment rate $\eta^{\alpha\beta}$. Following [56] we assume that the microscopic force depends on the position, age of the bonds and time through $\mathbf{r}^{\alpha\beta}$, i.e.,

$$\mathbf{F}^{\alpha\beta}_{mic}(X^\alpha, a, t) = \widehat{\mathbf{F}}^{\alpha\beta}_{mic}(\mathbf{r}^{\alpha\beta}(X^\alpha, a, t))\,. \tag{8.18}$$

The constitutive relation for $\eta^{\alpha\beta}$ follows from the physical intuition that a bond breaks up depending on the magnitude of the microscopic force exerted on it and on its age, reading:

$$\eta^{\alpha\beta}(X^\alpha, a, t) = \hat{\eta}^{\alpha\beta}(F^{\alpha\beta}_{mic}(X^\alpha, a, t), f^{\alpha\beta}(a, t), a)\,, \tag{8.19}$$

where $F^{\alpha\beta}_{mic} = |\mathbf{F}^{\alpha\beta}_{mic}|$. Actually, it is also reasonable to assume a linear relationship with $f^{\alpha\beta}$, so that

$$\begin{aligned}\eta^{\alpha\beta}(X^\alpha, a, t) &= \zeta^{\alpha\beta}(F^{\alpha\beta}_{mic}(X^\alpha, a, t), a) f^{\alpha\beta}(a, t) \\ &= \zeta^{\alpha\beta}(\widehat{F}^{\alpha\beta}_{mic}(\mathbf{r}^{\alpha\beta}(X^\alpha, a, t)), a) f^{\alpha\beta}(a, t)\,.\end{aligned} \tag{8.20}$$

In the next section we will explain how to deduce $\zeta^{\alpha\beta}$ from some experimental data. As an example we can state a simple linear isotropic map

$$\mathbf{F}^{\alpha\beta}_{mic}(X^\alpha, a, t) = -k^{\alpha\beta}_{mic}\mathbf{r}^{\alpha\beta}(X^\alpha, a, t)\,, \tag{8.21}$$

where $k^{\alpha\beta}_{mic}$ is the elastic constant of the microscopic bond. From (8.14) we have

$$\mathbf{m}^\alpha_{ad}(X^\alpha, t) = -k^{\alpha\beta}_{mic} \int_0^{+\infty} \mathbf{r}^{\alpha\beta}(X^\alpha, a, t) f^{\alpha\beta}(X^\alpha, a, t)\, da\,. \tag{8.22}$$

8.3 The Quasi-stationary Limit

The aim of this section is to relate the microscopic measurement with the macroscopic constitutive laws defining the interaction force $\mathbf{m}_{ad}^{\alpha}$. In order to have a more compact notation we drop in this section the indexes α and $\alpha\beta$. A way to upscale the information obtained at the sub-cellular level is suggested by Ölz and Schmeiser who solved in [52, 53, 54] a similar problem when dealing with the actin cytoskeleton. For doing that, we first need to join Eqn. (8.17) with a proper boundary condition. We could take the rate of bond formation to be constant, but as will be shown at the end of the Section, this would give rise to unreasonable results in some cases. A better boundary condition should take into account the fact that the cell can expose on the membrane a maximum number of adhesion bonds, so that the number density N_{max} of active bonds per unit volume is in a first approximation proportional to the volume ratio occupied by the cells, or better to the ratio of cell contact area per unit volume. We can then assume that the formation of new bonds is proportional to the bonds that can still be formed, i.e., recalling (8.16),

$$f(a=0,t) = \beta\left(N_{max} - N^{\alpha\beta}(t)\right) = \beta\left(N_{max} - \int_0^{+\infty} f(a,t)\,da\right), \tag{8.23}$$

Using the scaling introduced in Section 8.1, we can re-write in dimensionless form the problem constituted by (8.17), with η given by (8.20), and (8.23) as

$$\begin{cases} \epsilon\dfrac{\partial \tilde{f}}{\partial \tilde{t}} + \dfrac{\partial \tilde{f}}{\partial \tilde{a}} = -\tilde{\zeta}(\tilde{F}_{mic})\tilde{f}\,, \\ \\ \tilde{f}(\tilde{a}=0,\tilde{t}) = \tilde{\beta}\left(1 - \displaystyle\int_0^{+\infty} \tilde{f}(\tilde{a},\tilde{t})\,d\tilde{a}\right), \end{cases} \tag{8.24}$$

where we have defined:

- $\tilde{t} := t/T$, being T the characteristic time of cell motion introduced in Section 8.1,
- $\tilde{a} := a/A$, being A the characteristic time of adhesion bond lifetimes introduced in Section 8.1,
- $\varepsilon := A/T$
- $\tilde{f} := \dfrac{f}{N_{max}/A}$
- $\tilde{\zeta} = A\zeta$
- $\tilde{\beta} = A\beta$

In the limit $\epsilon \to 0$ the problem reduces to its quasi-stationary version, dropping the time derivative in the differential equation, so that time only taking the role of a parameter in the boundary condition. Preferring to work with dimensional variables, we go back to the dimensional quasi-stationary problem that writes

$$\begin{cases} \dfrac{\partial f}{\partial a}(a,t) = -\zeta(F_{mic}(a,t))f(a,t)\,, \\ \\ f(a=0,t) = \beta\left(N_{max} - \displaystyle\int_0^{+\infty} f(a,t)\,da\right). \end{cases} \tag{8.25}$$

For any ζ, the differential equation in (8.25) can be solved giving

$$f(a,t) = C(t) \exp\left[- \int_0^a \zeta(F_{mic}(\alpha,t))\, d\alpha \right], \tag{8.26}$$

where $C(t)$ can be determined through the boundary condition obtaining

$$C(t) = \frac{\beta N_{max}}{1 + \beta \displaystyle\int_0^{+\infty} \exp\left[- \int_0^a \zeta(F_{mic}(\alpha,t))\, d\alpha \right] da}. \tag{8.27}$$

Hence, dropping the dependence on t, for the sake of simplicity,

$$f(a) = \frac{\beta N_{max} \exp\left[- \displaystyle\int_0^a \zeta(F_{mic}(\alpha))\, d\alpha \right]}{1 + \beta \displaystyle\int_0^{+\infty} \exp\left[- \int_0^a \zeta(F_{mic}(\alpha))\, d\alpha \right] da}, \tag{8.28}$$

and, from (8.14),

$$\mathbf{m}_{ad} = \frac{\beta N_{max} \displaystyle\int_0^{+\infty} \mathbf{F}_{mic}(a) \exp\left[- \int_0^a \zeta(F_{mic}(\alpha))\, d\alpha \right] da}{1 + \beta \displaystyle\int_0^{+\infty} \exp\left[- \int_0^a \zeta(F_{mic}(\alpha))\, d\alpha \right] da}. \tag{8.29}$$

If we take $\mathbf{F}_{mic} = -k_{mic}\mathbf{r}^{\alpha\beta}$, by an argument similar to the one detailed in the previous section, it can be shown that in the limit $A \ll T$, (i.e., $\epsilon \to 0$), using (8.10)

$$\mathbf{F}_{mic} = k_{mic} a (\mathbf{v}^\beta - \mathbf{v}^\alpha),$$

and therefore

$$\mathbf{m}_{ad} = k_{mic}\beta N_{max}(\mathbf{v}^\beta - \mathbf{v}^\alpha) \frac{\displaystyle\int_0^{+\infty} a \exp\left[- \int_0^a \zeta(k_{mic} v_{rel}\alpha)\, d\alpha \right] da}{1 + \beta \displaystyle\int_0^{+\infty} \exp\left[- \int_0^a \zeta(k_{mic} v_{rel}\alpha)\, d\alpha \right] da}, \tag{8.30}$$

where $v_{rel} = |\mathbf{v}^\beta - \mathbf{v}^\alpha|$. Referring to the modulus of the microscopic force rather than the age of the bond, we can then write

$$|\mathbf{m}_{ad}| = \frac{N_{max} \displaystyle\int_0^{+\infty} e(F) F\, dF}{W + \displaystyle\int_0^{+\infty} e(F)\, dF}, \tag{8.31}$$

where $W = k_{mic} v_{rel}/\beta$ and

$$e(F) = \exp\left[- \frac{1}{k_{mic} v_{rel}} \int_0^F \zeta(\phi)\, d\phi \right]. \tag{8.32}$$

Example 1. If there is a continuous constant renewal of bonds, i.e., $\zeta = \zeta_0$ constant, then

$$f(a) = \frac{\beta \zeta_0 N_{max}}{\beta + \zeta_0} e^{-\zeta_0 a}, \tag{8.33}$$

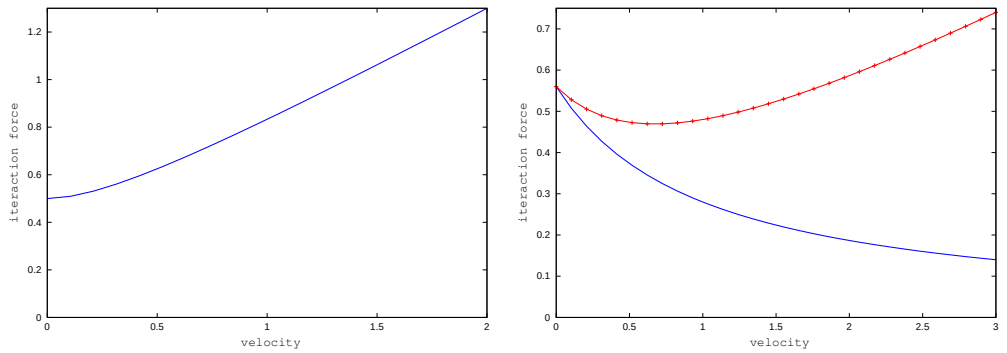

(a) (b)

Figure 8.2: Macroscopic adhesion laws for different cell-ECM microscopic interaction laws. In (a) $|\mathbf{m}_{ad}|/N_{max}F_0$ versus W/F_0 as given by Eq.(8.36) (Example 2) In (b), referring to the CHO cells data in [66], $|\mathbf{m}_{ad}|/N_{max}m_b$ (bottom curve) and $|\mathbf{m}|/N_{max}m_b$ (top curve), related to Example 3 and Eq.(8.46), are plotted versus W/m_b as $M/m_b = 0.2$.

and

$$\mathbf{m}_{ad} = -k_{mic}\frac{\beta N_{max}}{\zeta_0(\beta+\zeta_0)}(\mathbf{v}^\alpha - \mathbf{v}^\beta)\,. \tag{8.34}$$

One then finds the classical drag law asserting that in addition to $\mathbf{m}_D$ the adhesive interaction force is also proportional to the relative velocity, i.e., a Darcy's-like relationship. So, it does not add any new effect to $\mathbf{m}_D$ and the two terms can merge to single one.

Example 2. If the bond start breaking only after the microscopic force F_{mic} overcomes a threshold F_0, and being constant after this level, i.e.,

$$\zeta(F_{mic}) = \zeta_0 H(F_{mic} - F_0)\,, \tag{8.35}$$

where H is the Heavyside function, then

$$\frac{|\mathbf{m}_{ad}|}{N_{max}} = \frac{\hat{F}_0^2 + \hat{F}_0 F_0 + \frac{1}{2}F_0^2}{W + \hat{F}_0 + F_0}\,, \tag{8.36}$$

where

$$\hat{F}_0 = \frac{k_{mic}v_{rel}}{\zeta_0}\,. \tag{8.37}$$

For small velocities $|\mathbf{m}_{ad}|$ tends to $F_0N_{max}/2$ while for large velocities it goes back to the modulus of (8.34) that if the rates of bond formation and association are equal, as plausible, simplify to $k_{mic}N_{max}v_{rel}/(2\beta)$. This behaviour, shown in Fig.8.2a, is compatible with the one proposed in [58] where it is argued that if cells are not pulled strongly enough, they move together with the ECM. If the force overcomes the threshold $F_0N_{max}/2$, they detach from the ECM.

In spite of the simplicity of (8.34) and (8.36), however, it is more proper to obtain ζ from assumptions or experimental data on the bond-breaking distribution $b(F_{mic})$ (e.g.,

those in Fig.6.1). In order to do that we distinguish in ζ two contributions: the first, similar to the ones in the two examples above, related to the internal renewal of adhesion molecules, the second (ζ_r) related to the force-induced detachment, e.g.,

$$\zeta(F_{mic}(a)) = \zeta_0 H(F - F_0) + \zeta_r(F_{mic}(a))\,. \tag{8.38}$$

This last contribution is related to the breaking distribution b by

$$\zeta_r(F_{mic}(a)) = \frac{b(F_{mic}(a))}{B(F_{mic})} = -\frac{1}{B(F_{mic}(a))}\frac{dB}{da}(F_{mic}(a))\,, \tag{8.39}$$

or, because of the linear dependence of F_{mic} from a,

$$\zeta_r(F_{mic}) = -\frac{k_{mic}v_{rel}}{B(F_{mic})}\frac{dB}{dF_{mic}}(F_{mic})\,, \qquad \text{for} \quad F_{mic} < F_M\,, \tag{8.40}$$

where F_M is the supremum of the support of b, that is compact, and

$$B(F_{mic}) = \int_{F_{mic}}^{F_M} b(\phi)\,d\phi\,, \tag{8.41}$$

is the survival function. Of course, different breaking distributions would give rise to different macroscopic forces. However, we can state some general properties that can be easily proved.

Properties 1 (on B). *Since the function $b(F)$ is positive with compact support in $[F_m, F_M]$, then $B(F)$ is constant for $F < F_m$, decreases in (F_m, F_M), vanishes at $F = F_M$, and has an inflection point corresponding to the maximum of $b(F)$. In addition,*

$$\textit{if for} \quad F \simeq F_M, \quad b(F) \simeq C_M(F_M - F)^{\alpha_M} \Longrightarrow B(F) \simeq \frac{C_M}{\alpha_M + 1}(F_M - F)^{\alpha_M + 1}\,.$$

Integration by parts gives that the mean value of $b(F)$ is

$$m_b = F_m + \int_{F_m}^{F_M} \frac{B(F)}{B(F_m)}\,dF\,, \tag{8.42}$$

and the standard deviation σ is given by

$$\sigma^2 = F_m^2 + 2\int_{F_m}^{F_M} F\frac{B(F)}{B(F_m)}\,dF - m_b^2\,. \tag{8.43}$$

From the data by [9, 55, 66] reported in Fig. 8.1, we can argue that F_m is of about 10 pN, with a slightly larger value in [55] and a lower value (approximatively 4 pN) for the Chinese Hampster Ovary cells used in [66]. Regarding F_M from the graphs in [9] it is clear that it is about 200 pN and for the endothelial cells in [66] it is about 70 pN. The other graphs reported there as well as in [55] do not reach zero, so it is hard to evaluate F_M.

Properties 2 (on ζ_r). *The above properties on B imply that the function $\zeta_r(F)$ vanishes for $F \le F_m$ and blows up at F_M and is not integrable there. Therefore, for $F \in [F_m, F_M]$,*

$$\int_0^F \zeta_r(\phi)\,d\phi = \int_{F_m}^F \zeta_r(\phi)\,d\phi = -k_{mic}v_{rel}ln\frac{B(F)}{B(F_m)}\,. \tag{8.44}$$

Example 3. If $\zeta = \zeta_r$, corresponding to neglecting the continuous renewal of bonds which for instance may characterize epithelial cells, we have the strong simplification

$$e(F) = \frac{B(F)}{B(F_m)} \tag{8.45}$$

Obviously, $e(F) = 1$ for $F < F_m$, and $e(F_M) = 0$. We can then extend $e(F)$ and $B(F)$ assuming that they vanish for $F > F_M$. Hence, from (8.31), (8.42), and (8.43)

$$\frac{|\mathbf{m}_{ad}|}{N_{max}} = \frac{\dfrac{F_m^2}{2} + \displaystyle\int_{F_m}^{F_M} F \frac{B(F)}{B(F_m)}\, dF}{W + F_m + \displaystyle\int_{F_m}^{F_M} \frac{B(F)}{B(F_m)}\, dF} = \frac{\sigma^2 + m_b^2}{2(W + m_b)}\,, \tag{8.46}$$

that increasing the relative velocity decreases from $b_0 = (1 + \frac{\sigma^2}{m_b^2})\frac{m_b}{2}$ to zero. This is due to the fact that the high velocity breaks more bonds than the ones that are formed at a rate β. There is, however, a threshold stress determining cell detachment. We remark that m_b and σ are properties of the bond-breaking distribution function that are usually measured. For instance, in [66] $m_b = 28, 29, 29\, pN$ and $\sigma = 10, 9, 10\, pN$, respectively for Chinese hamster ovary cells, a malignant human brain tumor cell line, and human endothelial cells (EA hy926). Higher values can be deduced from the data in [9], giving $m_b \approx 73\, pN$ and $\sigma \approx 38\, pN$.

Referring to Fig.8.2b, it should be noticed that when $\mathbf{m}_{ad}$ and $\mathbf{m}_D$ are added to get

$$\mathbf{m} = -N_{max} \frac{\sigma^2 + m_b^2}{2(W + m_b)} \frac{\mathbf{v}^\alpha - \mathbf{v}^\beta}{v_{rel}} - M(\mathbf{v}^\alpha - \mathbf{v}^\beta)\,, \tag{8.47}$$

after a minimum reached for $v_{rel} = \sqrt{(\sigma^2 + m_b^2)\beta/(2k_{mic}M)}$, $|\mathbf{m}|$ grows to infinity because $|\mathbf{m}_D|$ becomes dominant. Starting from rest, when the interaction force overcomes the threshold value b_0, cells detach to crawl with a velocity given by the right branch, that we will denote Darcy-dominated behaviour. If now the interaction force decreases below the minimum, then the cells attach again, giving rise to a behaviour that is characteristic of bistable sytems.

We now consider that in addition to a force-driven detachment, there is a continuous renewal of the bonds. We will assume there this is triggered when $F > F_0$ and use (8.38). Therefore, we have

$$e(F) = \frac{B(F)}{B(F_m)} \exp\left[- \frac{(F - F_0)_+}{\hat{F}_0} \right]\,, \tag{8.48}$$

where h_+ stands for the positive part of h, and

$$\frac{|\mathbf{m}_{ad}|}{N_{max}} = \frac{\displaystyle\int_0^{F_m} F \exp\left[- \frac{(F - F_0)_+}{\hat{F}_0} \right] dF + \int_{F_m}^{F_M} F \exp\left[- \frac{(F - F_0)_+}{\hat{F}_0} \right] \frac{B(F)}{B(F_m)}\, dF}{W + \displaystyle\int_0^{F_m} \exp\left[- \frac{(F - F_0)_+}{\hat{F}_0} \right] dF + \int_{F_m}^{F_M} \exp\left[- \frac{(F - F_0)_+}{\hat{F}_0} \right] \frac{B(F)}{B(F_m)}\, dF} \tag{8.49}$$

Example 4. If the bonds always renew, i.e., $F_0 = 0$, which might resemble cells in a mesenchymal state, one has the behaviours shown in Fig.8.3a that is based on the experimental results reported in [9, 55, 66]. Considering the discussion in Example 3, adding

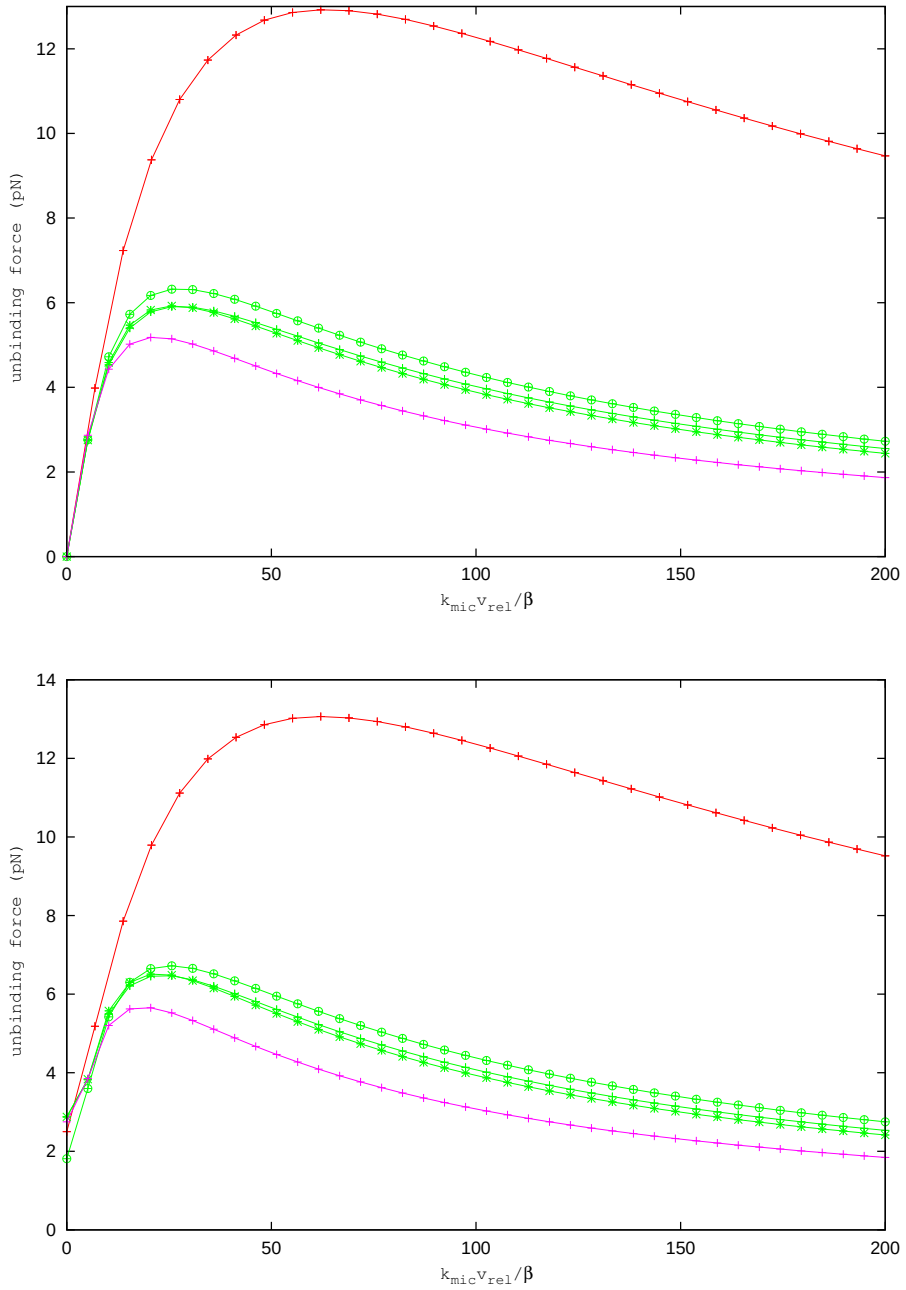

Figure 8.3: Macroscopic adhesion laws for the microscopic detachment rates given in [9] (top) [55] (bottom), and [66] (the three almost identical in the middle) as given by (8.49). In (a) $F_0 = 0$ and in (b) $F_0 = F_m/2$.

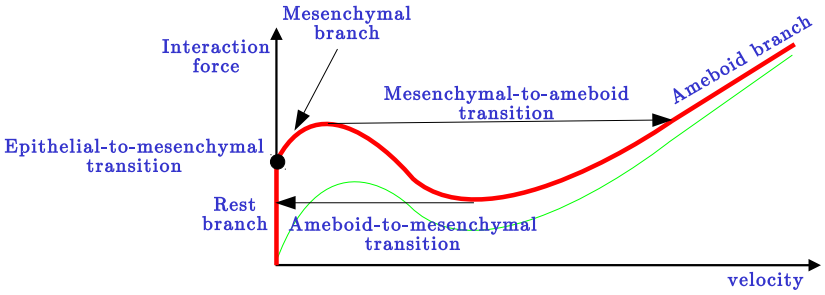

Figure 8.4: Sketch of the interaction forces when $F_0 = 0$ (bottom curve) and $F_0 \neq 0$ (upper curves). The right-pointed arrow indicates a transition that resembles the one between mesenchymal and ameboid motion. The left-pointed arrow, the reverse transition. The dot indicates a transition from rest to a mesenchymal-type motion.

the Darcy-like contribution, that is dominant for large relative velocities, we have again a total interaction force characterized by a cubic-like curve, as the one shown in Fig.8.4. In a descriptive way, we might call "mesenchymal-like branch" the increasing branch on the left and "ameboid-like branch" the one on the right, because the former is characterized by smaller velocities and is adhesion-dominated while the latter is characterised by larger velocities and is related to the difficulties in moving in the network of fibres. So, if the stress acting on the cells is too high, they might jump to the ameboid-like or Darcy branch and when it decreases again below the minimum in the graph they will jump to the adhesion-dominated or mesenchymal-like branch. We have then a transition that resembles an ameboid-mesenchymal transition. However, we need to warn the reader that the above description is a strong simplification, because there are chemical mechanisms that are not considered here, whilst they are at the basis of the ameboid-mesenchymal transition (see, for instance, [35, 37, 64, 65]).

Example 5. When $0 \neq F_0 < F_m$, i.e., the threshold for spontaneous renewal is lower than the one leading to bond rupture, the behaviour of (8.49) is similar to the one discussed in Example 2, presenting an initial increase from a non-null value that might be described as an epithelial-to-mesenchymal transition from rest to a slowly moving state. Again we would have a mesenchymal-like (or adhesion-dominated) branch and an ameboid-like (or Darcy-dominated) branch, as in the previous example and shown in Fig. 8.4. According to whether the local minimum is above or below the threshold value for low velocities, when decreasing the velocity from the ameboid-like branch the cell will go to the mesenchymal-like branch or to the rest branch.

As a final remark, as anticipated at the beginning of this section, we notice that if the rate of formation of bonds were simply constant, i.e., in absence of the integral in the boundary condition (8.23), then the above procedure would yield a force blowing up for small velocities because of the absence of the second term in the denominator, for instance of (8.29), and then of the last two terms in (8.36). This biologically corresponds to the fact that if the cell barely moves, bonds always form but never break. So, in the limit an infinite number of bonds form, corresponding to an infinite force. This is of course unphysical and justifies the presence of a saturation term in the boundary condition (8.23).

Chapter 9

Final Remarks

In this Part II of the dissertation we have shown how the information obtained performing experiments at the sub-cellular scale on the detachment forces of single adhesion bonds can be upscaled and used in a macroscopic model. For instance, an easy formula (8.36) linking the adhesive interaction force in the multiphase model with the mean and stardard deviation of the bond-breaking probability, the microscopic elastic constant, the bond renewal rate and the maximum number density of adhesive sites is found. An unexpected by-product of the study of cell-ECM interaction is the deduction of some laws that qualitatively lead to behaviours like the epithelial-mesenchymal transition and the mesenchymal-ameboid transition. We are well aware that the comparison can only be qualitative because our description is purely mechanical, neglecting all the chemical phenomena triggering such transitions (see, for instance, [35, 37, 64, 65]) and that, for instance, from the viewpoint presented here can at least change the parameters. However, in our opinion such constitutive laws for the interaction force present in the multiphase model is by itself very interesting also from the mathematical point of view. In fact, they are likely to give rise to bistable behaviours and to the presence of hysteresis cycles, localization and phase transition–like features. However, such characteristics were here only argued and not proved mathematically. Also from the numerical point of view, the use of such non-monotonic laws is not trivial and need some care. Other developments can be obtained taking into account several phenomena not considered here and that can influence the cell-cell adhesion and cell-ECM adhesion properties. For instance, it is known that in a tumour mass there are several clones characterized by different adhesive behaviours and motilities, that hypoxia can induce changes in the mechanisms of adhesion and trigger cell motility, and there are actually several chemical factors influencing the transition of cells towards a mesenchymal state.

Bibliography

[1] R.A. Adams and J.J.F. Fournier. *Sobolev Spaces*. Academic Press Elsevier, 2003. [cited at p. 17, 18, 33]

[2] D. Ambrosi. Cellular traction as an inverse problem. *SIAM J. Appl. Math.*, 66(6):2049–2060, 2006. [cited at p. 9, 32, 41, 43]

[3] D. Ambrosi, V. Peschetola, and A. Chauviere. Traction patterns of tumor cells. *J. Math. Biol.*, 58:163–181, 2009. [cited at p. 32, 43]

[4] D. Ambrosi and L. Preziosi. Cell adhesion mechanisms and stress relaxation in the mechanics of tumours. *Biomech. Modeling in Mechanobiology*, 8:397–413, 2009. [cited at p. 61]

[5] R.P. Araujo and D.L.S. McElwain. A history of the study of solid tumour growth: the contribution of mathematical modeling. *Bull. Math. Biol.*, 66:1039–1091, 2004. [cited at p. 61]

[6] N.J. Armstrong, K.J. Painter, and J. A. Sherratt. A continuum approach to modelling cell-cell adhesion. *Journal of Theoretical Biology*, (243):98–113, 2006. [cited at p. 61]

[7] N.J. Armstrong, K.J. Painter, and J. A. Sherratt. Adding adhesion to the cell cycle model for somite formation. *Bull. Math. Biol.*, (71):1–24, 2009. [cited at p. 61]

[8] J.P. Aubin. *Functional Analysys*. Wiley Interscience, 2000. [cited at p. 38]

[9] W. Baumgartner, P. Hinterdorfer, W. Ness, A. Raab, D. Vestweber, and H.D.D. Schindler. Cadherin interaction probed by atomic force microscopy. *Proc. Nat. Acad. Sci. USA*, 97:4005–4010, 2000. [cited at p. 61, 62, 74, 81, 82, 83]

[10] N. Bellomo. *Modeling complex living systems - Kinetic theory and stochastic game approach*. Birkhauser, 2008. [cited at p. 77]

[11] N. Bellomo, N.K. Li, and P.K. Maini. On the foundations of cancer modelling: Selected topics, speculations, and perspectives. *math. model meth. appl. sci.*, 18(4):593–646, 2008. [cited at p. 61]

[12] A. Bossavit. Applied differential geometry (a compendium). avaible on the website: `http://butler.cc.tut.fi/ bossavit`. [cited at p. 68]

[13] R.M. Bowen. Theory of mixtures. In A.C. Eringen, editor, *Continuum Physics*. Academic Press, New York, 1976. [cited at p. 65, 71, 72, 74]

[14] R.M. Bowen. Incompressible porous media models by the use of the theory of mixtures. *Int. J. Eng. Sci.*, (18):1129–1148, 1980. [cited at p. 65, 68, 72, 74]

[15] R.M. Bowen. Compressible porous media models by the use of the theory of mixtures. *Int. J. Eng. Sci.*, (20):697–735, 1982. [cited at p. 74]

[16] H. Byrne and L. Preziosi. Modeling solid tumor growth using the theory of mixtures. *Math. Med. Biol*, 20:341–360, 2004. [cited at p. 61]

[17] E. Canetta, A. Duperray, A. Leyrat, and C. Verdier. Measuring cell viscoelastic properties using a force-spectrometer: Influence of the protein-cytoplasm interactions. *Biorheology*, 42:298–303, 2005. [cited at p. 61]

[18] E. Casas. l^2 estimates for the finite element method for the dirichlet problem with singular data. *Numer. Math.*, 47:627–632, 1985. [cited at p. 10, 21]

[19] E. Casas. Control of an elliptic problem with pointwise state constraint. *SIAM J. Contr. Opt.*, 24(6):1309–1317, 1986. [cited at p. 10, 33]

[20] E. Casas. Boundary control of semilinear elliptic equations with pointwise state constraint. *SIAM J. Contr. Opt.*, 31(4):993–1006, 1993. [cited at p. 10, 21, 37, 38]

[21] P. G. Ciarlet. *Mathematical Elasticity*, volume 1. North Holland, 1988. [cited at p. 16, 19, 20, 36, 40]

[22] V. Cristini, X. Li, J. Lowengrub, and S.M. Wise. Nonlinear simulations of solid tumor growth using a mixture model: Invasion and branching. *J. Math. Biol.*, (58):723–763, 2009. [cited at p. 61]

[23] M. Dembo, T. Oliver, A. Ishihara, and K. Jacobson. Imaging the traction stresses exerted by locomoting cells with elastic substratum method. *Biophys. J.*, 70:2008–2022, 1996. [cited at p. 9]

[24] M. Dembo and Y. L. Wang. Stresses at the cell-to-substrate interface during locomotion of fibroblast. *Biophys. J.*, 76:2307–2316, 1999. [cited at p. 9, 43]

[25] Z. Ding. Optimal boundary control of linear elastostatics on lipschitz domains with point observation. *J. Dynamical and Control Syst.*, 7(2):181–207, 2001. [cited at p. 38]

[26] H. W. Engl, Hanke M., and Neubauer A. *Regularization of Inverse Problems*. Kluwer Academic Publisher, 2000. [cited at p. 22, 23, 24, 29]

[27] L. Graziano and L. Preziosi. Mechanics in tumour growth. In K. Rajagopal F. Mollica, L. Preziosi, editor, *Modeling of Biological Materials*, pages 267–328. Birkhauser, 2007. [cited at p. 61]

[28] A. Gurtin, M.E. Vargas. On the classical theory of reacting fluid mixtures. *Arch. Rat. Mech. Anal.*, (2), 1972. [cited at p. 71]

[29] M.E. Gurtin, E. Fried, and L. Anand. *The Mechanics and Thermodynamics of Continua*. Cambridge Press, 2010. [cited at p. 13, 14, 15, 68, 71]

[30] A.K. Harris, P. Wild, and D. Stopak. Silicone rubber substrata: a new wrinkle in the study of cell locomotion. *Science*, 208:177–179, 1980. [cited at p. 9]

[31] F. Hecht. *Free–FEM ++*. Laboratoire Jacques-Louis Lions, Université Pierre et Marie Curie, Paris. [cited at p. 41]

[32] T. Hillen, K. Painter, and C. Schmeiser. Global existence for chemotaxis with finite sampling radius. *Discr. Cont. Dyn. Syst.*, 7(1):125–144, 2007. [cited at p. 61]

[33] M. Hinze and F. Troeltzsch. Discrete concepts versus error analysis in pde constrained optimization. *GAMM-mitt.*, 33(2):148–162, 2010. [cited at p. 41]

[34] M. Iannelli, M. Martcheva, and F.A. Milner. Gender-structured population modeling - mathematical methods, numerics, and simulations. *SIAM Frontiers in Applied Mathematics*, 2005. [cited at p. 77]

[35] J. Jou and A. M. Diehl. Epithelial-mesenchymal transitions and hepatocarcinogenesis. *J. Clin. Invest.*, 120(4):1031–1034, 2010. [cited at p. 84, 85]

[36] Wilmanski K. Lagrangean model of a two phases porous material. *J. Non-Equil. Thermodyn.*, (20):50–77, 1995. [cited at p. 65, 72, 74]

[37] M. Novotny J. Brabek K. Pankova, D. Rosel. The molecular mechanisms of transition between mesenchymal and amoeboid invasiveness in tumor cells. [cited at p. 84, 85]

[38] K. Krumbiegel. *Numerical concepts and error analysis for elliptic Neumann boundary control problems with pointwise state and control constraints*. PhD thesis, Vom Fachbereich Mathematik der Universitat Duisburg-Essen (Campus Duisburg), 2009. [cited at p. 38]

[39] W. R. Legant, Miller J.S., Blakely B.L., Cohen D.M., Genin G.M., and C.S. Chen. Measurement of mechanical traction exerted by cells in three dimensional matrices. *Nature*, 7(12):969–971, 2010. [cited at p. 10, 41, 42, 45, 54, 57]

[40] J.L. Lions. *Optimal Control of Systems Governed by Partial Differential Equations*. Springer, 1972. [cited at p. 18, 25, 28, 29, 31]

[41] I-S. Liu. On chemical potential and incompressible porous media. *Journal de la Mecanique*, 19(2):329–337, 1980. [cited at p. 69]

[42] I-S. Liu. *Continuum Mechanics*. Springer, 2002. [cited at p. 14, 15, 69, 70, 71]

[43] I.S. Liu and A. Rincon. On numerical approximation of an optimal control problem in linear elasticity. *Divulgaciones Matematicas*, 11(2):91–107, 2003. [cited at p. 41]

[44] J. Lowengrub, S.M. Wise, H.B. Frieboes, and V. Cristini. Three dimensional multispecies nonlinear tumor growth ii: Tumor invasion and angiogenesis. *J. Theor. Biol.* to appear. [cited at p. 61]

[45] J. Lowengrub, S.M. Wise, H.B. Frieboes, and V. Cristini. Three-dimensional multispecies nonlinear tumor growth- i. model and numerical method. *J. Theor. Biol.*, 253:524–543, 2008. [cited at p. 61]

[46] J.S. Lowengrub, H.B. Frieboes, F. Jin, Y.L. Chuang, X. Li, P. Macklin, S.M. Wise, and V. Cristini. Nonlinear modelling of cancer: Bridging the gap between cells and tumours. *Nonlinearity*, 23, 2010. in press. [cited at p. 61]

[47] J. M. Marsden and T. J. R. Hughes. *Mathematical Foundations of Elasticity*. Prentice-Hall Inc., 1983. [cited at p. 16, 19, 20]

[48] A. Mazzuccato and V. Nistor. Well posedness and regularity for the elasticity equation with mixed boundary conditions on polyhedral domains with cracks. *Arch. Rat. Mech. An.*, 195(1):25–73, 2010. [cited at p. 20]

[49] J. Necas. *Les methodes directes en theorie des equations elliptiques*. Masson et Cie, Paris, 1967. [cited at p. 17, 18, 33]

[50] W. Noll. A frame-free formulation of elasticity. 2005. avaible on the website: `http://math.cmu.edu/wn0g/noll`. [cited at p. 13]

[51] W. Noll. *Finite Dimensional Spaces*, volume 1. 2006. avaible on the website: `http://math.cmu.edu/wn0g/noll`. [cited at p. 19, 32, 34]

[52] Schmeiser C. Oelz, D. Derivation of a model for symmetric lamellipodia with instantaneous cross-link turnover. *Archive Rat. Mech. Anal.*, (2). to appear. [cited at p. 63, 78]

[53] D. Olz and C. Schmeiser. How do cells move? mathematical modelling of cytoskeleton dynamics and cell migration. Chapman and Hall / CRC Press, 2010. [cited at p. 63, 78]

[54] D. Olz, C. Schmeiser, and V. Small. Modelling of the actin-cytoskeleton in symmetric lamellipodial fragments. *Cell Adhesion & Migration*, 2:117–126, 2008. [cited at p. 63, 78]

[55] P. Panorchan, M.S. Thompson, K.J. Davis, Tseng Y., K. Konstantopoulos, and D. Wirtz. Single-molecule analysis of cadherin-mediated cell-cell adhesion. *J Cell Sci*, (119):66–74, 2006. [cited at p. 61, 63, 81, 82, 83]

[56] J.J. Pop and R.M. Bowen. A theory of mixtures with a long range spatial iteraction. *Acta Mechanica*, (29):21–34, 1978. [cited at p. 65, 68, 71, 72, 74, 77]

[57] L. Preziosi and A. Tosin. Multiphase and multiscale trends in cancer modelling. *Math. Model. Nat. Phenom.*, 4:1–11, 2009. [cited at p. 61]

[58] L. Preziosi and A. Tosin. Multiphase modeling of tumor growth and extracellular matrix interaction: Mathematical tools and applications. *J. Math. Biol.*, 58:625–656, 2009. [cited at p. 80]

[59] L. Preziosi and G. Vitale. A multiphase model of tumour and tissue growth including cell adhesion and plastic re-organisation. *Mathematical Methods and Models in Applied Sciences*, 21(9):1901–1932, 2011. [cited at p. 5]

[60] S. Quiligotti, Dell'Isola F., and G.A. Maugin. An eshelbian approach to the nonlinear mechanics of constrained solid-fluid mixtures. *Springer-Verlag*, 2003. [cited at p. 65, 66, 67, 69, 70, 72]

[61] W. Rudin. *Functional Analysis*. McGraw-Hill Higher Education, 1990. [cited at p. 21, 28]

[62] S. Salsa. *Partial Differential Equations in Action*. Springer Verlag, 2008. [cited at p. 18, 20, 22]

[63] U. S. Schwartz, N. Q. Balaban, D. Riveline, A. Bershadsky, B. Geiger, and S. A. Safran. Calculation of forces at focal adhesion from elastic substrate data: The effect of localized force and the need for regularization. *Biophys. J.*, 83:1380–1394, 2002. [cited at p. 41]

[64] M. Scianna, R. Merks, L. Preziosi, and E. Medico. Individual cell-based models of cell scatter of aro and mlp-29 cells in response to hepatocyte growth factor. *J. Theor. Biol.*, 260:151–160, 2009. [cited at p. 84, 85]

[65] M. Scianna, L. Munaron, and L. Preziosi. A multiscale hybrid approach for vasculogenesis and related potential blocking therapies. *Progress in Biophysics and Molecular Biology*. submitted. [cited at p. 84, 85]

[66] M. Sun, J. Graham, B. Hegedus, F. Marga, Y. Zhang, G. Forgacs, and M. Grandbois. Multiple membrane tethers probed by atomic force microscopy. *Byophys J.*, 89:4320–4329, 2005. [cited at p. 61, 62, 63, 80, 81, 82, 83]

[67] P. Tracqui. Biophysical models of tumour growth. *Rep. Prog. Phys.*, 72(056701), 2009. [cited at p. 61]

[68] C. Truesdell. Sulle basi della termomeccanica. *Rend. Scient.. Fis. Mat. Nat.- Accademia dei Lincei*, (22):33–38, 158–166, 1957. [cited at p. 72]

[69] D. Valdembri, P.T. Caswell, K.I. Anderson, J.P. Schwartz, E. Astanina, F. Caccavari, J.C. Norman, M.J. Humphries, F. Bussolino, and G. Serini. Neuropilin-1/gipc1 signaling regulates a5b1 integrin traffic and function in endothelial cells. *PLOS Biology*, 7(1), 2009. doi:10.1371/journal.pbio.1000025. [cited at p. 74]

[70] G. Vitale, D. Ambrosi, and L. Preziosi. Force traction microscopy: an inverse problem with pointwise observation. *J. Math. Anal. Appl.* submitted. [cited at p. 5]

[71] C. R. Vogel. *Computational Methods for Inverse Problems*. SIAM Frontiers in Applied Mathematics, 2002. [cited at p. 22, 23, 24, 45]

[72] Lin Yuan, M.J. Fairchild, A.D. Perkins, and G. Tanentzapf. Analysis of integrin turnover in fly myotendinous junctions. *Journal of Cell Science*, 123:939–946, 2010. [cited at p. 74]

List of Principal Symbols and Abbreviations

Abbreviation	Description
Lin	Space of Continuous Linear Transformation
Skw	Subspace of Skew–Symmetric Transformation
Sym	Subspace of Symmetric Transformation
Sph	Subspace of Spherical Transformation
skw	Projection on Skw
sym	Projection on Skw
sph	Projection on Sph
tr	Trace of a Second Order Tensor
Ort	Group of Orthogonal Transformation
$\mathbb{T}$	Tangent Bundle of a Manifold
meas	Lebesgue Measure
$\square'$	Frechet Differential
∂_i	Derivative with respect to $i-$th Argument
∇	Gradient (Derivation in Space)
div	Divergence
$\dot{\square}$	Time Derivative
dom	Domain
ran	Range
dim	Dimension
$W^{k,p}$	Sobolev Functional Space
H^k	Hilbert Functional Space
$\cdot$	Scalar Product on Finite Dimensional Space
$\lvert\ \rvert$	Norm on Finite Dimensional Space
$\otimes$	Tensor Product on Finite Dimensional Space
$\times$	Exterior Product on two or Three Dimensional Space
$(\ \vert\ )$	Scalar Product on Infinite Dimensional Hilbert Space
$\lVert\ \rVert$	Norm on Infinite Dimensional Space
$\square^\dagger$	Moore-Penrose Generalized Inverse Map